AUTOTUNING OF A TRANSMISSION ELECTRON MICROSCOPE

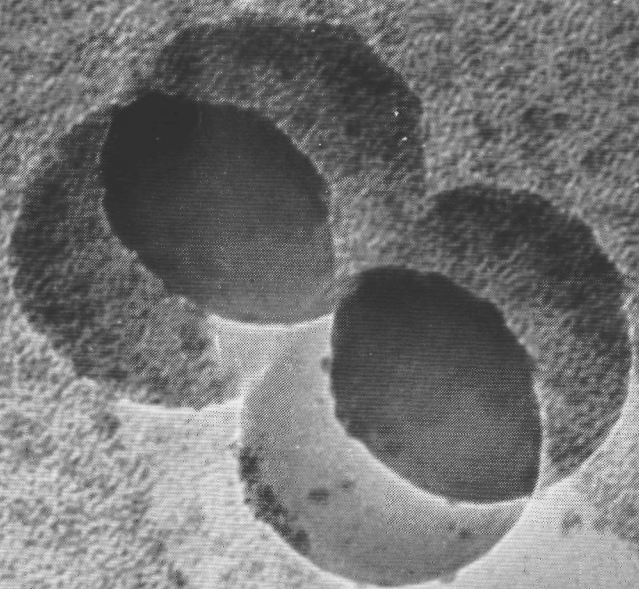

A.J. KOSTER

AUTOTUNING OF A TRANSMISSION ELECTRON MICROSCOPE

On the cover TEM images of latex particles with 0.22 μm diameter, shadowed with a coating of gold, are shown. The front cover illustrates the effect of tilting the illuminating beam in a TEM, when the TEM is not focused. The main effect of such a beam tilt is an image displacement. When the TEM is focused, no image displacement is visible, as is illustrated on the back cover.

AUTOTUNING OF A TRANSMISSION ELECTRON MICROSCOPE

Proefschrift

Ter verkrijging van de graad van doctor aan de
Technische Universiteit Delft, op gezag van
de Rector Magnificus, Prof.drs. P.A. Schenck,
in het openbaar te verdedigen ten overstaan van
een commissie aangewezen door het College van Dekanen
op dinsdag 6 juni 1989 te 14.00 uur

door

Abraham Johannes Koster

natuurkundig ingenieur
geboren te Velsen

Dit proefschrift is goedgekeurd door de promotoren
Prof.dr.ir. K.D. van der Mast en Dr.ir. A. van den Bos

Contents

1	Introduction	7
2	An Autofocus method for a TEM[1]	26
3	Signal processing for autofocusing by beam tilt induced image displacement[2]	40
4	Autotuning of a TEM using minimum electron dose[3]	58
5	Practical autotuning of a TEM[4]	81
6	Conclusions and Discussion	111
	Samenvatting	119
	Korte levensbeschrijving	123
	Nawoord	125

1. Published in Ultramicroscopy 21(1987)209-221.
2. Published in Scanning Microscopy Suppement 2, 1988, pages 83-92.
3. Published in Ultramicroscopy 27(1989)251-273.
4. Submitted to Ultramicroscopy.

1 Introduction

1.1	Scope of the research	7
1.2	Transmission electron microscopy	8
1.3	Resolution and electron bombardment	9
1.4	The tuning of the TEM parameters	13
1.5	Autotuning of a TEM - historical overview	15
1.6	Autotuning of a TEM - the research in Delft	18
1.7	Outline of the dissertation	19
	References	21

2 An Autofocus Method for a TEM

1	**Introduction**	27
2	**Focusing by measuring beam-tilt-induced image displacement**	28
3	**Achievable precision in estimating an image displacement**	28
3.1	Model of observations	28
3.2	Minimum variance bound	29
3.3	Signal-to-noise ratio, Poisson noise	29
3.4	Instrumentation noise	31
3.5	Sampling and its influence on the MVB	32
4	**Numerical experiments**	32
4.1	Defocus	33
4.2	Sampling distance	34
4.3	Sensor length	34
4.4	Instrumentation noise	34
4.5	Magnification	36
4.6	Measuring time	36
5	**The BID method as autofocus method**	36
6	**Conclusions and discussion**	37
	Appendix A. Power spectrum of the image	37
	Appendix B. Power spectrum of the Poisson noise in the image	38
	References	39

3 Signal Processing For Autotuning By Beam Tilt Induced Image Displacement

1	Introduction	41
2	Achievable precision in autofocusing a TEM	42
3	Image formation with tilted illumination	42
4	Achievable precision of the BID method	44
5	Achievable precision of the variance method	48
6	Estimating defocus with the BID method	51
7	Conclusions and discussion	55
	References	56

4 Autotuning of a TEM using Miminum Electron Dose

1	**Introduction**	**59**
2	**Autotuning method**	**61**
2.1	Models of the phase spectra derived from linear image formation	62
2.2	Estimation of the phase spectrum	65
2.3	Estimation of the TEM parameters	67
2.3.1	Achievable precision of defocus and astigmatism estimates	67
2.3.2	Estimator of defocus and astigmatism	67
2.3.3	Estimator of misalignment	68
2.3.4	Performance criterion for the estimation of defocus and astigmatism	68
3	**Practical design of the autotuning method**	**69**
3.1	Instrumental parameters determining the precision	70
3.2	Design strategy of the two-step autotuning procedure	71
3.3	Reference area for the estimation of defocus and astigmatism	72
4	**Simulations of the estimation of defocus and astigmatism**	**74**
4.1	Generation of noisy images	74
4.2	Numerical minimization	74
4.3	Simulation results	75
4.4	Numerical example : Electron dose required for tuning	77
5	**Conclusions and discussion**	**79**
	Appendix A : The influence of the TEM parameters on the equation errors	**79**
	Appendix B : Numerical computation of the tuning precision	**79**
	References	**80**

5 Practical Autotuning of a TEM

1	**Introduction**	82
2	**Theory of autotuning**	86
2.1	Effect of beam tilt : a mere image displacement	86
2.2	Measurement and correction of TEM parameters	89
2.3	Effect of beam tilt : image blurring	91
2.4	Expected accuracy and speed considering the noise	94
3	**Implementation of the autotuning method**	96
3.1	Requirements on the instrumentation	96
3.1.1	The Transmission Electron Microscope	96
3.1.2	The Camera	96
3.1.3	The computer - control of the TEM	98
3.1.4	The computer - image processing	98
3.1.5	The computer - the user interface	98
3.1.6	Some examples of measuring set-ups	99
3.2	The experimental set-up in Delft	99
3.2.1	The Philips EM420 TEM	99
3.2.2	The Gatan 622 camera	100
3.2.3	The DEC PDP 11/23	100
3.2.4	The TVDIPS image processing device	101
3.2.5	The IBM PC/AT	101
4	**Experimental results**	101
4.1	Calibration	101
4.2	Automatic rotation alignment	102
4.3	Automatic coma-free alignment	104
4.4	Automatic focusing and correction of astigmatism	104
4.5	Instrumental limitations for low SNR images	105
5	**Discussion and conclusions**	107
	References	108

1 Introduction

1.1 Scope of the research

A transmission electron microscope (TEM) is an instrument of importance for the research on biological and inorganic structures. Its application is restricted by the resolution of the instrument, the radiation sensitivity of the specimen, and the skill of the operator to tune the instrument accurately, sometimes under difficult imaging conditions. Consequently, research is done by many groups on a wide field of subjects to overcome these restrictions as much as possible.

This report is concerned with the instrumental limitations of a TEM related to the accuracy in tuning the beam tilt misalignment, the defocus and the astigmatism of the objective lens. The main reason for this research is that the optical and mechanical properties of a TEM are less a limitation for its application, than the skill of the operator to tune the TEM with the required accuracy. The operator makes a compromise between the tuning accuracy and the time (and thus the amount of electron irradiation) needed for tuning.

Therefore, the goal of the research is to design and test a method for the automatic correction of the beam tilt misalignment, defocus and astigmatism in a TEM (autotuning). The autotuning method has to tune the TEM as accurately as possible. In other words: the autotuning method has to be suitable for low dose-, and also for high resolution electron microscopy.

A characteristic aspect of low dose electron microscopy is that the specimens are sensitive to the electron irradiation. Consequently, the images recorded for autotuning are very noisy as the dose available to form the images is limited (only a few hundred electrons per nm^2). The autotuning method should therefore be designed to estimate the characteristic parameters for the beam tilt misalignment, defocus and astigmatism (TEM parameters) from noisy measurements as precise as possible (in the sense that the variance of the estimator is minimal).

Statistical methods are applied for the estimation of the TEM parameters, and not the conventional deterministic methods. Different from the deterministic methods, statistical methods for the measurement of parameters use a model of the observations that includes the influence of noise. Therefore, the autotuning method is first formulated as a statistical parameter estimation problem. With the statistical model of the measurements, the precision and systematic errors of the parameter measurements (estimates) can be analysed. Furthermore, with the techniques available for statistical parameter estimation problems, the performance of the autotuning method designed can be evaluated extensively with calculations and simulations of realistic measuring conditions. For textbooks on parameter estimation and signal processing, we refer to [1-4].

1.2 Transmission Electron Microscopy

In this section a short introduction to transmission electron microscopy is given. For a more complete discussion on electron microscopy and its applications we refer to [5-10].

In a transmission electron microscope (TEM), a specimen is irradiated with an electron beam of uniform current density. The electron energy is in the range of 20-400 keV for low and medium voltage electron microscopy. For high voltage electron microscopy, the electron energy is between the 400 keV and 3 MeV.

The electrons are emitted in the electron gun by thermionic emission from tungsten hairpin cathodes or LaB_6 rods, or by field emission from pointed tungsten filaments (when a high gun brightness is needed). A condensor-lens system permits variation of the illumination beam divergence and the area of the specimen illuminated (see figs.1 and 2). The electrons emerging from the specimen form an image by means of a projector lens system, on a fluorescent screen. The images can be recorded by direct exposure of a photographic emulsion inside the vacuum, or, for on-line image processing, with a camera system.

The objective lens of a TEM determines for the greater part the resolution of the image. The lens aberrations of the objective lens are so large that it is necessary to limit the objective apertures to 10-25 mrad, to achieve resolution of the order of 0.2-0.5 nm. The normal, bright-field, image contrast is produced either by absorption of the electrons scattered through angles larger than the objective aperture (scattering contrast) or by the interference of the scattered wave and the incident wave at the image point (phase contrast). The phase of the electron waves behind the specimen is modified by the wave aberration of the objective lens. These aberrations and the energy spread of the electron gun, together with the beam divergence of the illumination beam, limit the contrast transfer of high spatial frequencies.

Electrons interact strongly with atoms by elastic and inelastic scattering. The specimen must therefore be very thin,

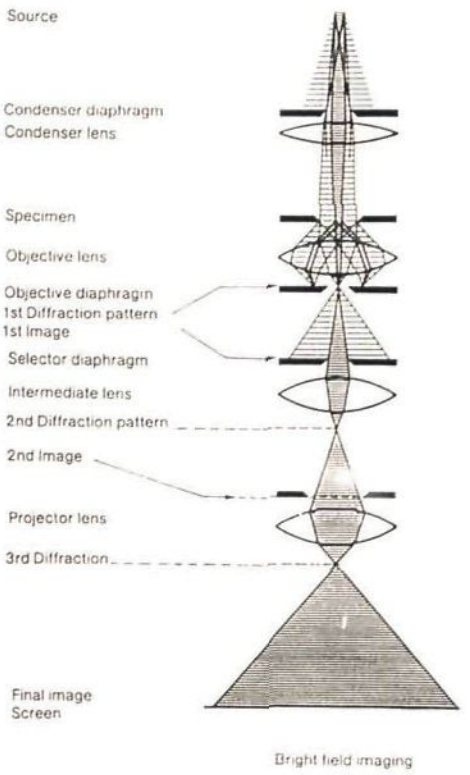

Fig.1 Ray diagram for a transmission electron microscope in the bright-field imaging mode (from: Reimer [8]).

typically of the order of 5 nm- 0.5μm for 100 keV electrons, depending on the density, the elemental composition of the structure and the resolution desired. Thicker specimens can be studied in a high voltage electron microscope.

A TEM can provide high resolution images as elastic scattering is an interaction process that is highly localized in the

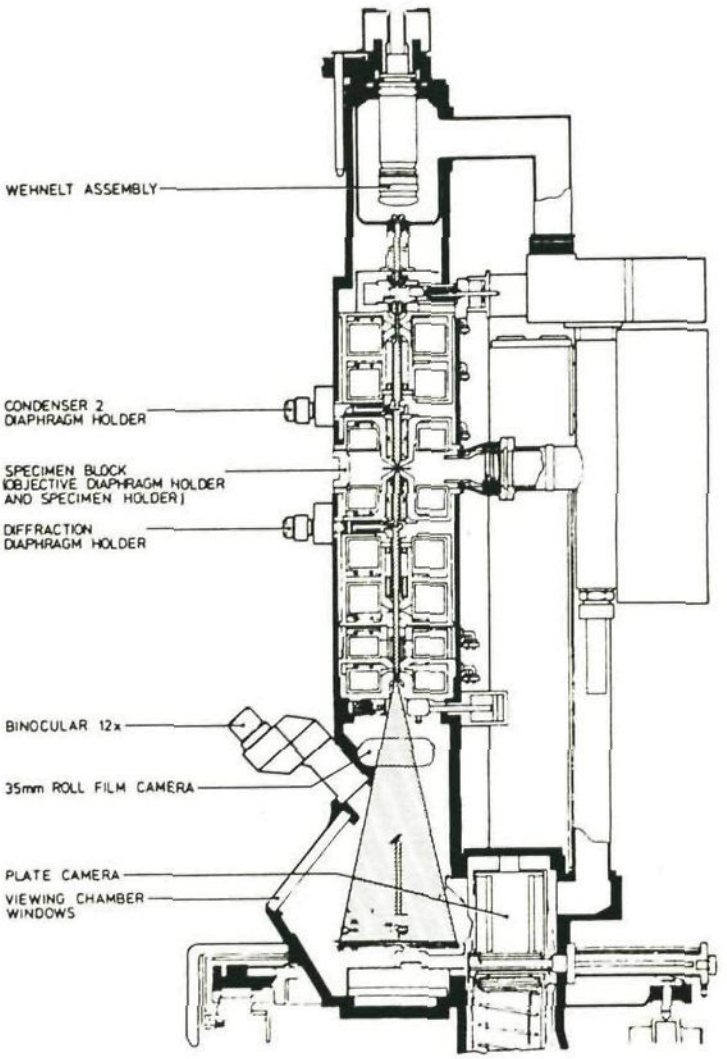

Fig.2 Cross-section of a transmission electron microscope (from: Philips Operating Instructions manual EM420).

region occupied by the screened Coulomb potential of an atomic nucleus. Inelastic scattering is, in general, more diffuse.

For the discussion of high resolution electron microscopy, the wave optical model of image electron propagation has to be employed. The Coulomb potential of a nucleus or the inner potential of a dense particle shifts the phase of the electron wave. Elastic scattering has to be treated quantum- mechanically by solving the Schrödinger equation of the scattering problem. In the wave optical theory of imaging, the phase shifts caused by the

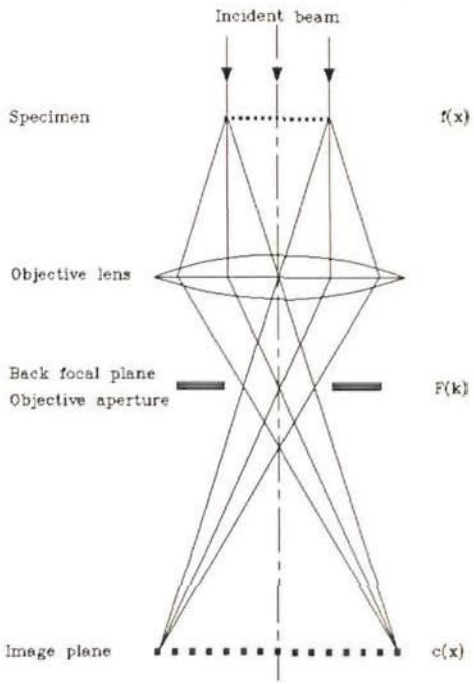

Fig.3 Schematic diagram of image formation in a TEM described by the wave propagation of electrons.

specimen and by the wave aberration of the objective lens are studied, and shown to create phase contrast as an interference effect between the primary and scattered electron waves.

1.3 Resolution and electron bombardment

In this report we restrict ourselves to the development of an autotuning method which is suitable for specimens which can be described as weak phase objects, and its image formation with the phase contrast transfer theory.

The imaging theory can be expressed in terms of a two-stage Fourier transform, see fig. 3. In the focal plane of the objective lens, the diffraction pattern of the specimen is formed; each scattering angle corresponds reciprocally with a periodic spacing in the specimen or, in other words, is proportional to a spatial frequency $\mathbf{k}$ of the specimen. The amplitude distribution of the electron wave in the focal plane is the Fourier transform $F(\mathbf{k})$ of the specimen transparancy $f(\mathbf{x})$. The wave aberration function describes the phase shifts of the electrons due to the objective lens as a function of the scattering angle and includes the effect of the defocus, the astigmatism and of the spherical aberration. This phase shift can be described as an exponential phase factor applied to the complex distribution of the electron wave in the focal plane. The image amplitude is then the inverse Fourier transform of this modified Fourier transform, in which the influences of the objective aperture, the illumination divergence and the energy spread of the electron gun (defocus spread) are in-

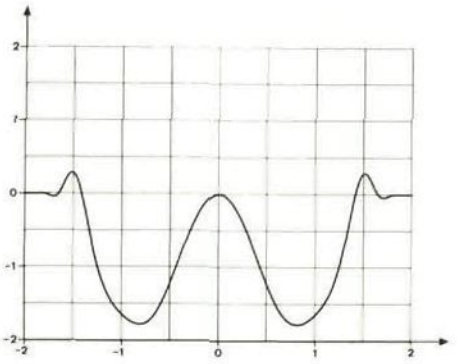

Fig.4 The phase contrast transfer function for axial illumination, without astigmatism, and in Scherzer defocus. The spatial frequencies are given in reduced coordinates (Glaser).

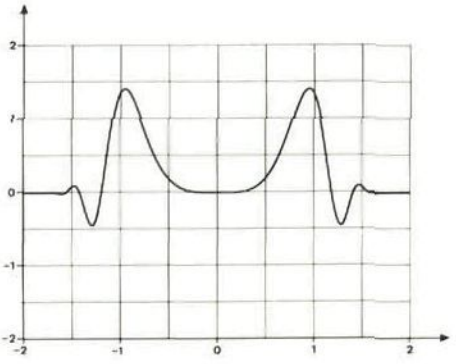

Fig.5 The phase contrast transfer function for axial illumination, without astigmatism and in focus. The spatial frequencies are given in reduced coordinates (Glaser).

cluded. The result may be expressed in terms of a contrast transfer function for the different spatial frequencies. This transfer function is important because it characterizes the effect of the instrument on image formation, independent of the particular specimen in question, see fig.4. The *full expression of the phase contrast transfer* function (PCTF) is written as

$$\Gamma(\mathbf{k}) = i[e(\mathbf{k}_0+\mathbf{k})e^{-i[\chi(\mathbf{k}_0+\mathbf{k})-\chi(\mathbf{k}_0)]} - e(\mathbf{k}_0-\mathbf{k})e^{i[\chi(\mathbf{k}_0-\mathbf{k})-\chi(\mathbf{k}_0)]}] \quad (1)$$

with $e(\mathbf{k})$ the envelope function modelling beam divergence and defocus spread, $\chi(\mathbf{k})$ the wave aberration function of the objective lens

$$\chi(\mathbf{k}) = \pi[0.5k^4-(D-0.5A)k^2-A(\mathbf{k}.\mathbf{a})^2] \quad (2)$$

with the spatial frequency $\mathbf{k}$ (linear with the scattering angle) expressed in Gl^{-1} with 1 Gl $= (C_s\lambda^3)^{0.25}$ and the beam tilt $\mathbf{k}_0$), C_s the constant of spherical aberration, λ the wavelength of the electrons, D the defocus expressed in Sch with 1 Sch $= (C_s\lambda)^{0.5}$, the astigmatism $\mathbf{a}A$ with A the amount of astigmatism and $\mathbf{a}$ the azimuthal direction of astigmatism pointing in the direction of maximal *defocus. In this expression of the PCTF,* three-fold astigmatism is assumed to be negligible relative to the other aberrations. The effect of beam divergence and defocus spread is modelled by the envelope function

$$e(\mathbf{k}) = e^{-s^2\nabla|\chi(\mathbf{k})-\chi(\mathbf{k}_0)|^2/4} \cdot e^{-\pi^2d^2[k^2-k_0^2]^2/2} \quad (3)$$

with the gradient of the wave aberration function given by

$$\nabla\chi(\mathbf{k}) = 2\pi\{[k^2-(D-0.5A)]\mathbf{k}-A(\mathbf{k}.\mathbf{a})\mathbf{a}\} \quad (4)$$

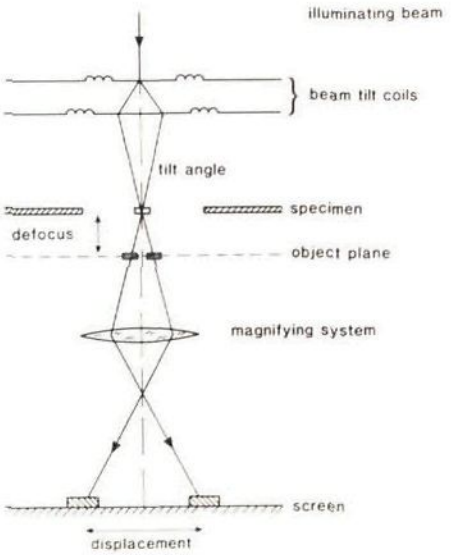

Fig.6 The principle of autotuning: measurement of an image displacement after inducing a beam tilt. An illustration of the effect on beam tilt an an image is given on the right: an image of latex particle (0.22 μm diameter) is displaced when the beam is tilted.

where s is the rms value of the beam divergence and d the rms of the defocus spread caused by both energy spread and objective lens variations. The optimum imaging condition in bright-field occurs at the Scherzer defocus ($D=(C_S\lambda)^{0.5}$) for which a broad band of spatial frequencies is imaged with positive phase contrast. This band has an upper limit which is often used to define a limit to resolution (point resolution), which is about 0.2 nm for a TEM operated at 100 kV and a spherical aberration of 1 mm. Narrow bands of higher spatial frequencies can be imaged if the image is not blurred by the energy spread of the electrons or the beam divergence of the illumination beam. These effects limit the resolution of todays microscopes to 0.1-0.3 nm (information resolution), see fig.5.

The resolution can be increased by lowering the spherical aberration of the objective lens by new designs. However, a substantial decrease of the spherical aberration is not to be expected, as the space available for manipulation (tilt) of the the specimen is very limited. Attempts were made to compensate for the spherical aberration of the objective lens by means of multipoles, but none has so far been successfully applied to routine high- resolution microscopy. Another approach is to decrease the wavelength of the electrons by increasing the accelerating voltage of the TEM. Unfortunately, the specimen damage increases with the accelerating voltage (knock-on damage). In practice the optimum accelerating voltage, as a compromise between these effects, has been found to be

200-300 keV. Furthermore, the resolution can be enhanced by not using a thermionic cathode as electron gun, but a field emission gun instead. The latter is brighter and has a lower energy spread.

However, some of these limitations on resolution can be compensated by applying a posteriori spatial-frequency filtering by digital computations. Several methods were proposed to reverse the phase in regions where the sign of the transfer function is wrong and to flatten the transfer function by amplitude filtering. Nevertheless, these (a posteriori) methods cannot restore information lost at gaps in the transfer function, unless a more complicated type of processing is applied. New techniques to enhance the resolution of the images recorded might become available if the TEM can be controlled very accurately, as discussed in chapter 6.

An obstacle in obtaining high resolution images of organic material is radiation damage, caused by ionisation and subsequent breakage of chemical bonds and by a loss of mass. The radiation damage depends on the electron dose incident on the specimen. Most amino-acid molecules are destroyed at a dose of about 500 electrons per nm^2, while the amount needed to record an image virtually free of statistical noise at high magnifications is about 50.000 electrons per nm^2. The dose incident on the specimen while tuning the microscope manually will exceed even this dose, many times.

The purpose of the autotuning method is to estimate and correct the TEM parameters from images formed with a dose far less than the dose needed by a human operator. Such an autotuning method may even need a lower dose for tuning the TEM parameters than that needed to record an image virtually free of statistical noise. Autotuning may thus increase considerably the number of meaningful micrographs that can be obtained from a sensitive object.

1.4 The tuning of the TEM parameters

The beam tilt misalignment, defocus and astigmatism are tuned by adjusting the currents through the deflection coils above the objective lens, the current through the objective lens coils and the currents through the objective lens stigmator. This tuning is done by adjusting those currents while observing the specimen image on the fluorescent screen. First of all, to minimize the chromatic rotation errors, the area of the specimen that is imaged has to be positioned on the axis of the objective lens (the so called image centering). The image centering is sometimes mechanically prealigned determined by the manufacturing process of the TEM. Secondly, the illumination beam tilt needs to be adjusted in such a way that the effect of spherical aberration of the objective lens is symmetric to the primary beam. We refer to this alignment as the coma-free alignment. Thirdly, the focus has to be adjusted, followed by the correction of astigmatism (after centering the stigmator). Next, some manual procedures for tuning the TEM will be given.

First, at low magnifications, a rough setting of focus is obtained using the so called wobbler: a dual image, the one

slightly shifted with respect to the other, will be seen when the illumination beam is continuously switched between two opposite tilt angles while the TEM is out of focus, see fig.6. The focus is adjusted until the two shifted images coincide. Next, a rough setting of alignment is obtained by varying the objective lens current (or the high tension). On the screen an image rotation will be observed. By changing the beam tilt angle, the centre of rotation can be positioned on the centre of the screen, and thus on the centre of the projector lens system. The astigmatism of the objective lens can now be corrected by adjusting the strength

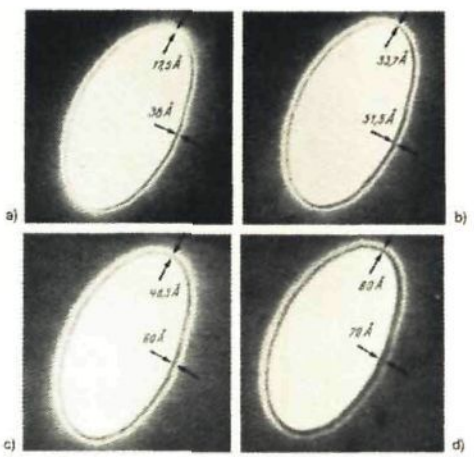

Fig.7 Focal series of an elliptical hole in a carbon foil, showing the asymmetry in distances of the first Fresnel fringe with defocus values of (a) 0.8 μm, (b) 2.85 μm, (c) 6.75 μm and (d) 8.85 μm. From the asymmetry the astigmatism can be estimated (from: Reimer [8]).

of the objective lens stigmator to obtain a symmetrical fresnel fringe on the screen (fig.7). For a more accurate setting of the TEM parameters, first the electron optical magnification has to be increased to a few hundred thousand. Then the following procedures may be carried out.

The defocus and astigmatism can be corrected by observing the structure (texture) of a thin amorphous carbon film. At a sharply defined setting, minimum image contrast is visible (focus). Underfocusing the objective lens by a few nm should show the granular carbon film structure without a preferential direction evident in the pattern (corrected astigmatism). This procedure for a high accuracy in tuning the TEM requires considerable expertise.

Prior to the correction of the defocus and astigmatism, the misalignment must be corrected. When the TEM is not aligned on the coma-free axis, it is not possible to distinguish between the effect of misalignment and that of the astigmatism in the image, by observing the texture of the image on screen (or by observing the digital diffraction pattern of the image). Compensation of misalignment by introducing more astigmatism may then be mistaken for the correction of astigmatism.

A procedure to align the TEM coma-free is by observing the granularity of an amorphous film, while tilting the illuminating beam in two opposite directions and over different azimuthal angles. The beam is aligned coma- free, when the granularity of the image is similar for the opposite beam tilt angles.

As stated previously, the dose needed for tuning the TEM and recording an image (free of statistical noise) exceeds, in general, the dose leading to a complete

destruction of the structures of interest to the microscopist. Therefore, a number of special low dose techniques have been developed.

An example of such a technique is to tune the TEM using images of an another area in the specimen than the area of interest. For the recording of the area of interest the deflection coils above and underneath the objective lens are adjusted in such a way that this area is only irradiated for the final recording of the image, and not for tuning. Some drawbacks of this technique are that the defocus and astigmatism may be different from those in the area which was used to tune the TEM, and that in the area which is recorded no structures of interest may be present (it is a blind recording).

Another technique may be applied if a large number of identical structures is imaged. The signal-to-noise ratio of such a structure can be enhanced by averaging many (thousands) of those structures with the help of a computer system (off-line). For many specimens this is the only available method to obtain information of the structure by means of electron microscopy. The reproducibility in tuning the TEM parameters, for each image prior to the recording, limits the applicability of these reconstruction techniques.

1.5 Autotuning of a TEM - historical overview

As is evident from the previous sections, it is important to tune a TEM accurately using a minimum electron dose. Consequently, much research has been done in the last few decades to realize a practical automatic system for the correction of the TEM parameters. Unfortunately, for theoretical and instrumental reasons, this has not been a trivial task.

In general, the high resolution image of a specimen of a known structure, with an arbitrary orientation and thickness, cannot be expressed in a simple, explicit mathematical model. Only for thin specimens, the relation between the setting of the TEM parameters and the image is less complicated. For weak phase objects (thin specimens which influence the phase of the electron wave only slightly and not its amplitude), the image formation can be described with the phase contrast transfer function (PCTF). The PCTF acts as a complex linear filter. The image contrast $C(\mathbf{x})$ of a weak phase object is given with

$$C(\mathbf{x}) = F^{-1}(\eta(\mathbf{k})\Gamma(\mathbf{k})) \qquad (5)$$

where $\mathbf{x}$ is the spatial coordinate scaled to the object plane, η the Fourier transform of the phase variation of the electron wave function emerging from the specimen, Γ the phase contrast transfer function (PCTF), and F^{-1} denotes the inverse Fourier transform. The image contrast distribution is defined as $C(\mathbf{x}) = (I(\mathbf{x})-I_a)/I_a$, where I_a is the average intensity of the image $I(\mathbf{x})$ over $\mathbf{x}$ (all dimensions scaled to the specimen).

In this work we restrict ourselves to those specimens which can be described as weak phase objects. This restriction is sufficient for high resolution electron microscopy if the material of interest is

positioned on a thin amorphous film, which is, generally, the case.

The realization of an autotuning system is also hampered for instrumental reasons. For instance, only in the last few years TEMs are available with computer control facilities. Before 1985, it was necessary to design and build an interface between the TEM and a computer, prior to any autotuning experiments. A large number of papers on interfacing a TEM to a computer were published, see, for instance [11-18]. The resolution and sensitivity of the commercially available image pick-up devices limit the applicability of an autotuning system. Research has also been done to improve the on-line image recording devices for TEM, see, for instance, [19-22].

Two main approaches to develop an autotuning system, in spite of the instrumental limitations, can be found in literature [23-42]. Next a short description of some of the proposed autotuning methods is given.

The first approach was to design the tuning method in such way that only a small set of input data was needed to estimate the TEM parameters. Koops and Walter [27] estimated the TEM parameters from images of a very special specimen: a specimen with a small hole. The position of the hole on the screen, measured as a function of the induced beam tilt angle, could be used to estimate the TEM parameters. The position of the hole was found by scanning the image over a single-element detector. The TEM parameters were computed from about 200 measured coordinates. The method corrected the TEM aberrations in 35 minutes with high accuracy, but was not generally applicable, as it requires a very special type of specimen. In 1980 Le Poole and de Groot [28] proposed a method to estimate the direction of an image displacement when the illuminating beam is tilted. Three arrays of detector elements were used as input device. The measured intensities of all elements were combined in an ingeneous way (in hardware) to estimate the direction of displacement. In an iterative way a change of in the direction of image displacement was found. The method worked, but hardware problems arose related to the synchronism of the scanning of the array elements. Van der Mast [29] proposed in 1984 to measure the amount of image displacement. In a preliminary set-up two one-dimensional images were recordeds, each formed at an opposite beam tilt angle. The defocus is linearly related to the image displacement and was corrected. The primary investigations were successful, but only at low magnifications. It was also necessary to implement astigmatism and misalignment correction procedures based on the same method.

The other approach to minimize the restrictions due to the instrumenation, was more dose efficient, see [31-42]. It was recognised that for a practical system the whole image has to be used for autotuning. For this approach a video camera was selected as the most suitable image pickup device.

Until 1985, the main problem with this approach was that a quarter of a million pixels are to be processed by an eight bit (or later sixteen bit) processor with a very

limited amount of memory (64 kByte). The solution to this problem was to build special hardware to extract from a series of measured images a (small) set of data to be used for tuning. To limit the problems related to the design of the hardware, simple algorithms were used for the tuning procedures.

Since 1979, work has been reported on autotuning procedures based on measuring the image variance, see Krivanek et al., Smith et al., Saxton et al., Erasmus and Smith [37-41]. The image variance depends on the setting of the defocus, astigmatism and beam tilt angle. The image has minimum image variance when the TEM is well aligned, focused and the astigmatism corrected, see fig. 8. The procedure is automatized by calculating the image variance as a function of the beam tilt angle, defocus and astigmatism. From a series of measured image variance values, the correct setting of the currents through the lenses and coils is found. This method is the only method which was found to work in practical situations for high resolution electron microscopy. Note, however, that this is an iterative method which compresses the information of a whole image into one number (the image variance). Consequently, the method is not dose efficient and not suitable for specimens which are dose sensitive. Five years ago, the method could tune a TEM within minutes. Nowadays, with faster hardware, the tuning is done in about 10 s, and with a high accuracy (2 nm defocus, 0.1 mrad alignment).

In the last few years, with the increasing computational power, more autotuning methods have been proposed. Most of these methods do not differ, basically, from the methods used for manual control and are used as tuning aid for the operator.

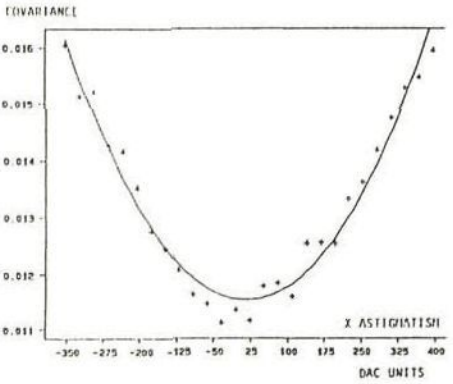

Fig.8 Covariance curve as a function of astigmatism taken with a JEM-4000EX (400 keV; 500,000 magnification; 4 A/cm^2) using a thin carbon film test sample (from: D.J. Smith et al. [14]).

Nowadays, the diffractogram of the image (modulus of the Fourier transform of the image) can be calculated and displayed within seconds. The diffractogram can be used as (manual) tuning aid, because it gives an impression of the amount of defocus and astigmatism in the TEM [35]. When no misalignment is present, the astigmatism can be corrected with the stigmator controls until the diffractogram becomes circular.

It is not often recognized that the TEM has to be aligned on a coma-free axis, before the correction of the astigmatism and defocus by observing the granularity or the diffractogram of the image. From one diffractogram it is not possible to derive the misalignment. If more than one diffractogram is used,

under different imaging conditions, the misalignment can also be derived. An elegant aid for aligning the TEM on a coma-free axis is by calculating a number of diffractograms as a function of the azimuthal angle of beam tilt. The diffractogram is the same for opposite beam tilt angles when the TEM is aligned on a coma-free axis. For some papers using the diffractograms of images to tune the TEM, see Zemlin, Kubler and Waser, Kunath et al., Typke and Kostler, Baba et al., and fig.9.

The diffractogram based methods are, in principle, not suitable for full automatic instrumental adjustment as the shape of the diffractograms is not specimen independent. Furthermore, the realization of an autotuning method which 'recognizes' the shape of the diffractogram (as used for the coma-free alignment procedure) will be difficult.

All the autotuning methods described in the previous section did not meet the requirements for radiation sensitive material: accuracy in tuning the TEM with minimum electron dose. The method discussed in the remainder of this work is based on measuring the effect of a beam tilt on an image and meets these demands.

1.6 Autotuning of a TEM - the research in Delft

The autotuning method described in this work is based on measuring the effect of a beam tilt on the image. The autotuning method is independent of the type of specimen if the image contrast can be described as small angle scattering contrast or (weak) phase contrast. The method tunes the misalignment, defocus and astigmatism in one step from measured image displacements, and is therefore a non-iterative method. The method is suitable for low dose electron microscopy, and was extended to high resolution electron microscopy.

In 1984, the so called 'autotuning project' started in Delft, with as its main

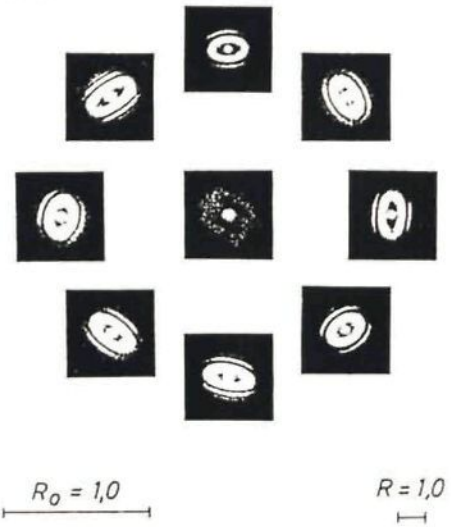

Fig.9 Diffractogram tableau after aligning the microscope onto the coma-free axis. Tilt angle 10 mrad (from: F.Zemlin et al. [13]).

goal the realization of an experimental set-up for the automatic tuning of a TEM. Several internal reports, master theses and papers were published on these activities [42-55]. For an overview of the autotuning method, its theory and its present experimental set-up in Delft, we refer to chapter 5. The basic idea of this research was that the autotuning method should be designed to be as accurate as possible. Consequently, the first step was to find, theoretically, the

relation between the achievable precision in tuning the TEM as a function of the instrumental specifications. The tool we used to find this relation is the minimum variance bound (MVB), also known as the Cramér and Rao Lower Bound on the variance (CRLB). This is a measure for the minimum variance of any unbiased estimator. For the estimation of image displacement D, the MVB is given by (see chapter 2 and 4),

$$\sigma_D^2 \geq 2\pi[L \int_{-k_h}^{k_h} \frac{SNR^2(\mathbf{k})}{1+2SNR(\mathbf{k})} k^2 d\mathbf{k}]^{-1} \quad (6)$$

where SNR(**k**) is the signal-to-noise ratio defined by

$$SNR(\mathbf{k}) = S_s(\mathbf{k})/S_n(\mathbf{k}) \quad (7)$$

with $\mathbf{k}_h$ the highest frequency present in the image C(**x**), L the area of the image, S_s (**k**) the power spectrum of the image C(**x**), S_n(**k**) the power spectrum of the noise in the image and σ_D^2 the variance in estimating D. The expression shows that the SNR(**k**) is important at high spatial frequencies. When the SNR(**k**) is large for high frequencies the MVB will be small. When the SNR(**k**) is small, the MVB will be largee and the tuning imprecise. The characteristics of the TEM and measuring set-up influence the SNR(**k**). With this expression the relation between tuning precision and instrumental specifications is found (chapter 2 and 3). Next, a specific estimator was designed to achieve this precision in tuning the TEM (chapter 4 and 5). After testing the autotuning method in simulations, the method was implemented (chapter 5).

In 1985, the measuring system consisted of a Philips EM 420 TEM (not equipped with facilities for external control) and a transmission detector (a single-detector). An image was measured (serially) by scanning the image over the single-detector element using the deflection coils underneath the objective lens. The computer connected to the transmission detector and the TEM, was based on a Motorola 6809 processor with 64 kB random access memory (RAM). For computational reasons the image size was restricted to about 256 datapoints.

The first experiments showed that autofocusing was possible with this measuring set-up, and took about 10 s. The linear relation between the image displacement and defocus was used to estimate the defocus. The method worked at low magnification ($<20{,}000$), if no astigmatism or misalignment was present.

In 1985/1986 the system was upgraded. The single-detector element was replaced by a video camera. The camera was connected to an image processing system (Crystal). The Crystal system could contain two images of 512^2 pixels and process the images within a fraction of a second in a pre-defined way (for instance, accumulation of images and contrast enhancement). For non pre-programmed processing it was necessary to transport the image (or parts of it) to

an external computer. This computer was a DEC PDP 11/23 with 256 kByte of RAM and a 10 Mbyte hard disc. It also controlled the defocus, astigmatism and misalignment of the Philips EM 420 TEM.

Meanwhile, the estimator of the TEM parameters was extendend from estimating only the defocus from two one-dimensional images, to the correction of defocus, astigmatism and misalignment from a number of two-dimensional images. From the theory it was derived that the effect of beam tilt is a mere image displacement **d**, given by

$$\mathbf{d} = \{-|\mathbf{t}+\mathbf{m}|^2 + (D\text{-}0.5A)\}(\mathbf{t}+\mathbf{m}) + A((\mathbf{t}+\mathbf{m}).\mathbf{a})\mathbf{a} \qquad (8)$$

provided that the highest spatial frequency $|\mathbf{k}|$ in the image is lower than $|-|\mathbf{t}+\mathbf{m}|^2 + (D\text{-}0.5A)|^{0.5}$ to ensure that the effect of image blurring due to the spherical aberration of the objective lens is smaller than the image displacement due to defocus D, astigmatism A**a** and/or misalignment **m**, with the induced beam tilt represented by **t**. The TEM parameters are given in the normalised units Sch and Gl.

Some remarks can be made on the relation between image displacement and beam tilt. Firstly, from (8) it is clear that the direction of the induced beam tilt (**t**) is, in general, not equal to the direction of image displacement (**d**). They are equal only if no astigmatism and misalignment is present (so there is only defocus). Therefore, the parameters **m**, D, A and **a** can only be estimated if more than one image displacement is measured. Secondly, to suppress the blurring effect due to the spherical aberration, the highest spatial frequency in the image must be lower than the limit mentioned. This can be effected by applying a low pass (digital) filter to the image.

The TEM parameters are estimated using (8) from six measured image displacements, and is described in chapter 5.

The system worked in 1986/1987, but its speed and accuracy was limited by the instrumentation. The transport of the images from Crystal to the DEC took 9 s. The available RAM (256 kByte), and the processing speed, were not sufficient for the processing of two-dimensonal images (one image of 512^2 pixels of 8 bit is 256 kByte). The set-up corrected the defocus in 5 s, using a few hundred data points and at low magnifications (< 20,000), but was too slow and limited to continue the development of the tuning algorithms.

So, in 1987 and 1988 the system was upgraded to its present configuration. The Crystal was replaced by a larger computer system (TVDIPS), based on a Motorola 68020 processor. This sytem has 5 Mbyte of RAM, a 80 Mbyte harddisc and special hardware for the Fourier transforms (16 bit integer arithmetic) of images and for image accumulation. With the present system the defocus can be corrected with 5 nm accuracy, the astigmatism with 10 nm and the beam tilt with 0.1 mrad. The system works fast and reliable: 6.5 s to correct the defocus and the astigmatism and 7.5 s to align the TEM.

We stress that the autotuning method and its realization is continuously refined

and adapted to the state of the art in TEMs and computers connected to it. Presently, the autotuning method is implemented on several computer controllable TEMs to continue its development so that it will be applicable and useful in practical research in the field of electron microscopy. In Delft, the system is, again, enhanced. The integer Fourier processor will be replaced by an 80 Mflop floating point array processor, and the DEC PDP 11/23 will be replaced with an IBM PC to control also the magnification and deflection coils underneath the objective lens.

1.7 Outline of the dissertation

The autotuning method selected and described in the remainder of this report, is based on inducing a beam tilt and measuring its effect on the specimen image. In chapter 2, a theoretical study is presented on the potential of this method for automatic focusing. The achievable accuracy in estimating the defocus is calculated as a function of the noise and other parameters of importance. The final conclusion of this study is that the potential is impressive: 5 nm accuracy in focusing using only 6500 electrons per nm^2.

Next, the potential of the beam tilt method is compared to another autotuning method based on measuring the image variance (chapter 3). The conclusion is that the beam tilt method requires, under realistic measuring conditions, about 30 times less dose for the same accuracy.

In chapter 4, the possibility to include the correction of the astigmatism and the beam tilt misalignment is studied, again using the method based on measuring image displacements. The method is tested in simulations of TEM, specimen and measuring set-up. The result of this study is an overview of the instrumental requirements, including the accuracy which can be expected in tuning the defocus, astigmatism and beam tilt misalignment under various measuring conditions.

In chapter 5, the implementation of the autotuning is discussed. The measuring set-up, the measured accuracy and speed and the latest developments in automatic control of a TEM are described.

Finally, chapter 6 is intended for those interested in future developments concerning the automatic control of transmission electron microscopes, and possible applications.

References

Textbooks on parameter estimation and signal processing

[1] Papoulis A. (1965). Probability, Random variables and Stochastic Processes. New York: McGraw Hill.

[2] Federov, V.V. (1972). Theory of Optimal Experiments. New York: Academic Press.

[3] Priestley M.B. (1981). Spectral Analysis and Time Series. New York: Academic Press.

[4] Bos A. van den (1982). Parameter Estimation - (Handbook of Measurement Science). Chapter 8. New York: Wiley.

Textbooks on transmission electron microscopy

[5] Hawkes P.W. (1972). Electron Optics and Electron Microscopy. London: Taylor&Francis.

[6] Misell D.L. (1978). Image Analysis, Enhancement and Interpretation. Amsterdam: North-Holland.

[7] Saxton W.O. (1978). Computer Techniques for Image Processing in Electron Microscopy. New York: Academic.

[8] Cowley J.M. (1981). Diffraction Physics. Amsterdam: North-Holland.

[9] Spence J.H. (1981). Experimental High-Resolution Electron Microscopy. Oxford: Clarendon Press.

[10] Reimer L. (1984). Transmission Electron Microscopy. Berlin: Springer-Verlag.

Papers on interfacing a computer to a TEM

[11] Rez, P. and Williams D.B. (1982). Electron microscope/computer interactions: a general introduction. Ultramicroscopy 8, p. 247.

[12] McCarthy, J.J., Fisher R.M. and Lee, R.J. (1982). Applications of computers in electron microscopy. Ultramicroscopy 8, p. 351.

[13] Atkin P., Erasmus S.J. and Smith K.C.A. (1982). Automatic correction of image drift in the HREM. Proc. 10th Int. Cong. EM (Hamburg, Federal Republic of Germany) 1, p.525.

[14] Boyes E.D., Muggridge B.J. and Goringe M.J. (1982). On-line image processing in high resolution electron microscopy. J. of Microscopy, Vol. 127, Pt. 3, p. 321.

[15] Jones J.C. (1984). High resolution electron microscopy in association with interactive computing. Journal of materials science 19, p. 533.

[16] Krakow, W. (1985). Applications of real-time image processing for electron microscopy. Ultramicroscopy 18, p. 197.

[17] Kokubo Y., Suzuki K., Mori S., Suzumi J., Taira M. and Skarnulis A.J. (1986). An electron microscope controlled by an external computer. Proc 11th Int. Cong. on Electron Microscopy (Kyoto, Japan), p. 497.

[18] Smith K.C.A., Smith T. and C.J.D. Catto. (1986). An integrated image processing system based on a personal computer. Proc. 11th Int. Cong. on Electron Microscopy (Kyoto, Japan), p. 483.

Papers on the development of an image pick-up device adequate for TEM

[19] Spence, J.C.H. and Bleha W.P. (1980). A real-time optical image projection system for electron microscopy. Journal of Microscopy, Vol. 120, Pt. 3, p. 1.

[20] Catto C.J.D., Smith K.C.A., Nixon W.C., Erasmus S.J. and Smith D.J. (1981). An image pickup and display system for the Cambridge University HREM. Inst. Phys. Conf. Ser. No. 61, p. 123.

[21] Kraus B., Krivanek O.L., Swann N.T., Ahn C.C. and Swann P.R. (1986). Performance of newvicon and CCD real-time EM observations systems. Proc. 11th Int. Cong. on Electron Microscopy (Kyoto, Japan), p. 455.

[22] Matsuura S., Hino T., Oba K. and Horiuchi S. (1986). Development of high sensitive imaging device for TEM. Proc. 11th Int. Cong. on Electron Microscopy (Kyoto, Japan), p. 441.

Papers on autotuning - beam tilt induced image displacements

[23] LePoole J.B. (1947). A new electron microscope with contnuously variable magnification. Philips Tech. Rev. 2, p.33.

[24] Curling, C.D., Deeley E.M and Temple J.A. (1969). Focusing aid for an electron microscope. Proc. IEE, Vol. 116, No. 3, p. 334.

[25] Frank J. (1975). Controlled focusing and stigmating in the conventional and scanning electron microscope. Journal of Physics E, Vol. 8, p.582.

[26] Guckenberger, R. and Hoppe W. (1978). On-line electron-optical correlation computing in the CTEM. Proc. 9th Int. Cong.EM (Toronto, Canada) 1, p. 88.

[27] Koops H. and Walter G. (1980). Automated compensation of lens aberrations, a simulation. Proc. 7th Eur. Cong. EM (The Hague, The Netherlands) 1, p.40.

[28] LePoole J.B. and Groot L.E.M. de (1980). Low intensity focusing. Proc. 7th Eur. Cong. EM (The Hague, The Netherlands) 1, p. 644.

[29] Mast K.D. van der (1984). Transmission electron microscopy: state of the art and future developments, Proc.8th Eur. Cong. EM (Budapest, Hungary) 1, p.3.

[30] Nomura S. and Isakozawa S. (1987). Autofocusing of CTEM using parallax. J. Electron Microsc., Vol. 36, No. 4, p. 157.

Papers on autotuning - diffractogram based methods

[31] Kubler O. and Waser R. (1973). A light-optical diffractometer for electron microscopical images operating on-line. Optik 37, Vol. 4, p. 425.

[32] Typke D. and Kostler D. (1977). Determination of the wave aberration of electron lenses from superposition diffractograms of images with differently tilted illumination. Ultramicroscopy 2, p.285.

[33] Zemlin F., Weiss K., Schiske P., Kunath W. and Herrmann K.-H (1978). Coma-free alignment of high resolution electron microscopes with the aid of optical diffractograms. Ultramicroscopy 3, p.49.

[34] Zemlin F. (1979). A practical procedure for alignment of a high resolution electron microscope. Ultramicroscopy 4, p. 241.

[35] Baba N., Oho E. and Kanaya K. (1987). An algorithm for on-line digital image processing for assisting automatic focusing and astigmatism correction in Electron Microscopy. Scanning Microscopy, vol. 1, No. 4, p.1507.

[36] Kunath W., Zemlin F. and Weiss K. (1987). Refinement procedures for high-resolution electron microscopy. Optik 76, No. 4, p. 122.

Papers on autotuning - image variance based methods

[37] Krivanek O.L., Isoda S. and Kobayashi K. (1977). Accurate stigmating of a high voltage electron microscope. Journal of Microscopy, Vol. 111, Pt. 3, p. 279.

[38] Erasmus S.J. and Smith K.C.A. (1982). An automatic focusing and astigmatism correction system for the SEM and CTEM. Journal of Microscopy, Vol. 127, Pt. 2, p. 185.

[39] Saxton W.O., Smith D.J., O'Keefe M.A., Wood G. and Stobbs W.M. (1983). Procedures for focusing, stigmating and alignment in high resolution electron microscopy. Journal of Microscopy 130, Part 2, p. 187.

[40] Smith D.J., Saxton W.O., O'Keefe M.A., Wood G. and Stobbs W.M. (1983). The importance of beam alignment and crystal tilt in high resolution electron microscopy. Ultramicroscopy 11, p. 263.

[41] Smith D.J., Higgs A. and Perkes P. (1987). Practical experience with computer-controlled high-resolution electron microscopy. Proc. 45th Annual Meeting EMSA (San Francisco, USA), p.62.

Internal reports and master theses on the autotuning of a TEM

[42] Bakker J.G. (1984). Automatic focusing in a transmission electron microscope. Master thesis, University of Technology Delft, Delft, The Netherlands.

[43] Koster A.J. (1985). Haalbare precisie bij autofocusing van een transmissie electron microscoop. Master thesis, University of Delft, Delft, Netherlands.

[44] Swaan R. (1986). Automatic objective lens alignment in a transmission electron microscope. Master thesis, University of Technology, Delft, Delft, The Netherlands.

[45] Heesterbeek L.T.M. (1987). Automatizing a transmission electron microscope - measuring an image shift. Master thesis, University of Technology Delft, Delft, The Netherlands.

[46] Ruijter W.J. de (1988). Autotuning a transmission electron microscope for low dose and high resolution applications. Master thesis, University of Technology, Delft, Delft, The Netherlands.

[47] Hoekstra T.S. (1988). Automatic correction of the objective lens misalignment of a transmission electron microscope for low and medium magnifications. Master thesis, University of Technology, Delft, Delft, The Netherlands.

[48] Hoek M. (1988). Automatic correction of the astigmatism and the defocus of a transmission electron microscope for low and medium magnifications. Master thesis, University of Technology, Delft, Delft, The Netherlands.

[49] Vliet L.K. van (1988). Afleiding samenhang defocus, astigmatisme en

misalignment van een transmissie electronenmicroscoop, te gebruiken bij automatische correctie. Master thesis, University of Technology, Delft, Delft, The Netherlands.

Papers on the autotuning of a TEM in Delft

[50] Koster A.J., Bos A. van den, Mast K.D. van der and Kruit P. (1986). Autofocus of a TEM through beam tilt induced image shift - dependence of its precision and speed on TEM characteristics and measuring set-up. Proc. XIth Int. Cong. on Electron Microscopy, Kyoto, p.501.

[51] Koster A.J., Bos A. van den and Mast K.D. van der (1987). An autofocus method for a TEM. Ultramicroscopy 21, p.209.

[52] Koster A.J., Bos A. van den and Mast K.D. van der (1988). Signal Processing for autofocusing by beam tilt induced image displacement. Scanning Microscopy Supplement 2, p.83.

[53] Koster A.J. and Ruijter W.J. de. (1988) Automatic control of a transmission electron microscope for high resolution electron microscopy. Inst. Phys. Conf.Ser. No.93: Vol.1, p. 83.

[54] Koster A.J., Ruijter W.J. de, Bos A. van den and Mast K.D. van der (1989). Autotuning of a TEM using minimum electron dose. Ultramicroscopy 27, p.251.

[55] Koster A.J., Vliet L.K. van, Hoekstra, T.S., Hoek, M., Bos A. van den and Mast K.D. van der. Practical autotuning of a transmission electron microscope. Submitted to Ultramicroscopy.

2 An Autofocus Method for a TEM

1	**Introduction**	**27**
2	**Focusing by measuring beam-tilt-induced image displacement**	**28**
3	**Achievable precision in estimating an image displacement**	**28**
3.1	Model of observations	28
3.2	Minimum variance bound	29
3.3	Signal-to-noise ratio, Poisson noise	29
3.4	Instrumentation noise	31
3.5	Sampling and its influence on the MVB	32
4	**Numerical experiments**	32
4.1	Defocus	33
4.2	Sampling distance	34
4.3	Sensor length	34
4.4	Instrumentation noise	34
4.5	Magnification	36
4.6	Measuring time	36
5	**The BID method as autofocus method**	**36**
6	**Conclusions and discussion**	**37**
	Appendix A. Power spectrum of the image	**37**
	Appendix B. Power spectrum of the Poisson noise in the image	**38**
	References	**39**

Ultramicroscopy 21 (1987) 209–222
North-Holland, Amsterdam

AN AUTOFOCUS METHOD FOR A TEM

A.J. KOSTER, A. VAN DEN BOS and K.D. VAN DER MAST

Department of Applied Physics, Delft University of Technology, Lorentzweg 1, 2628 CJ Delft, The Netherlands

Received 16 October 1986; revised version 4 February 1987

Autofocus and correction of astigmatism of a transmission electron microscope (TEM) based on measuring a beam-tilt-induced image displacement is proposed and its theoretical limitations are studied. Tilting the illumination beam displaces the specimen image on screen when the TEM is out of focus. This displacement has a known relationship with the defocus. Autofocusing is possible by tilting the beam, measuring the image displacement, calculating the defocus and correcting it. Correction of astigmatism is possible by measuring the defocus in different directions. The method is fast because it calculates and corrects the defocus in one step. It works with many types of specimens because it utilizes both the amplitude and phase contrast of a bright field image. The precision of this method depends on the precision of the image displacement estimation. The shifted and unshifted images differ because of shot noise, instrumentation noise, and aberrations caused by the beam tilt. An expression is derived, containing parameters of the TEM and measuring system, for the achievable precision in estimating the displacement. This expression is a tool for optimizing the automatic focussing procedure and the measuring system. It does not depend on any particular estimation method with which the displacement is calculated. Computer simulations for a TEM equipped with a Vidicon videocamera have been carried out. They show that at Scherzer defocus (86 nm) the minimum measuring time required for focussing the TEM with a precision of 5 nm is about 50 ms. The precision is less satisfactory (> 30 nm) when, with the same measuring time, the TEM is far out of focus or very near focus. The precision improves proportionally to the square root of the measuring time.

1. Introduction

Reliably interpretable high-resolution electron micrographs require an accurately focussed, stigmated and aligned transmission electron microscope (TEM). Incorrect objective lens and stigmator currents result in artifacts in the recorded image. Focussing and stigmating a TEM can be time consuming and requires an experienced operator, in the case of low-dose and high-resolution work in particular. The time factor is important since object structures are destroyed by prolonged radiation. A system which automatically focusses, stigmates and aligns a TEM is useful when it is:
(1) as *precise* as or more precise than a human operator;
(2) as *fast* as or faster than a human operator;
(3) *efficient*, in the sense that it uses the available observations exhaustively;
(4) *reproducible* (as is not the case with human operators);
(5) *applicable with most specimens*;
(6) *suitable to manufacture and to implement* in a TEM at a reasonable cost.

Several methods to automatically focus, stigmate and align a TEM have been proposed [1]. To our knowledge, the only published proposal for automatic focussing which has been tested in practice is based on minimum contrast of the image at focus [2]. Image contrast is measured as a function of the objective lens current. The object is in focus when the image has the lowest contrast. This minimum contrast is used by most microscopists while focussing, as it involves no special equipment. The same method is also applied for alignment of the illuminating beam [3]. Another method is based on the power spectrum of the image (diffractogram) [4]. The position of peaks and zeros in the spectrum make it possible to compute the defocus, astigmatism and misalignment. Unfortunately, there is considerable ambiguity in the imaging conditions which might be

0304-3991/87/$03.50

deduced from a single diffractogram. This limits the practical feasibility of the method.

2. Focussing by measuring beam-tilt-induced image displacement

The method for fast and direct defocus calculation considered in this paper is based on tilting the illuminating electron beam over a known angle, thus producing image displacement on the screen because of the large depth of field due to the very coherent illumination. This beam-tilt-induced image displacement (BID) has a known relationship with the defocus of the TEM [5] and can be used as focussing aid, see fig. 1. Le Poole [6] introduced in 1947 the beam tilt wobbler as a simple focussing aid. Most microscopists use this method for focussing a TEM at lower magnifications. Later LePoole and De Groot [7] proposed a special linear detector to measure the direction of the image displacement. A similar approach was followed by Curling et al. [8] using only one detector. Koops and coworkers [9,10] measured the aberrations of the objective lens with an aplanator. He used a special specimen for his measurements: a specimen with one very small hole, whose position was detected by scanning its image over a single detector.

Van der Mast [11] proposed to measure both magnitude and direction of the image displacement in order to calculate and correct the defocus in one step: the BID method. It uses a multi-element image pick-up system and an algorithm which calculates the image displacement directly, independently of the type of specimen. In the case of a properly aligned system the image displacement D for beam tilt angles $+\beta$ and $-\beta$ (as seen from the specimen) is given by McFarlane [5], and Zemlin et al. [12]

$$D = 2M\beta\left(\Delta f + C_s\beta^2 + C_s\omega^2\frac{2\lambda^2}{4\pi^2}\right), \qquad (1)$$

with M the magnification, Δf the defocus of the TEM, C_s the spherical aberration of the objective lens, λ the wavelength of an accelerated electron and ω the spatial frequency of the specimen ex-

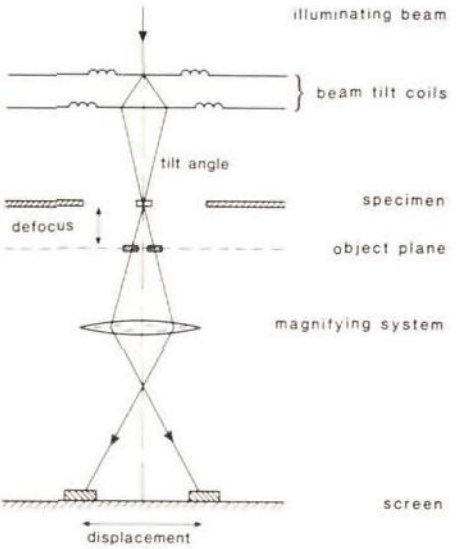

Fig. 1. Image displacement caused by beam tilt.

pressed in rad m^{-1}. For low frequencies and for large tilt angles the frequency-dependent term is negligible. The displacement is then given by:

$$D = 2M\beta(\Delta f + C_s\beta^2). \qquad (2)$$

The BID method is suitable as an autofocussing system when the requirements mentioned in the introduction are met. We will first discuss its precision.

3. Achievable precision in estimating an image displacement

3.1. Model of the observations

The specimen is supposed be imaged with axial, partly coherent illumination and producing phase contrast images. These assumptions are valid for high-resolution electron microscopic images when the beam tilt angle is not too large. Observations are made at the image of the specimen on the fluorescent screen at every point of a given interval of an x-axis. Measurements are done during T

seconds using a rectangular sensor with length Δx and width Δy (scaled to the specimen plane). The width Δy is supposed to be small enough to presume the image measured in the y-direction constant. This is done for simplicity; the theory can be extended to correct for this assumption. Measuring the image with the beam tilted first over an angle β and next over $-\beta$ results in the following observations:

$$r_1(x) = k(x) + n_1(x), \tag{3a}$$

$$r_2(x) = k(x - D) + n_2(x), \tag{3b}$$

with x the position of a sensor along the x-axis, $k(x)$ the image of the specimen, $k(x-D)$ the displaced image over a distance D, and $n_1(x)$ and $n_2(x)$ independent, zero-mean, Poisson-distributed noises with expectation

$$k = \Delta x \, \Delta y \, T\bar{k}, \tag{4}$$

where k is the total number of electrons passing through an area equal to $\Delta x \, \Delta y$ with $\bar{k}$ the number of electrons per second and per square meter (averaged over all sensors). The expectation of the Poisson noise can be considered independent of the coordinate x because of the low contrast in electron microscopic images (0–0.2) at high magnifications. Furthermore, the noise is considered normally distributed as the number of electrons counted per sensor is large with respect to its square root.

This model of the observations (3) is next used to derive an expression for the achievable precision with which the displacement can be estimated irrespective of the estimator used. In statistics the expression derived is called minimum variance bound (MVB) or Cramèr–Rao lower bound (Van den Bos [13]). The MVB is used for two purposes: (1) from it numerical values can be computed for the achievable precision of the measured image displacement; (2) the expression for the MVB shows the dependence of this precision on experimental conditions as defocus, image recording strategy, instrumentation noise and measuring time. This dependence is investigated numerically for various realistic experimental conditions in section 4.

3.2. Minimum variance bound

The minimum variance bound (MVB) is a lower bound on the variance of any unbiased estimator. In this particular case, the MVB of a one-dimensional image displacement has to be derived. This one-dimensional approach makes it possible to treat the problem as a time-delay-estimation problem in passive sonar theory, for which the MVB already has been derived by Carter [14] and is described by the following expression:

$$\sigma_D^2 \geq 2\pi \left[L \int_{-\omega_h}^{\omega_h} \frac{\eta^2(\omega)}{1 + 2\eta(\omega)} \omega^2 \, \mathrm{d}\omega \right]^{-1}, \tag{5}$$

where $\eta(\omega)$ is the signal-to-noise ratio (SNR) defined by

$$\eta(\omega) = S_m(\omega)/S_n(\omega), \tag{6}$$

with ω_h the highest frequency present in the image $k(x)$, L the length of the interval on which observations are made, $S_m(\omega)$ the power spectrum of $k(x)$ and $S_n(\omega)$ the power spectrum of both the noises $n_1(x)$ and $n_2(x)$. The expressions (5) and (6) show the importance of the SNR $\eta(\omega)$ at high frequencies. When the SNR is large for high frequencies the MVB will be small. When the SNR is small for high frequencies the MVB will be large. Characteristics of the TEM and measuring set-up influence $\eta(\omega)$ strongly and are studied in more detail below.

3.3. Signal-to-noise ratio, Poisson noise

In this section the SNR of the measured image is derived as a function of parameters describing the image formation on screen, and parameters describing the measuring system. The image formation at high magnification can be described with the phase contrast transfer function (PCTF). Several PCTFs are described in the literature [15]. A well known PCTF given by Reimer (see Hanszen [16]) includes the effect of partly coherent axial illumination of the specimen and of the energy spread of the electrons:

$$\begin{aligned} H(\omega; a) = & -2 \sin\left[a_1\omega^4 - a_2 \Delta f \omega^2 \right] \\ & \times \exp\left[-\left(a_3 \omega^2 \right)^2 \right] \\ & \times \exp\left[-\left(a_4 \omega^3 - a_5 \, \Delta f \, \omega \right)^2 \theta^2 \right], \end{aligned} \tag{7}$$

with

$$a_1 = \frac{C_s\lambda^3}{32\pi^2}, \quad a_2 = \frac{\lambda}{4\pi}, \quad a_3 = \frac{\lambda H_A}{16\pi(\ln 2)^{1/2}},$$

$$a_4 = \frac{C_s\lambda^2}{8\pi^2(\ln 2)^{1/2}}, \quad a_5 = \frac{1}{\pi(\ln 2)^{1/2}},$$

with θ the angle of the beam seen from the specimen, $a = (a_1 \ldots a_5)$ the vector of specifications of the TEM.

$$H_A = C_c\frac{\Delta V}{V}\left(\frac{1 + E/E_0}{1 + E/2E_0}\right), \tag{7a}$$

with C_c the chromatic aberration, $\Delta V/V$ the stability of the acceleration voltage, E_0 the rest-energy of an electron and E the energy of an accelerated electron. The envelope function of $H(\omega;a)$ related to the chromatic aberration is dominating and is reduced to 1% or less of its maximum value for frequencies higher than:

$$\omega_h = (2/\lambda H_A)^{1/2}. \tag{8}$$

where H_A is described by (7a). Fig. 2 shows the PCTF for the specifications in table 1 and for a defocus of $\Delta f = 2$ Sch.

The relationship between the power spectrum of the image on the screen $S_i(\omega)$ and the power spectrum of the specimen $S_s(\omega)$ is now given by

$$S_i(\omega) = |H(\omega;a)|^2 S_s(\omega). \tag{9}$$

The relationship of the image on the screen $S_i(\omega)$ with the power spectrum of the image measured is (see appendix A):

$$S_m(\omega) = T^2(\Delta x)^2(\Delta y)^2 \operatorname{sinc}^2(\omega\Delta x/2)\, S_i(\omega). \tag{10}$$

where

$$\operatorname{sinc}(p) = \frac{\sin(p)}{p}. \tag{11}$$

In the following it is convenient to normalize $S_s(\omega)$ with respect to the power spectrum on screen $S_m(\omega)$. This is done as follows.

Define the modulation depth as:

$$m = \sigma_k/k. \tag{12}$$

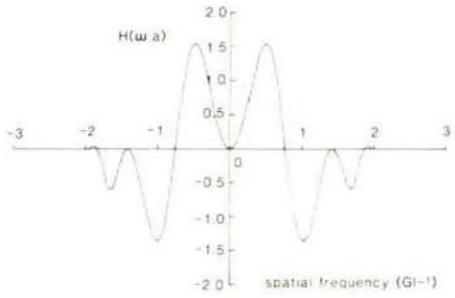

Fig. 2. The phase contrast transfer function. See table 1 for specifications of the TEM. $\Delta f = 2$ Sch.

where σ_k is the standard deviation of number of electrons counted per sensor (standard deviation of the image). Now suppose that at Scherzer defocus ($\Delta f = (C_s\lambda)^{1/2}$), and for a particular specified sensor length Δx_s, m has the value μ. Generally, σ_k must satisfy

$$\sigma_k^2 = \frac{1}{2\pi}\int_{-\infty}^{\infty} S_m(\omega)\, d\omega. \tag{13}$$

Hence, from (3), (9) and (10)

$$m^2 = \frac{1}{2\pi\bar{k}^2}\int_{-\infty}^{\infty} \operatorname{sinc}^2(\omega\Delta x/2)\,|H(\omega;a)|^2 \times S_s(\omega)\, d\omega. \tag{14}$$

Hence, in order to produce a modulation depth $m = \mu$ at Scherzer defocus with $\Delta x = \Delta x_s$, $S_s(\omega)$ must satisfy

$$S_s(\omega) = \mu^2\bar{k}^2 S_{ns}(\omega), \tag{15}$$

Table 1
Microscope parameters and measuring set-up; dimensions are those at specimen level; 1 Sch = 86 nm, 1 Gl = 0.56 nm

Specimen	TEM	Measuring set-up
$\mu = 0.05$	$C_c = 2$ mm	$\Delta x = 0.05$ nm
	$C_s = 2$ mm	$\Delta y = 0.5$ nm
Flat power spectrum	$V = 100$ kV	$L = 0.25$ μm
	$M = 10^5$	
	$\bar{k} = 10^{21}$ electrons m^{-2} s^{-2}	
	$\beta = 5$ mrad	
	$\theta = 1$ mrad	

with

$$\frac{1}{2\pi}\int_{-\omega_h}^{\omega_h} \operatorname{sinc}^2(\omega\,\Delta x_s/2)\,|H(\omega;a)|^2_{\text{Scherzer}} \times S_{ns}(\omega)\,\mathrm{d}\omega = 1, \quad (16)$$

and $S_{ns}(\omega)$ the normalized power spectrum of the specimen.

Of all spectra having the *shape* as $S_s(\omega)$, only one normalized spectrum $S_{ns}(\omega)$ gives rise to the supposed modulation depth μ for the given sensor length Δx, number of electrons counted per sensor k and PCTF $H(\omega;a)$. The power spectrum of the image $k(x)$ is therefore determined by the modulation depth μ of the specimen, the shape of the power spectrum of the specimen $S_s(\omega)$, the PCTF, the illumination $\bar{k}$, the measuring time T and sensor dimensions Δx and Δy.

It is shown in appendix B that the power spectrum of the Poisson noise $n(x)$ is described by:

$$S_{pn}(\omega) = (\bar{k}T)\,(\Delta x)^2\,\Delta y\,\operatorname{sinc}^2(\omega\,\Delta x/2). \quad (17)$$

Clearly the Poisson noise depends on the illumination, measuring time and the dimensions of the sensor.

It follows from (6), (10) and (17) that the SNR $\eta(\omega)$ is described by

$$\eta(\omega) = \mu^2\,(\bar{k}T)\,\Delta y\,|H(\omega;a)|^2\,S_{ns}(\omega). \quad (18)$$

This expression shows that the SNR $\eta(\omega)$ depends on the specimen ($S_s(\omega)$ and μ), the PCTF and measuring strategy ($\bar{k}$, T and Δy). It also shows that, under the assumption that the bandwidth of the specimen is larger than that of the PCTF, the frequency ω_h in (5) may be taken as the frequency at which the PCTF becomes negligible and remains so. Notice that the sensor length Δx is absent in expression (18). It could be concluded that the sensor length is of no importance for the achievable precision! In the next section it will be shown that this is no longer true when instrumentation noise is present in the model of the measured image and a finite number of sensors is used.

3.4. Instrumentation noise

Up to now it has been assumed that there is no instrumentation noise present in the image measured. Of course, in practice, there is always instrumentation noise present as, for instance, digital quantization noise or dark current in a video camera. Suppose there is additive instrumentation noise $n_i(x)$, not correlated with the Poisson noise $n_p(x)$. The total noise in the image can then be modelled by

$$S_n(\omega) = S_{pn}(\omega) + S_{in}(\omega), \quad (19)$$

with $S_{in}(\omega)$ the power spectrum of the instrumentation noise $n_i(x)$. To be able to handle the instrumentation noise in the same way as the Poisson noise, it is assumed that the instrumentation noise is normally distributed and that its power spectrum may be modelled by

$$S_{in}(\omega) = S_{ni}\,\operatorname{sinc}^2(\omega\,\Delta s/2), \quad (20)$$

where the constants S_{ni} and Δs define the intensity and the bandwidth of $S_{in}(\omega)$. To model (approximately) white instrumentation noise before and after sampling, Δs is small compared to Δx, so that $S_{in}(\omega) \approx S_{ni}$ over the bandwidth of PCTF, and band-limited. This finite power spectrum is of importance when (in the next subsection) sampling is introduced. Using (6) and (19), the SNR $\eta_i(\omega)$ is now given by:

$$\eta_i(\omega) = N(\omega)\,\eta_p(\omega), \quad (21)$$

where

$$N(\omega) = S_{pn}(\omega)/\big[S_{in}(\omega) + S_{pn}(\omega)\big], \quad (22)$$

$$\eta_p(\omega) = S_{in}(\omega)/S_{pn}(\omega). \quad (23)$$

Consider the factor $N(\omega)$ in (21); the envelope of $N(\omega)$ is less than 1 and the sensor length affects the function $N(\omega)$ (and so the SNR $\eta_i(\omega)$), but not its envelope, as can be seen in fig. 3. The number of electrons per square meter $\bar{k}T$ relative to S_{ni} and the sensor dimensions Δx and Δy are now also of importance for the MVB, see (17), (20) and (22). The influence of instrumentation noise on the MVB is minimal when the zeros of

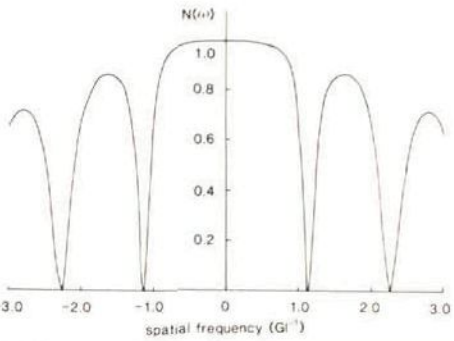

Fig. 3. Influence of instrumentation noise $N(\omega)$ on the SNR. See tables 1 and 2 for specifications of the TEM and measuring set-up. 1 GI = 0.56 nm.

the PCTF coincide as much as possible with the zeros of the function $N(\omega)$.

3.5. Sampling and its influence on the MVB

The image measurements are supposed to be made using a finite number of sensors. This is, in fact, sampling of the image, and it influences the power spectra $S_m(\omega)$ and $S_n(\omega)$. To what extent this is the case is determined by the sampling frequency ω_s, the bandwidth of the spectra, the sensor length and the spectrum of the instrumentation noise. An expression for the relationship of the power spectrum of a process before and after sampling is given in ref. [17]. In terms of $S_m(\omega)$ this relationship yields:

$$S_s'(\omega) = \sum_{n=-\infty}^{\infty} S_m(\omega + n\omega_s), \tag{24}$$

with

$$\omega_s = 2\pi/\Delta\xi, \tag{25}$$

where $S_s'(\omega)$ is the spectrum of $k(x)$ after sampling and $\Delta\xi$ is the sensor distance. The expression for the power spectrum of the sampled version of the Poisson noise is analogous to (24). Substituting (17) into this expression and subsequently applying Poisson's sum formula [17], one can easily show that

$$S_{pn}'(\omega) = \bar{k}T\,\Delta x\,\Delta y\,\Delta\xi\left[1 + 2\sum_{n=1}^{\infty} d_1(n\,\Delta\xi) \times\cos(n\omega\,\Delta\xi)\right], \tag{26a}$$

$$d_1(x) = \begin{cases} 1 - |x|/\Delta x & \text{for } |x| \leqslant \Delta x, \\ 0 & \text{elsewhere.} \end{cases} \tag{26b}$$

When the sampling distance equals the sensor length the sampled power spectrum of the Poisson noise after sampling is flat and given by

$$S_{pn}'(\omega) = k\,\Delta\xi. \tag{27}$$

Similarly, the power spectrum of the sampled instrumentation noise

$$S_{in}'(\omega) = S_{in}\frac{\Delta\xi}{\Delta s}\left[1 + 2\sum_{n=1}^{\infty} d_2(n\,\Delta\xi)\cos(n\omega\,\Delta\xi)\right] \tag{28a}$$

where

$$d_2(x) = \begin{cases} 1 - |x|/\Delta s & \text{for } |x| \leqslant \Delta s, \\ 0 & \text{elsewhere.} \end{cases} \tag{28b}$$

The SNR after sampling is now

$$\eta_i'(\omega) = N'(\omega)\eta_p'(\omega), \tag{29}$$

with

$$\eta_p'(\omega) = S's(\omega)/S_{pn}'(\omega), \tag{30}$$

$$N'(\omega) = S_{pn}'(\omega)/\left[S_{in}'(\omega) + S_{in}'(\omega)\right]. \tag{31}$$

Using formula (5) and substituting $\eta_i'(\omega)$ for $\eta(\omega)$, the influence of the various parameters on the MVB can be studied. A number of such numerical experiments are described in the next section.

4. Numerical experiments

The influence of relevant parameters in the measuring process is not directly clear from (5), (24), (26) and (28). Therefore, numerical experiments have been carried out to study the dependence of the MVB on some of these parameters (defocus, sampling distance, sensor length, instru-

mentation noise, magnification and measuring time, see table 2) in order to ascertain their influence on the precision with which the defocus can be estimated.

Table 1 shows the microscope characteristics and measurement parameters used (the reference conditions). It is supposed that the specimen has a flat power spectrum (up to ω_h or ω_s) and a modulation depth μ of 0.05. The specifications of the TEM are those of a Philips EM 420: $C_c = 2$ mm, $C_s = 2$ mm, stability of the acceleration voltage $\Delta V/V = 10$ ppm. The acceleration voltage is 100 kV. The screen current density is 16 nA m^{-2} (10^{21} electrons m^{-2} s^{-1}). The angle of the beam seen from the specimen is 1 mrad. The defocus is expressed in Sch [18] and in m. For these specifications of the TEM 1 Sch is about 86 nm. The tilt angle is 5 mrad, small enough to allow the use of the expression in Reimer [15] for the PCTF of an axially illuminated specimen. The magnification influences the scaling from screen to specimen level; chosen is 10^5. The measuring set-up simulated is one line of a videocamera with a noise intensity half the Poisson noise intensity for the reference conditions. A pixel of the video image is considered as sensor with dimensions $\Delta x\, \Delta y$. The measuring time is 5 s. The length of the measuring interval is 2.5 cm and the width and length of a pixel on screen of 50 μm.

To make the results easier to interpret, not the MVB for estimation of the displacement is plotted but three times the square root of the corresponding MVB for estimation of the defocus:

$$3\sigma_{\Delta f} = 3(\mathrm{MVB})^{1/2}/(2\beta). \qquad (32)$$

This can be interpreted as the 99.5% confidence level for estimation of the defocus. In what follows (32) will be referred to as precision.

4.1. Defocus

The precision of focussing depends on the image modulation depth (or contrast). Since the latter is a function of the defocus (fig. 4), the precision is a function of the defocus. Fig. 5, calculated from (5) and (32), shows this. Notice the global minimum near Scherzer defocus and the local maximum

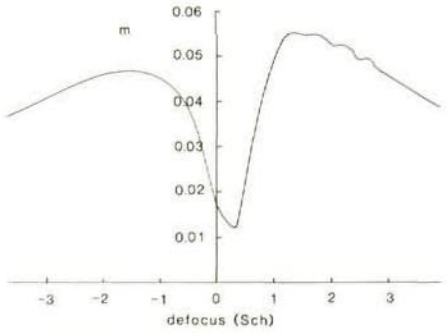

Fig. 4. Modulation depth m of the image on screen as a function of defocus Δf. 1 Sch = 86 nm.

near focus. The figure also shows that if the absolute defocus is less than 1 Sch, or more than 5 Sch, estimates of the defocus may be very imprecise. Then autofocussing the TEM on the basis of image displacement estimates no longer makes sense.

The smallest focus step in a Philips EM 420 is 5 nm. To obtain this accuracy using the BID method a measuring time of more than 5 s is necessary, using only one line of the measured image for calculating the image displacement. When more independent lines are used in calculating the image displacement, the required measuring time decreases proportionally with the square root of the number of lines. The strategy in focussing the

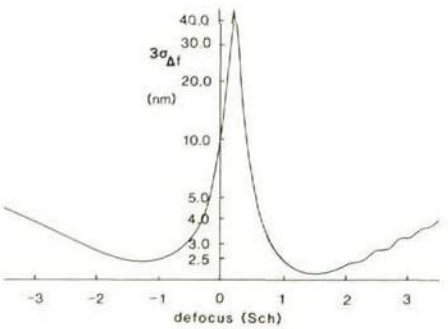

Fig. 5. Precision of the estimation of defocus as a function of defocus. 1 Sch = 86 nm.

TEM can efficiently make use of the relationship between the precision in estimating the defocus and the defocus itself by focussing the TEM in two steps. During the first step the defocus of the TEM is estimated, and the TEM is set at about Scherzer defocus. During the second step the defocus is again estimated and this time the TEM is focussed more precisely.

4.2. Sampling distance

Results related to the sampling distance are presented in fig. 6. The length of the individual sensor elements is set to 0.5 nm. The sampling distance is varied from about one fifth of the sensor length to 5 times the sensor length. When the sampling distance is less than 0.2 nm hardly any new information is gathered, while for sampling distances of more than 1 nm only the phase contrast at low frequencies is used. So a relatively smooth changing of the MVB for both large and small sampling distances is to be expected. A sampling distance of 0.5 nm seems to be optimum under the reference conditions. The smallest sampling distance in a videocamera equals the sensor length, in this case 0.5 nm.

4.3. Sensor length

The sensor length is varied from 0.1 nm up to 3 nm, see fig. 7. This figure shows that the precision in estimating the defocus varies periodically with the sensor length. For very small sensor lengths the SNR is small because of the few electrons

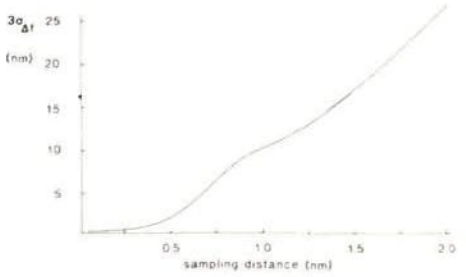

Fig. 6. Precision of the estimation of defocus as a function of sampling distance $\Delta\xi$. Sensor length is 0.5 nm.

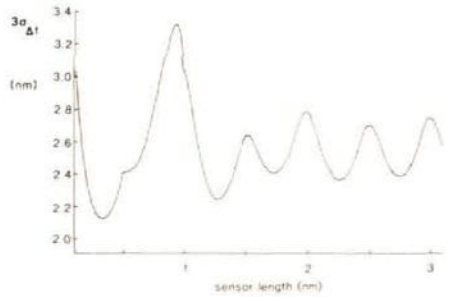

Fig. 7. Precision of the estimation of defocus as a function of sensor length.

counted per sensor. The estimation of the image displacement is therefore imprecise. The peaks in the figure can be understood from (18), (21) and (22): The SNR with respect to the Poisson noise has the same shape as the PCTF (see fig. 8) and the sensor length determines which frequencies of the SNR $\eta(\omega)$ are suppressed by the transfer function $N(\omega)$. The dips in $N(\omega)$ are periodic with Δx (fig. 3), so the MVB will increase (while the SNR decreases) periodically with Δx. By adjusting the sensor length, optimal measuring conditions can be created.

4.4. Instrumentation noise

The influence of the instrumentation noise on the precision is described by (21), (22) and (23)

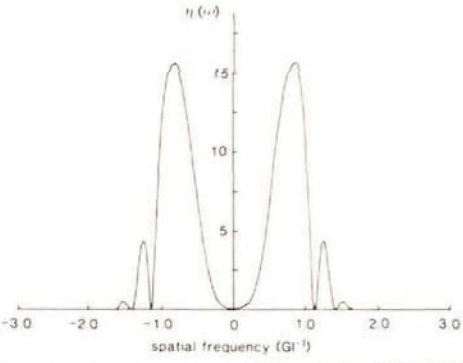

Fig. 8. Signal-to-noise ratio $\eta_i(\omega)$ before sampling. 1 Gl = 0.56 nm.

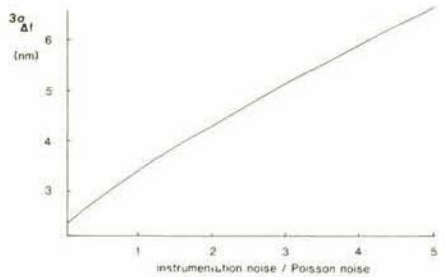

Fig. 9. Precision of the estimation of defocus as a function of the ratio of the Poisson noise to the instrumentation noise.

combined with (5). The ratio of intensities of the instrumentation noise S_{ni} to that of the Poisson noise is varied from 0.1 up 5, and the precision varies as shown in fig. 9. This result can be explained as follows. From (22) it follows that $N(\omega)$ and, therefore, the SNR $\eta_i(\omega)$ described by (21) decreases monotonously with S_{ni}. Since the integrand of (5) decreases monotonously with the SNR, the precision increases monotonously with S_{ni}. Furthermore, if the SNR $\ll 1$ the integrand is approximately quadratic in the SNR. For the SNR $\gg 1$ it is linear. This is also in agreement with fig. 9. So, not surprisingly, the instrumentation noise should be kept as small as possible .

4.5. Magnification

The influence of the magnification on the precision can be seen in fig. 10. The magnification influences the dimensions of a sensor, the sampling distance and the interval of the image in which measurements can be done on specimen level. The total effect of these four parameters on the precision while varying the magnification is rather complex, see (24), (26), (29) and (5). For low magnifications the estimation of the image displacement is relatively imprecise because of the large dimensions of Δx, Δy and $\Delta\xi$ on specimen level. For high magnifications the precision is also less because of the very small dimensions Δx, Δy and $\Delta\xi$, which results in a small SNR, see section 4.3. The magnification best suited for estimating an image displacement is about 200,000 times.

4.6. Measuring time

The measuring time influences the signal-to-Poisson-noise ratio $\eta_p(\omega)$ following (18). The precision is plotted against the measuring time in fig. 11. The precision increases inversely with the square root of the measuring time. The influence of the measuring time on the precision is described by (18), (21) and (22) combined with (5). Expression (18) shows that $\eta_p(\omega)$ is proportional to T. Furthermore, it follows from (17) and (22) that the function $N(\omega)$ monotonously increases to one if T increases. So, by (21), $\eta_i(\omega)$ is somewhat more than proportional to T. Then, by the same arguments as used in section 4.4, the MVB, eq. (5), is more than inversely proportional to T for small T, and becomes for increasing T purely inversely proportional. This is precisely the type of behaviour shown by fig. 11.

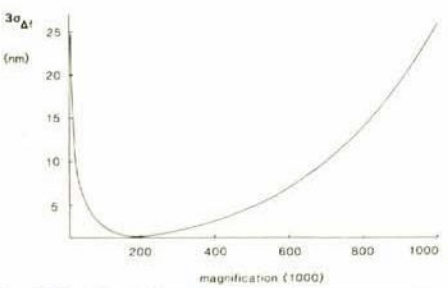

Fig. 10. Precision of the estimation of defocus as function of magnification.

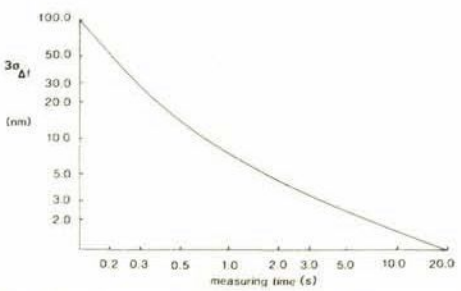

Fig. 11. Precision of the estimation of defocus as a function of measuring time T.

The minimum time necessary to autofocus the TEM up to a certain precision can be calculated using the MVB. In the following it is assumed that precision better than 5 nm is desired. Fig. 6 shows that a measuring time of 5 s is enough, using one line of a video camera, provided the TEM is not more than 3.5 Sch out of focus. When more (independent) video lines are used for calculating the image displacement, the required measuring time is less. Moreover, the precision is inversely proportional to the square root of the number of statistically independent lines used:

$$3\sigma_D \sim 1/n^{1/2}. \tag{33}$$

When 500 independent lines are available (n = 500), the minimum measuring time will be about 25 ms instead of 5 s when one line is used to calculate the image displacement. In order to autofocus using the BID method, two measurements have to be done. So the minimum time required is 50 ms. To measure other aberrations (such as astigmatism and misalignment) more images have to be measured [10]. Of course, the time necessary to measure these aberrations increases linearly with the number of image displacements to be estimated.

5. The BID method as autofocus method

We now return to the feasibility requirements to be met by BID autofocus listed in section 1:

(1) As to the *precision*: we have assessed in sections 4 and 5 the ultimate precision than can be achieved with a particular set of observations, automatically or manually. So, any automatic method getting near this precision is unlikely to be outperformed by a human operator.

(2) The BID method is inherently *fast*, because it calculates the defocus directly from two measured images; there are, in principle, no intermediate iterative steps. Limitations in speed depend on the measuring system used.

(3) A practical and natural measure for the *efficiency*, used in statistical literature, is the extent to which an estimation method achieves the minimum variance bound. Methods are available for the construction of estimation methods optimal in this sense [13]. These methods can, in principle, be applied to the problem of image displacement [19]. However, this has not yet been tried out in TEM practice. Several straightforward, non-optimal methods such as cross-correlation, minimum square error, and determination of the phase angle of the cross-power spectrum between the images are available [20]. Whichever of these methods is chosen, all are based on straightforward signal processing operations as correlation or discrete Fourier transform. An example of an estimator, which has been used in the first experiments by Van der Mast [11], is relatively fast and easy to implement in hardware:

$$F(s) = \sum_{i=1}^{IP} |r_1(i) - r_2(i-s)|, \tag{34}$$

where s is the displacement, i the location of an image point along the line considered, IP the number of image points, $r_1(i)$ and $r_2(i)$ the image intensities measured. The value for s for which $F(s)$ is minimal is taken as the image displacement, see fig. 12.

(4) *Reproducibility* is determined by the signal-to-noise ratio in the observed images and can therefore, in principle, be made arbitrarily high by increasing the measuring time.

(5) No *special kind of contrast* in the image is needed to focus the TEM; the BID method functions with both phase and amplitude contrast.

(6) These operations can be carried out with *inexpensive* small computers. For practical reasons it may be wise to use a one-dimensional approach in estimating the image displacement. The amount of data to be processed is small when only one row of pixels in a measured image is used. The

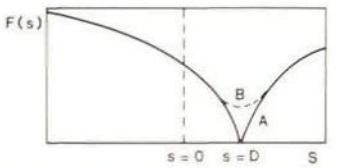

Fig. 12. The function $F(s)$ without noise (A) and with noise (B). D is the displacement between the two images.

Table 2
Summary of experiments; values of parameters are: $\Delta x = 0.5$ nm, $\Delta f = (\Delta f)_{Sch} = 1$ Sch, $S_{ni} = 5 \times 10^{-9}$ electrons m, $T = 5$ s, $\Delta \xi = 0.5$ nm, $k = 1250$; dimensions are those at specimen level; 1 Sch = 86 nm

Experiment	Varied
1	Δf: −3.4 to +3.5 Sch
2	$\Delta \xi$: 0.1–0.2 nm
3	Δx: 0.1–7.0 nm
4	$S_{ni}/(k\,\Delta x)$: 0.1–5.0
5	M: 10^3–10^6
6	T: 0.1–20.0 s

direction of the image displacement is known, because the shift is in the direction of the beam tilt. Thus when after a certain measuring time the precision is unsatisfactory, more rows of pixels can be processed to obtain a higher precision.

6. Conclusions and discussion

The theoretical limitations of a procedure to autofocus a TEM based on measuring a beam-tilt-induced image displacement (BID) have been studied. Simulations of a TEM and measuring system show that:

- The minimum measuring time necessary to focus the TEM with a precision of 5 nm (under normal operating conditions) with a vidicon camera attached is about 0.05 s. This is the *measuring* time. Image processing time is not taken into account.
- The precision with which the defocus can be estimated depends strongly on the defocus itself. A strategy is proposed for focussing a TEM using this dependence.
- The magnification can be chosen such that the precision in estimating the defocus is optimal. For a TEM under normal operating conditions and normal Vidicon video camera, this magnification is about 200,000.

In studying the theoretical limitations of the BID method, effects of inaccurate modelling of the measuring process are not taken into account. It is assumed, for instance, that the frequency-dependent shifts due to beam tilt in the two images may be neglected.

Furthermore, a well aligned TEM is assumed in studying the theoretical limitations of the BID method. Work is being done in extending the BID method to be able to align the illuminating beam and to apply the BID method to dark field images.

Assumptions have also been made with respect to the power spectrum and modulation depth of the image of the specimen (flat and 0.05, respectively). Automatic focussing with a specimen whose image contains only low frequencies (crystalline) and with a very small modulation depth will be extremely difficult using the BID method.

The time necessary to autofocus a TEM consists of the measuring time necessary to obtain the precision required, and the time necessary to process the measured images and to control the TEM. Limitation of the total autofocussing time is therefore mainly determined by the image pick-up device (afterglow in the fluorescent layer), transport and storage of images, computation time, and settling time of the currents through the beam tilt coils and objective lens currents.

Experiments with the BID method are presently carried out at Delft University of Technology. Results show that the method works under normal operating conditions and that the total time necessary to autofocus the TEM is limited by the processing of the images (10 s). Practical problems arise when calculating the image displacement because of the spatial inhomogeneity of the camera. A system which can align, focus and correct astigmatism using the BID method is being developed.

Acknowledgements

These investigations were supported by the Netherlands Technology Foundation (STW) and by Philips Nederland B.V.

Appendix A. Power spectrum of the measured image of the specimen

Suppose $f(x)$, the image on the screen, has a power spectrum $S_{ff}(\omega)$. Our problem is to derive an expression for the power spectrum of $g(x)$, the

image on the screen *measured* with an infinite number of sensors of finite dimensions. In other words, we wish to establish the relation between the power spectra of $f(x)$ and $g(x)$:

$$g(x) \overset{\text{def}}{=} \int_{-\Delta x/2}^{\Delta x/2} f(x'-x)\,\mathrm{d}x', \tag{A.1}$$

where Δx is the length of a sensor.

Suppose the expectation of $g(x)$ is $E(g(x)) = \mu_g$ and $E(f(x)) = \mu_f$. Then

$$\mu_g = \int_{-\Delta x/2}^{\Delta x/2} \mu_f\,\mathrm{d}x'. \tag{A.2}$$

$$g(x) - \mu_g = \int_{-\Delta x/2}^{\Delta x/2} \left[f(x'-x) - \mu_f \right] \mathrm{d}x'. \tag{A.3}$$

With $g'(x) \overset{\text{def}}{=} g(x) - \mu_g$ and $f'(x) \overset{\text{def}}{=} f(x) - \mu_f$, it follows that

$$g'(x) = \int_{-\Delta x/2}^{\Delta x/2} f'(x'-x)\,\mathrm{d}x'. \tag{A.4}$$

The autocovariance function $C_{gg}(\xi)$ of $g'(x)$ is given by

$$\begin{aligned} C_{gg}(\xi) &= E(g'(x)g'(x+\xi)) \\ &= \int_{-\Delta x/2}^{\Delta x/2} \mathrm{d}x_1' \int_{-\Delta x/2}^{\Delta x/2} \mathrm{d}x_2'\, E(f'(x_1'-x) \\ &\quad \times f'(x_2'-x-\xi)) \\ &= \int_{-\Delta x/2}^{\Delta x/2} \mathrm{d}x_1' \int_{-\Delta x/2}^{\Delta x/2} \mathrm{d}x_2'\, C_{ff}(x_2'-x_1'-\xi). \end{aligned} \tag{A.5}$$

If $x_2' - x_1' = r$, then

$$\begin{aligned} C_{gg}(\xi) &= \int_{-\Delta x/2}^{\Delta x/2} \mathrm{d}x_1' \int_{0}^{\Delta x/2 - x_1'} C_{ff}(r-\xi)\,\mathrm{d}r \\ &\quad + \int_{-\Delta x/2}^{\Delta x/2} \mathrm{d}x_1' \int_{-\Delta x/2 - x_1'}^{0} C_{ff}(r-\xi)\,\mathrm{d}r \\ &= \int_{0}^{\Delta x} C_{ff}(r-\xi)\,(\Delta x - r)\,\mathrm{d}r \\ &\quad + \int_{-\Delta x}^{0} C_{ff}(r-\xi)\,(\Delta x + r)\,\mathrm{d}r, \end{aligned} \tag{A.6}$$

or

$$C_{gg}(\xi) = \Delta x \int_{-\infty}^{\infty} C_{ff}(p)\, d_1(\xi - p)\,\mathrm{d}p. \tag{A.7}$$

with

$$d_1(x) = \begin{cases} 1 - \dfrac{|x|}{\Delta x} & \text{for } |x| \leqslant \Delta x, \\ 0 & \text{elsewhere.} \end{cases}$$

The power spectrum of $g(x)$ is then given by

$$S_{gg}(\omega) = (\Delta x)^2\, S_{ff}(\omega)\, \mathrm{sinc}^2(\omega\, \Delta x/2), \tag{A.8}$$

with Δx the sensor length, ω the spatial radian frequency and $S_{ff}(\omega)$ the power spectrum of the image on screen.

Appendix B. Power spectrum of the Poisson noise in the measured image of the specimen

An expression is derived for the power spectrum $S_{pn}(\omega)$ of the Poisson noise for the hypothetical case that a sensor is placed in every point of a selected interval of the x-axis (this is the spatial equivalent of making "continuous-time" observations during a selected time interval).

Suppose sensors of length Δx are present in the interval $0 \leqslant x \leqslant L$. This means the noise is covariant over a length Δx. This covariance is first computed. The desired power spectrum is the Fourier transform of this covariance.

Fig. 13 shows two sensors which overlap over a distance $\alpha \Delta x$. Let the expectation of the number of electrons counted by a sensor be k. Then the expectations of these numbers for processes p, q and r are approximately αk, $(1-\alpha)k$ and αk respectively. The covariance of the electron counts $p+q$ (sensor 1) and $q+r$ (sensor 2) then satisfies

$$E((p+q)(q+r)) = E(q^2) \tag{B.1}$$

since p and r are not covariant. The right-hand member of this equation equals the variance of q and, since q is Poisson-distributed, this variance is

Fig. 13. Two sensors of length Δx overlapping over a distance $\alpha \Delta x$.

equal to $(1-\alpha)k$. So, since

$$\alpha = |x|/\Delta x, \tag{B.2}$$

the covariance $C_{pn}(x)$ of the electron counts of two sensors at a distance x is described by

$$C_{pn}(x) = \begin{cases} \left(1 - \frac{|x|}{\Delta x}\right)k & \text{for } |x| < \Delta x, \quad \text{(B.3a)} \\ 0 & \text{for } |x| \geq \Delta x. \quad \text{(B.3b)} \end{cases}$$

The power spectrum $S_n(\omega)$ of the Poisson noise is now given by the Fourier transform of $C_{pn}(x)$:

$$S_n(\omega) = k\,\Delta x\,\mathrm{sinc}^2(\omega\Delta x/2), \tag{B.4}$$

with ω the spatial radian frequency in the image on screen. Note that in the above considerations the simplification has been made that the standard deviation of the number of electrons counted per sensor is constant; this is true when the modulation depth of the image is small.

References

[1] S.J. Erasmus and K.C.A. Smith, J. Microscopy 127 (1982) 185.

[2] S.J. Erasmus, J. Microscopy 127 (1982) 29.

[3] W.O. Saxton, D.J. Smith and S.J. Erasmus, J. Microscopy 130 (1983) 187.

[4] R. Guckenberger, in: Proc. 9th Intern. Congr. on Electron Microscopy, Toronto, 1978, Vol. 1, Ed. J.H. Sturgess (Microscopical Soc. of Canada, Toronto, 1978) p. 88.

[5] S.C. McFarlane, J. Phys. C8 (1975) 2819.

[6] J.B. LePoole, Philips Tech. Rev. 9 (1947) 33.

[7] J.B. LePoole and L.E.M. de Groot, in: Proc. 7th European Congr. on Electron Microscopy, The Hague, 1980, Vol. 2, Eds. P. Brederoo and W. de Priester (7th European Congr. on Electron Microscopy Foundation, Leiden, 1980) p. 644.

[8] C.D. Curling, E.M. Deeley and J.A. Temple, Proc. IEEE 116 (1969) 334.

[9] G. Kobolt, H. Koops, A. Nauber, K. Weindel and B. Westerwald, in: Proc. 10th Intern. Congr. on Electron Microscopy, Hamburg, 1982, Vol. 1 (Wiss. Verlagsges., Stuttgart, 1982) p. 199.

[10] H. Koops and G. Walter, in: Proc. 9th Intern. Congr. on Electron Microscopy, Toronto, 1978, Vol. 3, Ed. J.H. Sturgess (Microscopical Soc. of Canada, Toronto, 1978) p. 185.

[11] K.D. van der Mast, in: Proc. 8th European Congr. on Electron Microscopy, Budapest, 1984, Vol. 1, Eds. A. Csanády, P. Röhlich and D. Szábo (Budapest, 1984) p. 3.

[12] F. Zemlin, K. Weiss, P. Schiske, W. Kunath and K.-H. Herrmann, Ultramicroscopy 3 (1978) 49.

[13] A. Van den Bos, Parameter estimation, in: Handbook of Measurement Science Fundamentals, Ed. P.H. Sydenham (Wiley, New York, 1982).

[14] C.G. Carter, IEEE Trans. Acoust. Speech, Signal Processing 29 (1981) 463.

[15] L. Reimer, Transmission Electron Microscopy (Springer, Heidelberg, 1984).

[16] K.-J. Hanszen, Advan. Opt. Electron Microsc. 4 (1971) 1.

[17] A. Papoulis, The Fourier Integral and its Applications (McGraw-Hill, New York, 1962).

[18] P.W. Hawkes, Ultramicroscopy 5 (1980) 67.

[19] D. Hertz, IEEE Trans. Acoust. Speech, Signal Processing 1 (1986) 1.

[20] M.B. Priestley, Spectral Analysis and Time Series (Academic Press, London, 1981).

3 Signal Processing For Autotuning By Beam Tilt Induced Image Displacement

1	Introduction	41
2	Achievable precision in autofocusing a TEM	42
3	Image formation with tilted illumination	42
4	Achievable precision of the BID method	44
5	Achievable precision of the variance method	48
6	Estimating defocus with the BID method	51
7	Conclusions and discussion	55
	References	56

A.J. KOSTER, A. van den BOS and K.D. van der MAST

Delft University of Technology, Department of Applied Physics, Lorentzweg 1, 2628 CJ Delft, The Netherlands

Abstract

Autofocus is possible by measuring a Beam-tilt- induced Image Displacement (BID). This can be done by having a computer tilt the beam, measuring the displacement, calculating the defocus and correcting it. The method works with many types of specimen because it utilizes both the amplitude and phase contrast of a bright field image. Image blurring due to the beam-tilt can be corrected by a phase correcting filter, derived from the phase contrast transfer function. Simulations for a TEM equipped with a video camera show that at Scherzer defocus (86 nm) the minimum measuring time required for focusing the TEM with a precision of 5 nm is about 50 ms. The measuring time for the minimum variance autofocus method is about 1.5 s to obtain the same precision.

1. Introduction

Automatic focusing and automatic stigmating of a Transmission Electron Microscope (TEM) is desirable, especially for high resolution electron microscopy. Reliable and interpretable electron micrographs require an accurately focused, stigmated and aligned TEM. Focusing and stigmating a TEM can be time consuming and requires an experienced operator, in the case of low dose work in particular. The time factor is important since object structures are destroyed by prolonged radiation.

Several methods to focus, stigmate and align a TEM automatically have been proposed [5]. The only published proposal for automatic focusing which has been tested in practice is based on minimum image variance (MV) at focus [17]. Image variance is measured as a function of the objective lens current. The object is in focus when the image variance is minimal. In fact, the MV method is used by most microscopists while focusing at high magnifications, as it involves no special equipment. The MV method is also applied for alignment of the illuminating beam [17].

Another proposed method is based on tilting the illuminating beam over a known angle. This beam-tilt results in image displacement on the screen due to the coherent illumination, see fig. 1.

This Beam-tilt-induced Image Displacement (BID) has a known relationship with the defocus of the TEM [5] and can be used as a focusing aid. Le Poole [12] introduced in 1947 the beam tilt wobbler as a simple focusing aid and most microscopists use this method for focusing a TEM at lower magnifications. Presently Nomura et al [15] are implementing this autofocus method. A similar approach was followed by Curling [3] and Koops [8,9]. Van der Mast [13] proposed to measure both

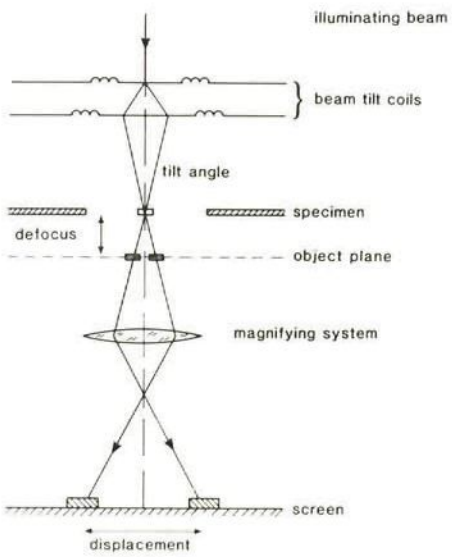

Fig. 1. Image displacement as result of beam-tilt.

magnitude and direction of the image displacement in order to calculate and correct the defocus in one step. An expression for the achievable precision of the BID method as function of TEM and measuring set-up has been derived by the present author [10,11]. The BID method is inherently fast, reproducible, applicable to most

specimens and suitable for implementation in a TEM. However, tilting the beam introduces image aberrations (Zemlin [19]) which makes it difficult to estimate defocus at high magnifications.

In this paper signal processing aspects of the BID method are discussed and the achievable precision in estimating the defocus of the BID method and MV method are calculated. Furthermore, a method is proposed for correcting the image aberrations introduced by the beam-tilt. The next section describes briefly image formation in a TEM for weak phase objects with tilted illuminations from which expressions are derived for the achievable precision of both the BID and MV method for a particular measuring set-up.

2. Achievable Precision in Autofocusing a TEM

Simulation and statistical modeling are tools for calculating the expectation and variance of an estimator for a parameter in a model of observations of a physical process before really making the observations, and can be used in optimizing the final measuring conditions. The bias, defined as the difference between the expectation and the true value of the parameter, represents the systematic error, that is, the accuracy of the estimator. similarly, the variance is a measure of the non systematic errors, that is, the precision of the estimator. Bias and variance are objective qualities suitable for the comparison of different estimators of a parameter applied to the same observations.

In this section the precision of the MV method is compared to the precision of the BID method. In other words: the (minimum) variances of both estimators are compared. The approach to calculating the achievable precision is as follows: first an expression is derived for the TEM image of a thin carbon film. Using this expression simulations are done to calculate the achievable precision of both the BID and MV method. This is done by taking into account the influence of Poisson noise, characteristics of the TEM and measuring set-up. In the next section a model of the observations, and the relation between defocus, beam-tilt and image displacement, is derived.

3. Image Formation with tilted Illumination

Image contrast of a weak phase object (WPO) in a TEM can be described by [18]

$$c(\mathbf{x}) = \left| F^{-1}\{\eta(\mathbf{k})\ T(\mathbf{k})\} \right| \qquad (1)$$

with $c(\mathbf{x})$ the contrast at position $\mathbf{x}$ scaled to the object plane (in $G\ell$, $1G\ell = 0.6$ nm for a 100 kV microscope with a C_s of 2 mm), F^{-1} the inverse Fourier transform, $\eta(\mathbf{k})$ the Fourier transform of the transparency of the phase object, $T(\mathbf{k})$ the phase contrast transfer function (PCTF) and $\mathbf{k}$ the spatial frequency scaled to the object plane (in $G\ell^{-1}$). The PCTF for a beam tilted over κ (measuring beam-tilt via the point at which

the primary beam intercepts the Fourier plane, in $G\ell^{-1}$) is given by

$$T(\mathbf{k}) = i\ \{e^{-i[\gamma(\kappa+\mathbf{k})-\gamma(\kappa)}.E(\kappa+\mathbf{k},\kappa) - e^{i[\gamma(\kappa-k)-\gamma(\kappa)]}.E(\kappa-\mathbf{k},\kappa)\} \quad (2a)$$

with the wave aberration function

$$\gamma(\mathbf{k}) = \pi k^2(k^2-D)$$

and the envelope function E describing attenuation of transfer as a result of finite beam divergence and focus spread:

$$E(\mathbf{k}_1,\mathbf{k}_2) = e^{-(s^2/4)|\Delta\gamma(\mathbf{k}_1)-\Delta\gamma(\mathbf{k}_2)|^2}\ e^{-\pi^2d^2(\mathbf{k}_1{}^2-\mathbf{k}_2{}^2)^2} \quad (2b)$$

$$\Delta\gamma(\mathbf{k}) = 2\pi(k^2-D)\mathbf{k}$$

with underfocus D (in Sch, 1 Sch = 86 nm for a 100 kV microscope with a C_s of 2 mm), s the rms divergence of the beam (in Sch) and d the rms focus spread (in Sch). The real and imaginary part of the PCTF for a defocus of 1 Sch and a beam-tilt of 0.2 $G\ell^{-1}$ are shown in fig. 2.
The PCTF works as a spatial filter in imaging the specimen. It transfers details up to 0.5 $G\ell$ for the TEM specifications of table 1. For objects having (in expectation) a flat power spectrum (1) can be simplified to

$$c(\mathbf{x}) = |F^{-1}\{T(\mathbf{k})\}|. \quad (3)$$

For small tilt angles (< 0.2 $G\ell^{-1}$)

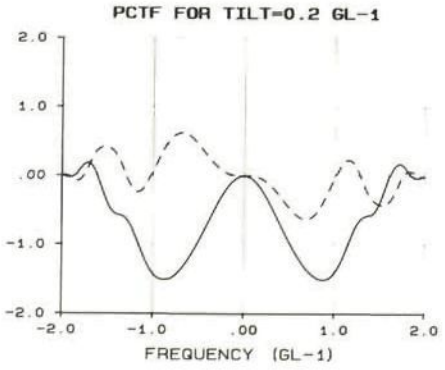

Fig. 2. The real (solid) and imaginary (dashed) parts of the PCTF for a defocus of 1 Sch and a beam-tilt of 0.2 $G\ell^{-1}$.

the relation between beam-tilt, defocus and image displacement can be approximated by:

$$c(\mathbf{x}) = |F^{-1}\{G(\mathbf{k})\ e^{-2\pi i(k^2-D)\mathbf{k}.\kappa}\}| \quad (4)$$

with

$$G(k) = 2\ \sin[\gamma(\mathbf{k})]\ E(0,\mathbf{k}).$$

The problem of focusing a TEM is transformed to the problem of estimating the parameter D in (4). Fortunately, this problem is similar to the problem of time delay estimation in passive sonar theory and much work has been done in estimating time delay [14]. This analogy is apparent when the image contrast for tilted illumination is compared with image contrast for axial illumination. For axial

illumination the image contrast is given by

$$c_a(\mathbf{x}) = \left|F^{-1}\{G(\mathbf{k})\}\right|. \qquad (5)$$

Comparing (5) with (4) we see that tilting of the beam results in phase shifts of the PCTF and modifies the image on screen. Its effect would be simply an image displacement if the phase shift depended only linearly on the frequency **k**, or with (4)

$$c_f(\mathbf{x}) = \left|F^{-1}\{G(\mathbf{k})\ e^{2\pi i D.\kappa.\mathbf{k}}\}\right| \qquad (6)$$

then

$$c(\mathbf{x}) = c_d(\mathbf{x}-\mathbf{d}) \qquad (7)$$

with the image displacement **d** (in $G\ell$) given by

$$d = D\kappa. \qquad (8)$$

Unfortunately, the phase shift does not only depend linearly on the frequency **k**, but also on the third power of it. To be able to use the BID method for autofocusing a TEM, it is essential to correct this blurring effect of beam-tilt on the image measured on screen. However, the achievable precision in estimating defocus with the BID method only depends on stochastic properties and not on deterministic effects resulting in systematic errors. These errors can, in principle, be corrected (section 3).

4. Achievable Precision of the BID Method

Using the BID method to focus the TEM at high magnifications, signal processing facilities are indispensable. First, two images have to be measured corresponding to well defined tilt angles. Then an algorithm has to be applied to those images in order to calculate the image displacement. This algorithm determines the precision of the focus estimation and must be carefully designed to obtain optimal precision. Finally, from this displacement the objective lens current can be adjusted to correct defocus, according to (8). In this sub section the achievable precision is calculated, the precision of a carefully designed optimal image displacement estimator.

An expression was derived [11] for the achievable precision for the BID method as a function of parameters describing the TEM and the simulated measuring set-up. This achievable precision is independent of any particular algorithm which calculates the displacement. It is an expression which assumes that all the information available in the images is used. This lower bound on the precision can, in principle, be achieved using a well designed estimator [7]. In this paper this expression is applied to a specific measuring set-up and TEM. It is assumed that measurements are done at the image of the specimen with a video- or CCD camera. Furthermore, it is assumed that measurements are done with a one-dimensional array of adjacent rectangular sensors (a line from a CCD or video camera, N

sensors on a line), each with a length Δx and a width Δy. The sensor width is small enough to assume the image measured in y-direction constant. This is done for simplicity; the theory can be extended to correct for this assumption. Specifications of the TEM and measuring conditions are given in table 1 (hereafter: reference conditions). In this model of observations instrumentation noise is added with an intensity equal to the Poisson noise. All dimensions are in $G\ell$ and Sch.

In focusing the TEM with the BID method, the beam is first tilted over κ (in $G\ell^{-1}$) and next over $-\kappa$ in the direction of the sensor array. This will result in two images measured (6):

$$\underline{r}_1(x_i) = c(x_i) + \underline{n}_1(x_i)$$

$$\underline{r}_2(x_i) = c(x_i - d) + \underline{n}_2(x_i)$$

$$\text{for } i=1,\ldots,N \qquad (9)$$

with x_i the position of sensor i, $c(x_i)$ the image contrast, d the image displacement and $n_{1,2}(x_i)$ independent, zero-mean noise, consisting of Poisson noise and instrumentation noise. The variance of the Poisson noise has an expectation equal to the number of electrons counted:

$$n = \Delta x\, \Delta y\, t\, j \qquad (10)$$

with n the number of electrons counted per sensor, t the measuring time and j the number of electrons per second and per unit area (averaged over all sensors). The achievable precision (in Sch) in estimating the defocus D is then given by

$$3\sigma_D = \frac{3\sigma_d}{2\kappa}, \qquad (11)$$

with

$$\sigma_d = \{4\pi^2 N \Delta x \int_{-k_s}^{k_s} \frac{SNR^2(k)}{1+2SNR(k)} k^2\, dk\}^{-0.5} \qquad (12)$$

where k_s the sampling frequency Δx^{-1}, $SNR(k)$ the signal to noise ratio, determined by the power spectra of the image contrast $S_c'(k)$ measured after sampling:

$$SNR(k) = \frac{S_c'(k)}{S_n} \qquad (13)$$

with

$$S_c'(k) = \sum_{i=-\infty}^{\infty} S_c(k + i\Delta x^{-1}) \qquad (14)$$

and

$$S_c(k) = n^2\mu^2 \mathrm{sinc}^2(k\pi\Delta x)\,|T(k)|^2 S_s \qquad (15)$$

with

$$\mathrm{sinc}(p) = \frac{\sin(p)}{p}. \qquad (16)$$

The noise is assumed to be white and consisting of Poisson noise S_{pn} and instrumentation noise S_{in}:

Table 1: Specifications of the model of observations, el = electrons, $G\ell = (C_s\lambda^3)^{0.25}$, Sch = $(C_s\lambda)^{0.5}$.

TEM

Coefficient of spherical aberration	: C_s = 2 mm
accelaration voltage	: E = 100 kV
defocus	: D = 1Sch(86 nm)
beam tilt	: $\kappa = 0.2\ G\ell^{-1}$ (1.2 mrad)
rms focus spread	: d = 0.2 Sch
divergense illuminating beam	: $s = 0.14\ G\ell^{-1}$
magnification	: M = 200,000

Set-up

illumination	: $j = 1000\ elG\ell^{-2}s^{-1}$
length sensor	: $\Delta x = 0.2\ G\ell$
width sensor	: $\Delta y = 0.2\ G\ell$
number of sensors	: N = 500
measuring time	: t_{BID} = 5 scR, $t_{MV} \approx$ 1s

intensity instrumentation noise: S_{ni}=400 $elG\ell$ (BID), Sni=80 $elG\ell$ (MV)

Specimen

modulation depth in Scherzer defocus	: $\mu = 0.05$
flat power spectrum (thin carbon film)	

$$S_n(k) = S_{pn} + S_{in} \qquad (17)$$

$$= n\Delta x + S_{in}.$$

The power spectrum of the specimen S_s is assumed to be flat [6] and has to be scaled to correspond to the image on screen. Therefore, an image contrast measure is introduced: the modulation depth (equivalent to the rms fractional image contrast) at Scherzer defocus:

$$\mu = \frac{\sigma_c}{n} \qquad (18)$$

with the image variance after sampling given by

$$\sigma^2_c = \int_{-1/2k_s}^{1/2k} S_c'(k)dk. \qquad (19)$$

The achievable precision of the BID method can be calculated using (11). As the modulation depth (18) varies as function of defocus and of beam-tilt the achievable precision varies as function of defocus and beam-tilt, see fig. 3 and 4.

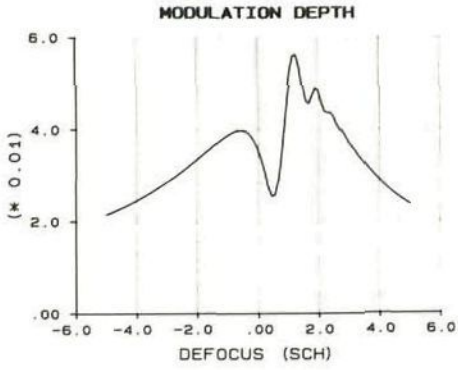

Fig. 3. The modulation depth as function of defocus for a beam-tilt of 0.2 $G\ell^{-1}$.

The modulation depth is large when the TEM is in Scherzer defocus compared to the TEM in focus. A beam-tilt value of 1.0 $G\ell^{-1}$ gives rise to a large modulation depth [18]. For a small modulation depth it is more difficult to estimate an image displacement than for a large modulation depth. This can be seen in fig. 5 and 6:

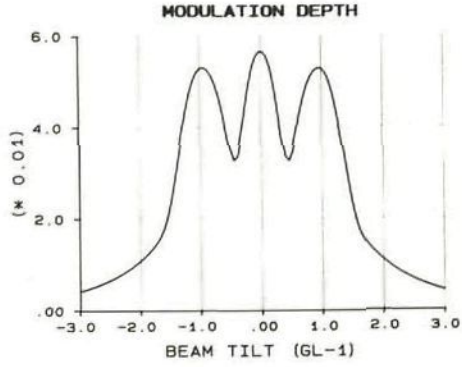

Fig. 4. The modulation depth as function of beam-tilt at Scherzer defocus.

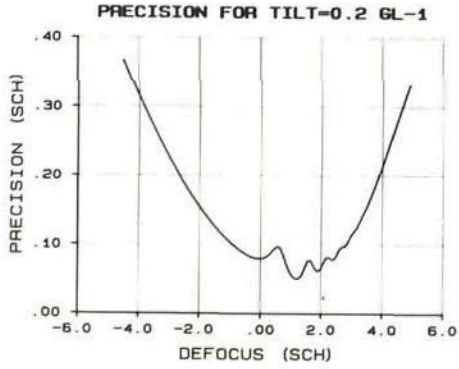

Fig. 5. The achievable precision as function of defocus for a beam-tilt of 0.2 $G\ell^{-1}$.

The achievable precision for a TEM in focus is less than for a TEM in Scherzer defocus. It can be concluded that for a beam-tilt of 0.5 to 1.5 $G\ell^{-1}$ the achievable precision in estimating defocus is optimal. The precision of the BID method is 0.055 Sch (5 nm) for a 100 kV TEM in Scherzer defocus, a

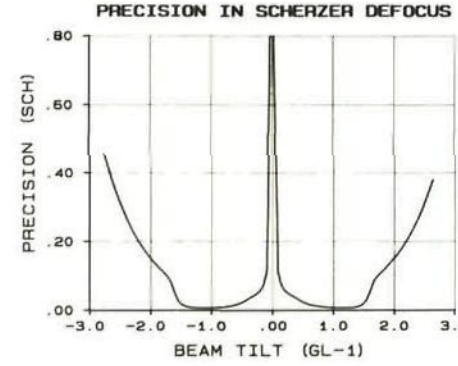

Fig. 6. The achievable precision as function of beam-tilt at Scherzer defocus.

beam-tilt of 0.2 $G\ell^{-1}$ (1.2 mrad), a magnification of 200000, a measuring time of 5 s (or 0.25 s when 400 video lines are used), and an illumination such that 400 electrons are counted per pixel.

5. Achievable Precision of the Variance Method

The MV method requires a series of image variance estimates to be able to estimate defocus of the TEM. The change in variance while varying defocus of the TEM is known for a weak phase object (19) and is given in fig. 3 and enlarged in fig. 7.
A defocus of about 0.5 Sch gives, for reference conditions, minimum image variance. The achievable precision of the MV method is determined by the precision in estimating the defocus value of this minimum variance. This precision depends on parameters determining the stochastic properties per image measurement. For the MV method these are the number of focus steps which are used, the amount of noise and the number of electrons counted per sensor for each defocus step. A measured image for each focus step is modeled by

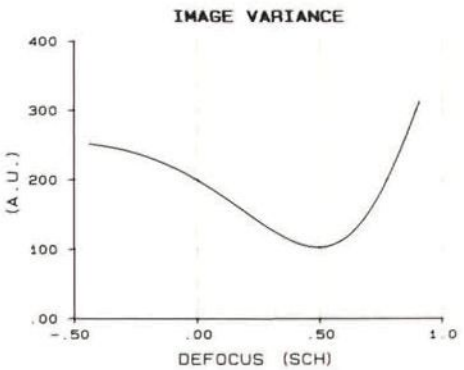

Fig. 7. The image variance as a function of defocus for a beam-tilt of 0.2 $G\ell^{-1}$.

$$r_j(x_i) = c_j(x_i) + n_j(x_i)$$

$$\text{for } i = 1, \ldots, N \quad \text{and } j = 1, \ldots, Nm \qquad (20)$$

with N the number of sensors positioned at x_i, Nm the number of focus steps, $c_j(x_i)$ the number of electrons counted corresponding to the specimen image intensity (signal), and $n_j(x_i)$ the number of electrons counted corresponding to the noise in measurement j. The variance of the signal variance is then

$$\text{var } r_j = \text{var } c_j + \text{var } n_j$$

$$\text{for } j = 1, \ldots, Nm \qquad (21)$$

with var c_j the signal (specimen image) variance after sampling and var n_j the noise variance for each measurement. The noise variance consists of Poisson noise variance and instrumentation noise variance (17), and is calculated as in (19):

$$\text{var } n_j = n + S_{inks}, \qquad (22)$$

and is determined by the measuring time (10). An estimator for the signal variance is

$$s_j^2 = \frac{1}{N-1} \sum_{i=1}^{N} (r_j(x_i))^2, \qquad (23)$$

which has itself a variance of at least [16]

$$\text{var } s_j^2 \approx \frac{2(\text{var } r_j)^2}{N} \qquad (24)$$

$$= \frac{2}{N} (\text{var } c_j + \text{var } n_j)^2.$$

The precision in estimating the signal variance $3(\text{var } s_j^2)^{0.5}$ varies therefore with the signal variance itself (var c_j) for each focus step. For simplicity it is assumed that the TEM is near focus (somewhere between -0.5 Sch and +1 Sch) and that the change in signal variance can be approximated by a quadratic polynomial:

$$w_j = b_0 + b_1 f_j + b^2 f_j^2 + \nu_j$$

$$j = 1, \ldots, Nm \qquad (25)$$

with w_j the signal variance estimated for a defocus f_j, b_0, b_1 and b_2 the parameters to be estimated and ν_j the noise. Or in vector (of dimension Nm) notation:

$$w = Fb + \upsilon \qquad (26)$$

with

$w = (w_1 \ \ldots \ w_{Nm})T$ the signal variances estimates

$$F = \begin{pmatrix} 1 & f_1 & f_{12} \\ . & . & . \\ . & . & . \\ 1 & f_{Nm} & f_{Nm}^2 \end{pmatrix}$$ the 3x Nm matrix containing the defocus values,

$b = (b_0 b_1 b_2)^T$ the 3 parameters of the polynomial, and

$\upsilon = (\upsilon_1 \ldots \upsilon_{Nm})^T$ the noise on the estimated signal variances (dim. Nm)

The best linear unbiased estimator is [1]

$$b = (F^T V^{-1} F)^{-1} F^T V^{-1} w \qquad (27)$$

with a covariance matrix (3x3) given by

$$\text{cov}(b,b) = (F^T V^{-1} F)^{-1} \qquad (28)$$

where the covariance matrix V is of uncorrelated, noise:

$$V = (\sigma_n^2{}_1 \ \ldots \ \sigma_n^2{}_{Nm})^T \ I \qquad (29)$$

with I the unity matrix. The estimator (27) achieves the minimum variance bound when the noise distribution is Gaussian.

Fortunately, the only parameter of interest is that one indicating the minimum of the polynomial. From (25) we derive the parameter to be

$$b_{min} = -\frac{b_1}{2_b^2} \qquad (30)$$

indicating the defocus value of minimal signal variance. The variance in estimating this parameter is given by

$$\text{var } b_{min} = \frac{\partial b_{min}}{\partial b}^{T} \text{cov}(b,b) \frac{\partial b_{min}}{\partial b}, \quad (31)$$

where

$$\frac{\partial b_{min}}{\partial b} = \left(-\frac{1}{2b_2}, \frac{b_1}{2b_2^2}, 0 \right).$$

To be able to compare the BID method with the MV method, the available measuring time is taken the same for both methods. This implies a measuring time per focus step of the MV method of

$$t_{MV} = 2/Nm \; t_{BID} \quad (32)$$

with t_{BID} the measuring time available per image measurement for the BID method. This results in a different SNR per measurement, as the Poisson noise and instrumentation noise depend on the measuring time (13). Fig. 8 shows the precision of each image variance estimate as function of defocus. Fig. 9 shows the achievable precision in estimating bmin as function of the number of measurements. A precision of 1.5 Sch (140 nm) can be achieved with 5-15 focus steps in estimating bmin, for the reference conditions, using 50-160 electrons per sensor for each focus step. To obtain a precision of 0.055 Sch, the available measuring time should be 300 s instead of 10 s needed for the BID method. The precision of both methods in estimating focus increases approximately linear with the measuring time (29).

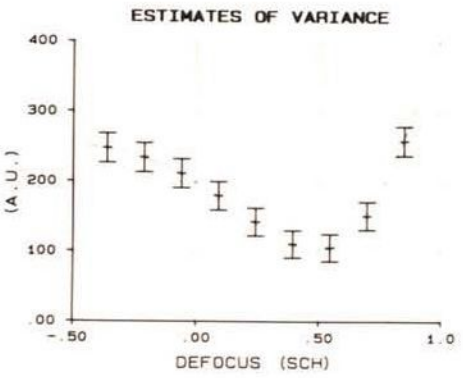

Fig. 8. The precision in estimating image variance as function of defocus, using 10 focus steps at Scherzer defocus and for a beam-tilt of 0.2 $G\ell^{-1}$.

Using 500 lines of the video camera instead of only one line, the minimum measuring time to focus the TEM is about 0.5 s for the BID method and 13 s for the MV method. This corresponds to 1.5 nAm^{-2} on the fluorescent screen of the TEM. Some remarks can be made concerning the accuracy of the minimum variance estimation using this quadratic polynomial. Firstly, the quadratic polynomial is not an accurate model of the observations. This can be seen in fig. 10: the position of minimum variance varies with the number of measurements used.

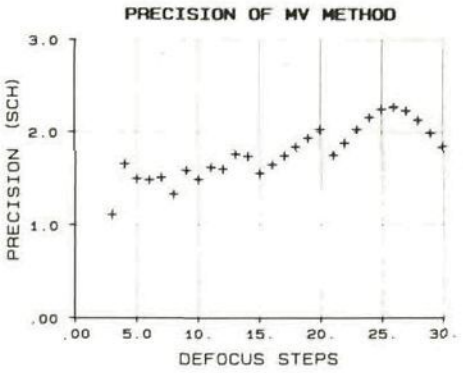

Fig. 9. The precision in estimating defocus as function of the number of focus steps at Scherzer defocus and for a beam-tilt of 0.2 $G\ell^{-1}$.

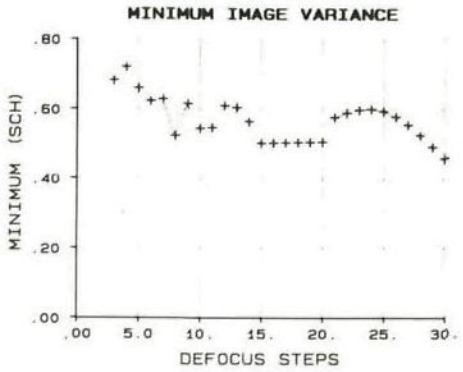

Fig. 10. The accuracy of the MV method modeling the change in image variance with a second order polynomial as function of the number of measurements at Scherzer defocus and for a beam-tilt of 0.2 $G\ell^{-1}$.

Nevertheless, conclusions concerning the precision hold and the final fit of the model has only a minor influence on this (24). Modeling with a higher order polynomial will be more accurate, but less precise, as more parameters have to be estimated. Therefore, the precision calculated can be regarded as the achievable precision.

6. Estimating Defocus with the BID Method

From the previous section it is concluded that the BID method requires less electrons than the MV method. This achievable precision of the BID method is the precision of an ideal, optimal estimator of defocus. Such an estimator can, in principle, be derived [2], making use of the a-priori knowledge concerning the PCTF for tilted illumination. However, irrespective of the image displacement estimator used, deterministic pre-filtering of the images is a necessity as the frequency shifts due to beam-tilt blur the image. This section describes some deterministic aspects in estimating defocus with the BID method.

The necessity of pre-filtering can be illustrated by a simulation of a thin carbon film. The phase of this carbon film is modeled by white, uniformly distributed noise [6]. The filtering effect is clear for axial illumination (see fig. 11 and 12): white noise is transformed to an image containing one small dominating frequency band.

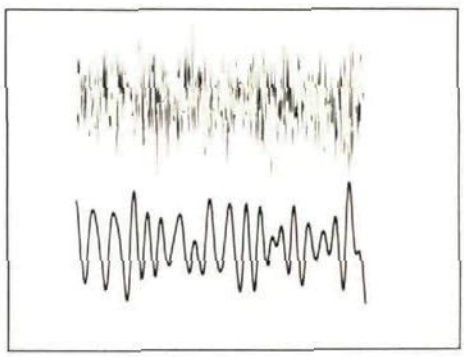

Fig. 11. Simulated 1;D intensities before (upper) and after (lower) imaging with the TEM with axial illumination and at Scherzer defocus. The length of the specimen image corresponds to 20 $G\ell$.

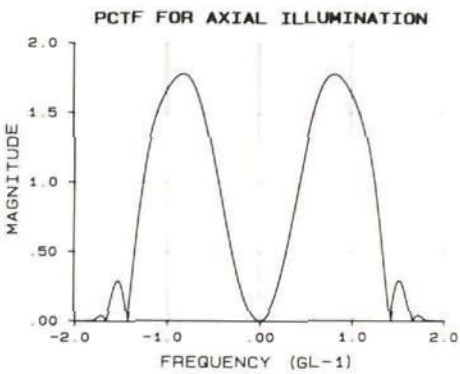

Fig. 12. Magnitude of the PCTF for axial illumination and at Scherzer defocus.

Imaging this specimen with a beam-tilt of +0.2 and -0.2 $G\ell^{-1}$ respectively, should result in an image displacement. However the result of beam-tilting is contrast reversal and blurring, see fig. 13.

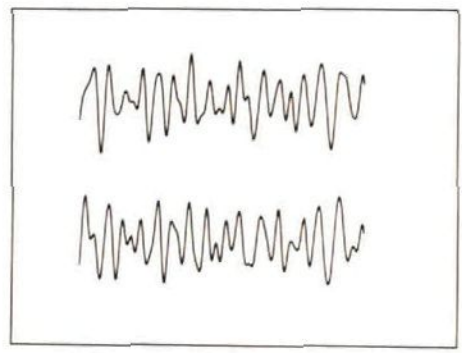

Fig. 13. Simulated 1-D intensities corresponding to a beam-tilt of +/-0.2 $G\ell^{-1}$ and at Scherzer defocus. An image displacement is not visible due to image blurring. The length of the specimen corresponds to 20 $G\ell$.

The effect of blurring on the estimation of image displacement can be illustrated by a straightforward estimator such as the cross correlation function. The position of the maximum of this function should indicate the image displacement, the height of, of the peak the influence of noise, and the width the influence of noise and contrast transfer function. Fig. 14 shows the correlation function corresponding to a beam-tilt of +/- 0.2 $G\ell^{-1}$ (about 1.2 mrad). The blurring due to the beam-tilt introduces bias: the position is not located at 0.4 $G\ell$, as was to be expected at Scherzer defocus, but at 0.1 $G\ell^{-1}$.

Another method to estimate image displacement makes use of the phase part of the cross spectrum of

the images [15]. An image displacement then corresponds to a phase shift linearly with the frequency of the cross spectrum. For the BID method the phase of the cross spectrum of the images measured corresponding to opposite tilt angles, is determined by the phase of the PCTF and can be used as defocus estimation.

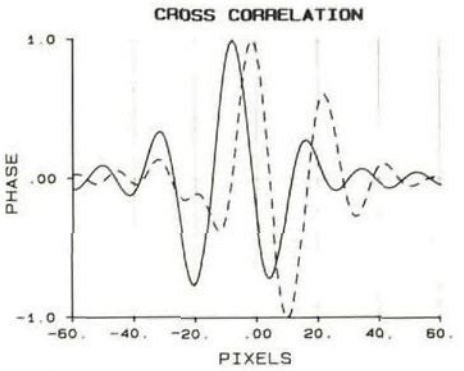

Fig. 14. Image blurring illustrated by the cross correlation function for a beam-tilt of +/-0.2 $G\ell^{-1}$ (dashed) at Scherzer defocus. The cross correlation function after filtering both images is plotted with a solid line.

The cross spectrum is given by

$$S_{12}(\mathbf{k}) = F\{r_1(\mathbf{x})\}\ F\{r_2(\mathbf{x})\}^*, \qquad (33)$$

with $r_{1,2}(x)$ the two images measured for a beam-tilt of $+/-\kappa$ and the * denoting the complex conjugate. Using (6) it can be derived that

$$D\kappa = \frac{\partial}{\partial \mathbf{k}} \text{phase}[S_{12}(\mathbf{k})]\mathbf{k}=0. \qquad (34)$$

Using (34) the defocus can be estimated from the phase of the cross spectrum. The phase of the cross spectrum for a beam-tilt of 0.2 $G\ell^{-1}$ is shown in fig. 15. Image displacement can be estimated from the linear relation between phase and frequency for frequencies up to +/- 0.4 $G\ell^{-1}$. For higher frequencies the linear relation is disturbed following (1). Fortunately, an analytical approximation of (1) for the extra phase shifts is available for small tilt angles (4).

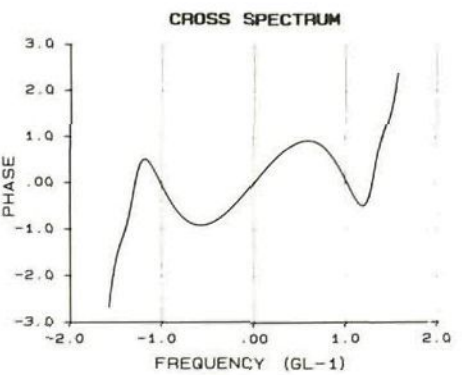

Fig. 15. Frequency shifts (coma) as result of beam-tilt +/-0.2 $G\ell^{-1}$ illustrated by the pahse part of the cross spectrum.

Fig. 16 shows the phase of both the exact (1) and approximated PCTF (4).

The approximation is valid between -1.2 and 1.2 $G\ell^{-1}$ for a beam-tilt of 0.2 $G\ell^{-1}$. Thus, a suitable phase correcting pre-filter can be calculated with (4) for spatial frequencies between -1.2 and 1.2 $G\ell^{-1}$ for a beam-tilt specified and defocus set to 0. This filter for a

tilt of 0.2 $G\ell^{-1}$ is shown in fig 17.

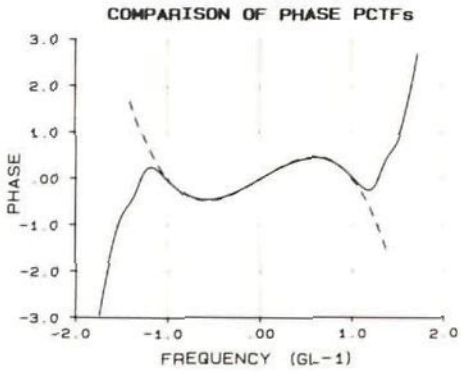

Fig. 16. The phase calculated with the exact description of the PCTF and the approximation (dashed) for a beam-tilt of 0.2 $G\ell^{-1}$ and at Scherzer defocus.

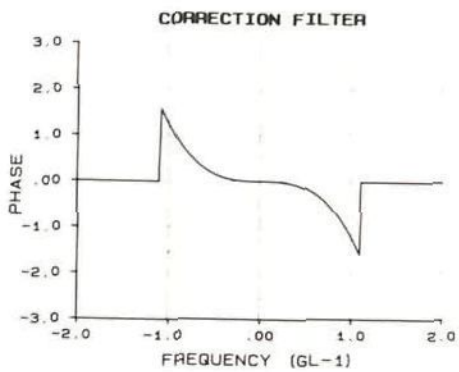

Fig. 17. Phase correcting pre-filter for a beam-tilt of 0.2 $G\ell^{-1}$.

Results of applying this filter for a beam-tilt of 0.2 $G\ell^{-1}$ are shown in fig. 18, 19 and 14.

Fig. 18 shows the two images of fig. 13 after filtering. Only an image displacement and no blurring is the result. Fig. 19 shows the phase of the corresponding cross spectrum. In contrast to fig. 15, the result is a linear relationship between phase and frequency. The cross correlation function, calculated after filtering is shown in fig. 14. The maximum is positioned correctly at 0.4 $G\ell$.

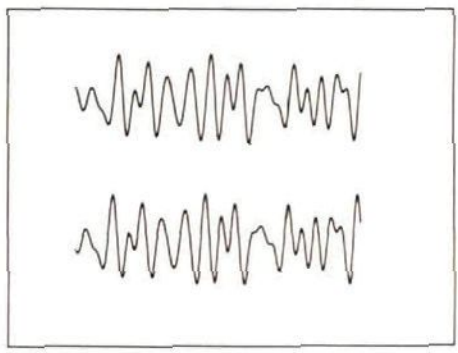

Fig. 18. Simulated 1-D intensities corresponding to a beam-tilt of +/-0.2 $G\ell^{-1}$, after filtering the images and at Scherzer defocus. An image displacement is clearly visible. The length of the specimen corresponds to 20 $G\ell$. The displacement is 0.4 $G\ell$.

Summarizing, an unbiased estimator of defocus is derived from the cross spectrum of the images corresponding to opposite beam-tilt angles. The TEM must be well aligned as the beam-tilt angle determines the pre-filter.

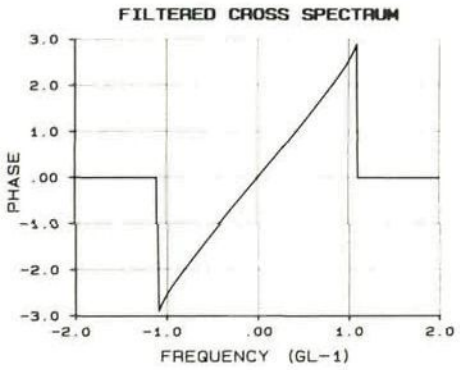

Fig. 19. The phase of the cross spectrum with pre-filtering the images for a beam-tilt of +/-0.2 $G\ell^{-1}$ and at Scherzer defocus.

7. Conclusions and Discussion

The theoretically achievable precision in autofocusing a TEM with the beam-tilt induced image displacement (BID) method and the minimum variance (MV) method were compared. It is concluded that, for a particular set of parameters describing the TEM and measuring set-up, the measuring time of the MV method is about 30 times the measuring time of the BID method to achieve a precision of 0.055 Sch. Furthermore, an estimator of defocus is proposed using the cross spectrum of the images measured. Pre-processing of the images is a necessity to correct for image blurring introduced by beam-tilt using the phase part of the phase contrast transfer function. Simulations show that the estimator proposed is unbiased.

Applying the BID method for autofocusing a TEM requires software and hardware to tilt the illuminating beam, measure the images [4], correct for the blurring due to the beam-tilt, estimate the displacement and calculate the focus adjustment. The hardware and software required to apply the MV method consists only of a focus facility and image variance estimator. Consequently, the MV method requires less computation and data handling time compared to the BID method.

Developments in signal processing techniques show an increase computation performance and it is therefore to be expected that in the near future computation time will be negligible compared to the required measuring time.

In experimental systems the spatial inhomogeneity, instability and computation time of the image measuring system influence the result of autofocusing the TEM using the BID method. Work is in progress to design optimal estimators taking these effect into account. Application of the BID method, as proposed in this paper, requires a well aligned TEM, but research is also in progress to extend the BID method for automatic correction of astigmatism and alignment.

References

[1] Bos A van den. (1982). Parameter estimation, in: Handbook of Measurement Science Fundamentals. PH Sydenham (ed), Wiley, New York.

[2] Carter CG. (1981). Time delay estimation for passive sonar signal processing. IEEE Trans. Acoust. Speech, Signal Processing, 29, 463.

[3] Curling CD, Deeley DM, Temple JA. (1969). Focussing aid for an electron microscope, Proc. IEE 116, 334-338.

[4] Erasmus SJ. (1982). Reduction of noise in TV rate electron microscope images by digital filtering. J. Microscopy 127, 29-37.

[5] Erasmus SJ, Smith KCA. (1982). An automatic focussing and astigmatism correction system for the SEM and CTEM. J. Microscopy 127, 185-199.

[6] Fan GY, Cowley JM. (1987). The simulation of high resolution images of amorphous thin films. Ultramicroscopy. 21, 125-130.

[7] Hannon EJ, Thomson PJ. (1981). Delay estimation and the estimation of coherence and phase. IEEE Trans. Acoust. Speech. Signal Proccessing, 29, 485.

[8] Kobolt G, Koops H, Nauber A, Weindel K, Westerwald B. (1982). Computer Controlled Measurement and compensation of axial aberrations of an electron microscope. in: Proc. 10th Intern. Congr. on Electron Microscopy, Hamburg, Wiss. Verlagsges, Stuttgart, 1:199-200.

[9] Koops H, Walter G. (1978). Automated compensation of lens aberrations, a simulation. in: Proc. 9th Intern. Congr. on Electron Microscopy, Toronto, JH Stutgess (Ed), Microscopical Soc. of Canada, Toronto, 1:185-186.

[10] Koster AJ, Bos A van den, Mast KD van der, Kruit P. (1986). Autofocus of a TEM through beam tilt induced image shift - dependence of its precision and speed on TEM characteristics and measuring set-up. Proc. 11th Intern. Congr. on Electron Microscopy, Kyoto, T Imura, S Maruse and T Suzuki (Eds), Japanese Soc. of Electron Microscopy, Kyoto, 1:501-502.

[11] Koster AJ, Bos A van den, Mast KD van der. (1987). An autofocus method for a TEM. Ultramicroscopy 21, 209-221.

[12] Le Poole JB, de Groot LEM. (1980). Low intensity focusing. in: Proc. 5th Europ. Congr. Electron Microsc. The Hague, 644-645.

[13] Mast KD van der. (1984). Automizing Electron Microscopes. in: Proc. 8th European Congr. on Electron Microscopy, Budapest, A Csanada, P Rohlich, D Szabo (Eds), Budapest, 1:3-9.

[14] Nagai K. (1986). Measurement of Time Delay using the Time Shift Property of the Discrete Fourier Transform (DFT). IEEE Trans. Acoust. Speech, Signal Processing, 34, 1006-1008.

[15] Nomura S, Isakozawa S, Kamimura S. (1986). Automatic focusing of CTEM using image wobbler. in: Proc. 11th Intern. Congr. on Electron Microscopy, Kyoto, T Imura, S Maruse, T Suzuki (Eds.), Japanese Soc. of Electron Microscopy, Kyoto, 1:499-500.

[16] Priestley MB. (1981). Spectral Analysis and Time Series. Academic Press, London, 702-703.

[17] Saxton WO, Smith DJ, Erasmus SJ. (1983). Procedures for focusing, stigmating and alignment in high resolution electron microscopy. J.Microscopy 130, 187-201.

[18] Smith DJ, Saxton WO, O'Keefe MA, Wood GJ, Stobbs WM. (1983). The importance of alignment and crystal tilt in high resolution electron microscopy. Ultramicroscopy 11, 263-282.

[19] Zemlin F, Weiss K, Schiske P, W Kunath, K-H. Herrmann. (1978). Coma-free alignment of high resolution electron microscopy with the aid of optical diffractograms. Ultramicroscopy 3, 49-60.

4 Autotuning of a TEM using Miminum Electron Dose

1	**Introduction**	**59**
2	**Autotuning method**	**61**
2.1	Models of the phase spectra derived from linear image formation	62
2.2	Estimation of the phase spectrum	65
2.3	Estimation of the TEM parameters	67
2.3.1	Achievable precision of defocus and astigmatism estimates	67
2.3.2	Estimator of defocus and astigmatism	67
2.3.3	Estimator of misalignment	68
2.3.4	Performance criterion for the estimation of defocus and astigmatism	68
3	**Practical design of the autotuning method**	**69**
3.1	Instrumental parameters determining the precision	70
3.2	Design strategy of the two-step autotuning procedure	71
3.3	Reference area for the estimation of defocus and astigmatism	72
4	**Simulations of the estimation of defocus and astigmatism**	**74**
4.1	Generation of noisy images	74
4.2	Numerical minimization	74
4.3	Simulation results	75
4.4	Numerical example : Electron dose required for tuning	77
5	**Conclusions and discussion**	**79**
	Appendix A : The influence of the TEM parameters on the equation errors	**79**
	Appendix B : Numerical computation of the tuning precision	**79**
	References	**80**

Ultramicroscopy 27 (1989) 251–272
North-Holland, Amsterdam

AUTOTUNING OF A TEM USING MINIMUM ELECTRON DOSE

A.J. KOSTER, W.J. de RUIJTER, A. VAN DEN BOS and K.D. VAN DER MAST

Research Group Particle Optics, Department of Applied Physics, Delft University of Technology, Lorentzweg 1, 2628 CJ Delft, The Netherlands

Received 26 August 1988; in revised form 27 December 1988

A new method is proposed to measure and correct defocus, astigmatism and beam tilt misalignment of a transmission electron microscope (TEM) automatically. The method is applicable to low-dose, high-resolution electron microscopy if the specimen may be described as a weak-phase object. Defocus and astigmatism are estimated from two different pairs of images. These are obtained, respectively, by tilting the illumination in two perpendicular directions over two equal but opposite angles. Beam tilt misalignment is estimated from three images, one formed without beam tilt and two with equal but opposite tilt angles. In all cases use is made of the cross-spectra of the images involved. An optimal measuring strategy has been designed and tested with simulations for the estimation of defocus and astigmatism. The design shows that the TEM should be tuned in two steps. The first step adjusts the defocus and astigmatism to 1.5 (in Sch), with a precision of 1. The second step adjusts the TEM with high precision. The simulations show that defocus and astigmatism can be estimated with a precision of 0.02 from images with an average intensity of 6500 electrons per nm^2. First measurements show a promising agreement of measured and simulated cross spectra.

1. Introduction

Application of a transmission electron microscope (TEM) in research is restricted by the resolution of the instrument, the sensitivity of the specimen to the electron irradiation and the skill of the operator. In the last two respects, an automatic system for the control of defocus, astigmatism and beam tilt misalignment (autotuning) could improve the TEM performance considerably, and thus increase the field of applications [1].

In the last decade, the resolution of the instrument has been pushed up to atomic resolutions as a result of many instrumental innovations. The energy spread of the electron gun is lowered from 1.5 to 0.5 eV (or possibly lower) by using a field emission gun (FEG) instead of a thermionic cathode. Coherent illumination conditions are nowadays nearly met by decreasing the illuminating aperture from 0.1 to 0.01 mrad in combination with a brighter electron source (such as a FEG). Also, the wavelength of the electrons has been shortened by increasing the acceleration voltage; widely used nowadays are 300–400 keV instruments. In addition, the spherical aberration of the objective lens has been reduced by improvement of the design and higher excitation. Finally, special imaging techniques, such as hollow cone illumination [2], holography [3] and image synthesis [4], can now be used to overcome the limitations due to the aberrations of the objective lens.

A more fundamental limit to the application of electron microscopy in materials research is set by the damage to the specimen due to the electron irradiation [5–7]. The maximum dose for which the chemical and structural change of a specimen remains negligible (allowable dose) is specimen and application dependent. Many specimen preparation and preserving techniques have been developed to increase the allowable dose. In spite of lowering the specimen temperature, increasing the acceleration voltage, improving the vacuum conditions, and developing new preparation techniques, it is inevitable to have radiation damage to the specimen. The range in allowable dose for organic

0304-3991/89/$03.50

material is between 50 to 5000 electrons per nm^2 at a specimen temperature of 300 K and an accelerating voltage of 100 kV [8].

Unfortunately, the dose needed to record the images (minimal dose) is relatively high. The dose needed to sufficiently expose photographic emulsion with a density $S = 1$ at a magnification of 100,000 is between 5000 and 50,000 electrons per nm^2. The dose needed for the same emulsion but at a magnification of a 1000 is 0.5 to 5 electrons per nm^2. Thus, the dose needed to record an image is determined by the density of the emulsion and the electron-optical magnification. A low magnification is often preferable to enable one to apply averaging techniques over a large specimen area [9]. Unfortunately, the magnification cannot be chosen too low when we consider the resolution of the recording material and the microscope aberrations such as stray fields and distortion. The smallest detail which can be recorded with photographic material is about 5 μm. Therefore, a detail of 0.1 nm in the specimen must be recorded with magnifications higher than 50,000.

Another factor is the skill of the operator. The operator must find a compromise between resolution and dose. Time (and thus dose) and sufficient electron optical magnification is required to be able to correct defocus, astigmatism and beam tilt misalignment manually up to the desired precision. The dose needed for tuning is much higher than the dose needed for recording an image. Therefore, when a specimen is radiation sensitive, sometimes micrographs are recorded without tuning the TEM precisely (e.g. by tuning the TEM at a different specimen location). Often, only a small fraction of many micrographs taken are useful due to the imprecise setting of the TEM.

Therefore, a system for automatic correction of defocus, astigmatism and beam beam tilt misaligment (or short: misalignment) that offers a better compromise between the tuning precision and dose than a human operator is highly desirable.

In general, such an autotuning system will be a closed loop system [10,11] (see fig. 1) with a video camera as image pickup device and a digital computer attached to the camera and TEM. Only recently, computer systems became available with sufficient computational power to perform complex computations on two-dimensional images of 512^2 pixels (Fourier transforms, numerical minimization) within seconds. For example, the computer system applied in this project (TVDIPS) has dedicated hardware modules for image transfer, Fourier transform and image arithmetic to speed up computational performance (for a brief description of this system, see ref. [12]). Other systems with comparable specifications are available (for example, IMAGINE with SEMPER [13]). Furthermore, the external control of a TEM is simplified by the new generation of TEMs (such as the Philips CM series) which are controllable through a serial communication port. In practice, the image pickup device most widely used is a video camera combined with an image intensifier (for example a Gatan camera). A measure of the quality of an image pickup device is the detection quantum efficiency (DQE), a normalized measure between 0 and 1 [14]. A well designed video camera combined with an image intensifier has a

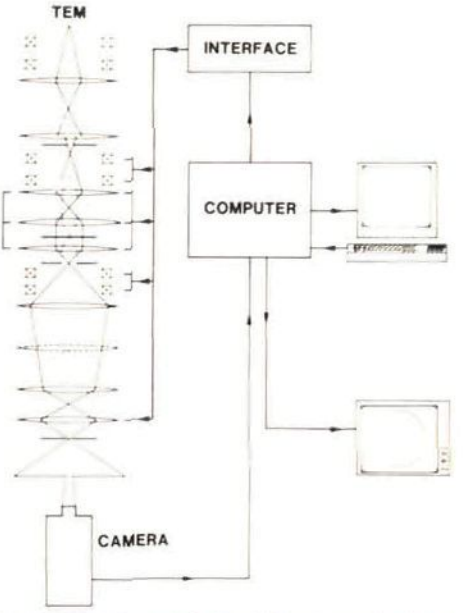

Fig. 1. Automatic control of a TEM using a closed loop construction.

DQE of nearly one and will outperform the human eye looking at the fluorescent screen in the TEM as to resolution and electron efficiency [15].

So, the instrumentation and computing power is available for implementation of an autotuning method that can, in principle, outperform a human operator. There remains the task to determine and design the best autotuning method. We require that the method functions with most specimens, and up to the same precision as a human operator, but with minimum electron dose. For many applications it is essential that the precision of the corrections after tuning is known [16–19]. Several methods for measurement and (automatic) correction of defocus, astigmatism and misalignment have been proposed and applied [20–24]. The only autotuning method tested in practice is based on measuring the image variance as a function of the parameter which is to be corrected [25,26]. The image variance is maximal for a TEM in Scherzer focus and minimal for a TEM in focus, well aligned and without astigmatism. Unfortunately, the method is specimen dependent and not electron-dose efficient.

In 1984 an autofocusing method was proposed [27] based on measuring a one-dimensional image displacement after inducing a beam tilt. The method was tested with simulations [27–29] and found to be electron-dose efficient and specimen independent, but not very robust in practice [30]. In this paper the method is extended to the estimation of defocus, astigmatism and beam tilt misalignment. The method is modified to be suitable for low-dose high resolution electron microscopy, if the specimen is a weak phase object. The method consists of measuring defocus, astigmatism and misalignment from pairs of two-dimensional images, formed with equal but opposite tilt angles in several azimuthal directions. Defocus and astigmatism is corrected subsequent to the correction of misalignment.

The structure of this paper is as follows: First the image formation in a TEM for tilted illumination is discussed (section 2.1). This is followed by measurement and modelling of the image measurements (section 2.2). Then, in section 2.3 a statistical parameter estimation approach is proposed leading to an estimator of defocus, astigmatism and misalignment. Next an optimal measuring strategy is designed for the estimation of defocus and astigmatism (section 3), which is tested with simulations in section 4. Finally, discussion and conclusions are presented in section 5.

2. Autotuning method

In this section the autotuning method is described which measures the defocus, astigmatism and beam tilt misaligment from images formed with induced tilts of the illuminating beam. Defocus and astigmatism are estimated from two different pairs of images. The images are obtained respectively by tilting the illumination in two perpendicular directions over two equal but opposite angles. Beam tilt misalignment (or: misalignment) is estimated from three images, one formed without beam tilt and two with equal but opposite tilt angles.

For large image detail (the low spatial frequencies in the image), the misalignment, the defocus and astigmatism can be derived from the beam tilt induced image displacement: For two images, formed with opposite beam tilt angles, the image displacement has a linear dependence on defocus; the defocus can be calculated from a measured image displacement. By measuring the image displacement for several azimuthal beam tilt angles, the astigmatism can be calculated. Because of spherical aberration, the image displacement is not exactly linear with beam tilt; it contains also higher-order terms. The beam tilt misalignment can be derived from the difference between two image displacements corresponding to zero beam tilt and beam tilts in two, opposite, directions.

However, also due to the spherical aberration, the amount of displacement of a particular image detail depends on its size, its spatial frequency. Especially the higher spatial frequencies are influenced by the lens aberrations and misalignment. Furthermore, the displacements corresponding to the higher frequencies can be estimated more precisely than those of the lower spatial frequencies. Consequently, it is important to measure the image displacement per spatial frequency in the image.

The cross correlation function is often used to estimate image displacements. Indeed, for the low spatial frequencies (visible at low magnifications) a mere image displacement results after inducing a beam tilt when the TEM is out of focus (wobbler). At higher magnifications (higher spatial frequencies), image displacement is not visible due to image blurring as result of the spherical aberration of the objective lens. Consequently, at high magnifications the cross-correlation function is not applicable to estimate the TEM parameters. However, the cross spectrum (defined as the Fourier transform of the cross-correlation function) is applicable, as the first derivative of the phase of the cross-spectrum (hereafter phase spectrum) with respect to the spatial frequency is equivalent to image displacement at a particular spatial frequency [31]. In other words: the image displacement at a spatial frequency is known if the phase of the cross-spectrum is known at that spatial frequency. Comparison of the measured phase spectrum with a mathematical model enables us to measure and correct the TEM parameters.

Thus, the TEM parameters are estimated from several pairs of images, obtained after tilting the illumination in several azimuthal directions. The TEM parameters are estimated from the phase of the cross-spectra of the pairs of images involved (phase-spectra). The method functions with weak phase objects as specimen, but is not sensitive to the power spectrum of the specimen. The method will tune the TEM, in principle, in one single step.

Bright field illumination, with a Weak Phase Object (WPO) as specimen, can be expressed in terms of a linear filter [32]. This filter, the phase contrast transfer function (PCTF), relates the (complex) spatial spectrum of the object to the (complex) spatial spectrum of the image. Hence, the PCTF is available as a mathematical model whose phase spectrum can be fitted – with respect to its unknown parameters – to the measured phase spectrum. Unfortunately, the measured images will be corrupted by shot noise, as the allowable electron dose used to image the specimen is limited [9]. Consequently, a heuristic parameter estimation procedure (e.g. procedure not especially adapted to noisy measurements) will result in parameter estimates which have an unknown precision (defined as the variance of the estimator), and is, in general, biased.

Therefore, a statistical parameter estimation approach [33] is essential to develop an autotuning method with a maximum precision for a given electron dose (or noise). First a model of the observations is derived: an expression for the phase spectrum (and its stochastic properties) which is estimated from two measured images. Secondly, an optimal estimator is designed for the estimation of defocus and astigmatism, with an expression for the achievable precision. Next a method is presented for the estimation of beam tilt misalignment. Finally, a practical performance criterion of the estimator is proposed.

2.1. Models of the phase spectra derived from linear image formation

For a WPO as specimen, there is a linear relation between the contrast variation in the bright field electron image C and the phase variation η of the electron wave function emerging from the specimen. Therefore, the image contrast can be modelled as [34]

$$C(\boldsymbol{x}, \theta) = F^{-1}(\tilde{\eta}(\boldsymbol{k})\, \Gamma(\boldsymbol{k}; \theta)), \tag{1}$$

where $\boldsymbol{x}$ is the place scaled to the object plane, θ a vector of TEM parameters describing defocus, astigmatism and beam tilt, $\boldsymbol{k}$ the spatial frequency of the image measured (related to a position in the back focal plane), $\tilde{\eta}$ the Fourier transform of η and Γ the (complex) transfer function known as the PCTF; F^{-1} denotes the two-dimensional inverse Fourier transform. The contrast C is defined as

$$C(\boldsymbol{x}; \theta) = \left[I(\boldsymbol{x}; \theta) - \bar{I} \right] / \bar{I}, \tag{2}$$

where $\bar{I}$ is the average intensity $I(\boldsymbol{x}; \theta)$ over $\boldsymbol{x}$.

Consider two images, $C_1(\boldsymbol{x}; \theta_1)$ and $C_2(\boldsymbol{x}; \theta_2)$, formed with parameter vectors θ_1 and θ_2 respectively. The parameter vectors θ_1 and θ_2 are unknown, except for an induced and known adjustment $\Delta\theta$, or

$$\theta_2 = \theta_1 + \Delta\theta, \tag{3}$$

where θ_1 is an unknown vector of TEM parameters and $\Delta\theta$ the vector of known adjustments.

The full expression of the PCTF is written as [35]

$$\Gamma(\boldsymbol{k};\,\theta) = \mathrm{i}\left[e(\boldsymbol{k}_0+\boldsymbol{k})\,\mathrm{e}^{-\mathrm{i}[\chi(\boldsymbol{k}_0+\boldsymbol{k})-\chi(\boldsymbol{k}_0)]} - e(\boldsymbol{k}_0-\boldsymbol{k})\,\mathrm{e}^{\mathrm{i}[\chi(\boldsymbol{k}_0-\boldsymbol{k})-\chi(\boldsymbol{k}_0)]}\right], \quad (4)$$

with $e(\boldsymbol{k})$ the envelope function modelling beam divergence and defocus spread (given in ref. (13)), $\chi(\boldsymbol{k})$ the wave aberration function of the objective lens

$$\chi(\boldsymbol{k}) = \pi\left[0.5k^4 - (D-0.5A)k^2 - A(\boldsymbol{k}\cdot\boldsymbol{a})^2\right], \quad (5)$$

with the spatial frequency $\boldsymbol{k}$ expressed in Gl^{-1} with

$$1\ \mathrm{Gl} = \left(C_s\lambda^3\right)^{1/4}, \quad (6)$$

and the beam tilt $\boldsymbol{k}_0 = (K_{0_x},\ K_{0_y})^{\mathrm{T}}$ expressed in Gl^{-1} with K_{0_x} and K_{0_y} the components of the beam tilt in perpendicular directions (T indicates the transpose of the vector), C_s is the constant of spherical aberration, and λ the wavelength of the electrons. The parameter vector θ is defined as

$$\theta = \left(D,\ A_x,\ A_y,\ K_{0_x},\ K_{0_y}\right)^{\mathrm{T}}, \quad (7)$$

with the defocus D expressed in Sch with

$$1\ \mathrm{Sch} = \left(C_s\lambda\right)^{1/2}, \quad (8)$$

astigmatism $\boldsymbol{a}A = (A_x,\ A_y)^{\mathrm{T}}$ with T the amount of astigmatism (defined as the difference between maximal and minimal defocus), A_x and A_y the components of astigmatism in perpendicular directions, and $\boldsymbol{a}$ the azimuthal direction of the astigmatism pointing in the direction of maximal defocus. In this expression of the PCTF, three-fold astigmatism is assumed to be negligible relative to the other aberrations.

The phase terms in the PCTF can be rewritten in an even (E) and odd (O) term with respect to the frequency [36], changing the expression of the PCTF into

$$\Gamma(\boldsymbol{k};\,\theta) = \mathrm{i}\left[e(\boldsymbol{k}_0+\boldsymbol{k})\,\mathrm{e}^{-\mathrm{i}[\mathrm{E}(\boldsymbol{k};\,\theta)+\mathrm{O}(\boldsymbol{k};\,\theta)]} - e(\boldsymbol{k}_0-\boldsymbol{k})\,\mathrm{e}^{\mathrm{i}[\mathrm{E}(\boldsymbol{k};\,\theta)-\mathrm{O}(\boldsymbol{k};\,\theta)]}\right], \quad (9)$$

with

$$\mathrm{E}(\boldsymbol{k};\,\theta) = 2\pi\left\{\tfrac{1}{4}|\boldsymbol{k}|^4 + \tfrac{1}{2}\left[|\boldsymbol{k}_0|^2 - \left(D-\tfrac{1}{2}A\right)\right]|\boldsymbol{k}|^2 + (\boldsymbol{k}\cdot\boldsymbol{k}_0)^2 - \tfrac{1}{2}A(\boldsymbol{k}\cdot\boldsymbol{a})^2\right\}, \quad (10)$$

$$\mathrm{O}(\boldsymbol{k};\,\theta) = 2\pi\left\{\left[|\boldsymbol{k}|^2 + |\boldsymbol{k}_0|^2 - \left(D-\tfrac{1}{2}A\right)\right]\boldsymbol{k}\cdot\boldsymbol{k}_0 - A(\boldsymbol{k}\cdot\boldsymbol{a})(\boldsymbol{k}_0\cdot\boldsymbol{a})\right\}. \quad (11)$$

Beam tilt misalignment is separated from the induced beam tilt $\boldsymbol{t}$ by modelling it as an extra beam tilt $\boldsymbol{m} = (M_x,\ M_y)^{\mathrm{T}}$, with

$$\boldsymbol{k}_0 = \boldsymbol{t} + \boldsymbol{m}, \quad (12)$$

where $\boldsymbol{t} = (T_x,\ T_y)^{\mathrm{T}}$ is the induced beam tilt.

The effect of beam divergence and defocus spread is modelled by an envelope function

$$e(\boldsymbol{k}) = \mathrm{e}^{-s^2|\nabla\chi(\boldsymbol{k})-\nabla\chi(\boldsymbol{k}_0)|^2/4}\,\mathrm{e}^{-\pi^2d^2[|\boldsymbol{k}|^2-|\boldsymbol{k}_0|^2]^2/2}, \quad (13)$$

with the gradient of the wave aberration function given by

$$\nabla\chi(\boldsymbol{k};\,\theta) = 2\pi\left\{\left[|\boldsymbol{k}|^2 - \left(D-\tfrac{1}{2}A\right)\right]\boldsymbol{k} - A(\boldsymbol{k}\cdot\boldsymbol{a})\boldsymbol{a}\right\}, \quad (14)$$

where s is the rms value of the beam divergence and d the rms value of the defocus spread caused by both energy spread and objective lens variations.

The envelope function e (eq. (13)) can be interpreted as a virtual aperture, positioned in the back focal plane [37–40]. This virtual aperture is not a real aperture, but is a mathematical description for the effect of beam divergence and defocus spread. Beam tilt causes a displacement of the Fourier transform of the object in the back focal plane along his (virtual) aperture, see fig. 2. Consequently, on the one side more spatial frequency components are included in the non-zero region of the envelope than on the other side of the aperture. We define the region where three beams interfere which are (almost) equally attenuated by the envelope function as the double side band (DSB) imaging region. In the frequency region

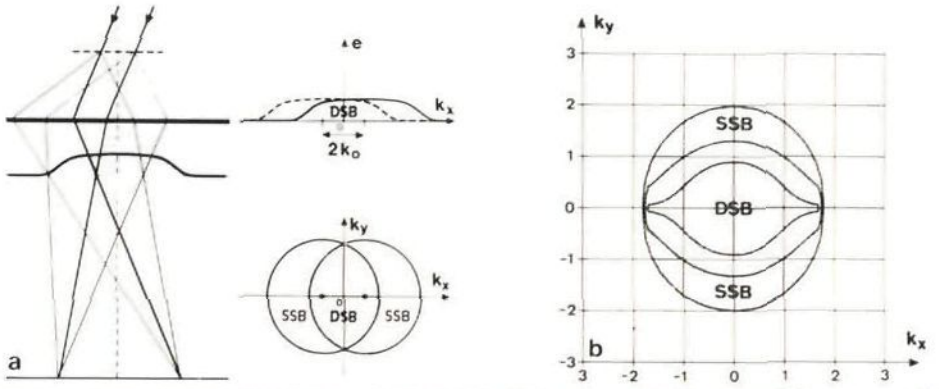

Fig. 2. (a) Double and single sideband imaging (DSB and SSB). Imaging of one spatial frequency of the specimen with tilted illumination (top left), and a contour of the corresponding envelope functions as a function of the frequency (top right). (b) Illustration of a DBS and SSB frequency region.

where one side is included within the envelope, two-beam interference takes place. This type of imaging is generally known as single side band (SSB) imaging. All estimators derived in this paper are valid for the DSB frequency region. The estimators for the SSB frequency region can be derived similarly. Note that the DSB and SSB frequency regions are determined by the defocus spread, beam divergence, the TEM parameters and the induced beam tilt. DSB imaging is the main type of imaging for relatively small tilt angles (fig. 3), SSB is the main type of imaging for relatively large tilt angles.

Thus, in the DSB region the attenuation by the envelope is (almost) equal for all frequency components, or:

$$e(\boldsymbol{k}_0 - \boldsymbol{k}) \approx e(\boldsymbol{k}_0 + \boldsymbol{k}) = e_{\mathrm{DSB}}(\boldsymbol{k}), \tag{15}$$

with the corresponding PCTF given by

$$\Gamma(\boldsymbol{k};\, \theta) = 2e_{\mathrm{DSB}}(\boldsymbol{k}) \sin\{E(\boldsymbol{k};\, \theta)\}\, \mathrm{e}^{\mathrm{i}O(\boldsymbol{k};\, \theta)}, \tag{16}$$

and the model for the phase spectrum

$$\begin{aligned} P(\boldsymbol{k};\, \theta) &= \arg\{\Gamma(\boldsymbol{k};\, \theta)\, \Gamma^*(\boldsymbol{k};\, \theta + \Delta\theta)\} \\ &= -O(\boldsymbol{k};\, \theta) + O(\boldsymbol{k};\, \theta + \Delta\theta). \end{aligned} \tag{17}$$

Beam tilt misalignment is estimated from three images, one formed without an induced beam tilt ($\boldsymbol{t}_1 = 0$), and two with equal but opposite tilt angle ($\boldsymbol{t}_2 = -\boldsymbol{t}_3$)). Consider the two phase models of the image without beam tilt ($\boldsymbol{t}_1$) and with induced beam tilt ($\boldsymbol{t}_2$ and $\boldsymbol{t}_3$). The difference of those two phase models P' is given by

$$\begin{aligned} P'(\boldsymbol{k};\, \theta) &= P_{\mathrm{m1}}(\boldsymbol{k};\, \theta) - P_{\mathrm{m2}}(\boldsymbol{k};\, \theta) \\ &= 4\pi\left[t^2(\boldsymbol{k}\cdot\boldsymbol{m}) + 2(\boldsymbol{m}\cdot\boldsymbol{t})(\boldsymbol{k}\cdot\boldsymbol{t})\right], \end{aligned} \tag{18}$$

with $\theta = (D,\, A_1,\, A_2,\, M_x,\, M_y)^{\mathrm{T}}$, and $P_{\mathrm{m1}}(\boldsymbol{k};\, \theta)$ and $P_{\mathrm{m2}}(\boldsymbol{k};\, \theta)$ the phase models of the image without an induced beam tilt ($\boldsymbol{t} = 0$), and the images with an induced beam tilt of $\boldsymbol{t}$ and $-\boldsymbol{t}$, respectively. In the absence of beam tilt misalignment ($\boldsymbol{m} = 0$), P' equals zero, as P_{m1} and P_{m2} are equal, independent of defocus or astigmatism. This alignment method aligns the TEM, in fact, on a coma-free axis. In section 2.3 we will discuss the estimation procedure for the TEM parameters in detail.

Defocus and astigmatism are estimated when beam tilt misalignment has been corrected, from two different pairs of images. One pair of images is obtained by tilting the illumination over two equal but opposite angles ($\pm\boldsymbol{t}_1$). The other pair of images is obtained by tilting the illumination in the perpendicular direction over two equal but opposite directions ($\pm\boldsymbol{t}_2$, with $\boldsymbol{t}_1 \cdot \boldsymbol{t}_2 = 0$ and $|\boldsymbol{t}_1| = |\boldsymbol{t}_2|$). The corresponding model of the phase of

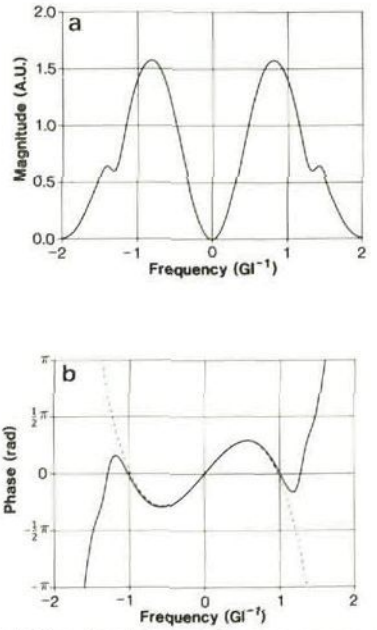

Fig. 3. DSB model (dashed) of the phase spectrum when varying beam tilt compared to the phase spectrum directly calculated from the PCTF (solid). The magnitude (a) and phase (b) with $t = (0.2, 0)^T$ and $D = 1$, and without astigmatism.

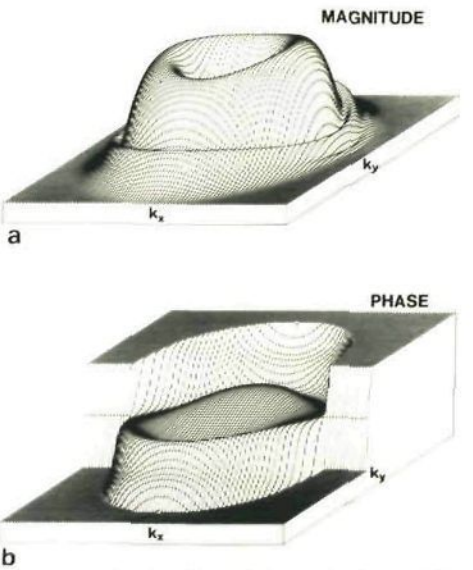

Fig. 4. A two-dimensional plot of the magnitude (a) and the phase of the PCTF (b), with a defocus $D = 1.5$, beam tilt $t = (0.2, 0)^T$ and without astigmatism. For scaling, see fig. 3.

the cross spectrum (phase spectrum) of each pair of images is given by

$$P_\alpha(k;\theta_\alpha) = 4\pi\{[k^2 + t_\alpha^2 - (D - \tfrac{1}{2}A)]k\cdot t_\alpha - A(k\cdot a)(t_\alpha\cdot a)\}, \quad \alpha = 1, 2, \quad (19)$$

with $\theta_\alpha = (D,\ A_x,\ A_y,\ -T_{\alpha x},\ -T_{\alpha y})^T$, and $T_{\alpha x}$ and $T_{\alpha y}$ known. The phase and magnitude of the PCTF with a defocus of 1 and a beam tilt of $(0.2, 0)^T$ is given in fig. 4. Note that two pairs of images are needed to estimate defocus and astigmatism; one pair of images is ambiguous for the determination of three parameters (D, A_x, A_y) from the two independent terms in eq. (19).

To develop a precise estimator of the TEM parameters, the stochastic properties of the phase disturbances in the calculated phase spectra must be known. Therefore, first an analysis of the estimation of the phase spectrum and its stochastic properties will be carried out.

2.2. Estimation of the phase spectrum

Images C_1 and C_2 have to be sampled before they can be processed by a digital computer. Therefore, the images are modelled as two-dimensional discrete spatial processes. The theoretical analysis, leading to a precise estimator of defocus and astigmatism, will employ discrete Fourier analysis of discrete processes. To prevent mismodelling, it is essential that there be no aliasing of frequencies. Therefore, it is assumed that the magnification is chosen properly. Furthermore, it is assumed that an image is (over)sampled with equally sized, rectangular, adjacent sensors which detect every incident electron (DQE ≈ 1). Consequently, noise in a measured image is due to contribution of a finite number of electrons to it. This type of noise is known as shot noise.

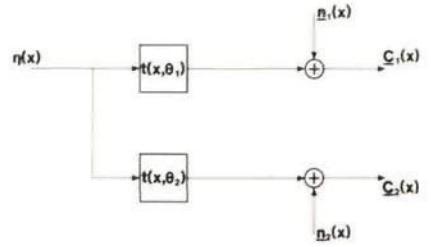

Fig. 5. Formation of two noisy images. The wave function emerging from the specimen $\eta(x)$ is influenced by the TEM, modelled as a convolution with t, a deterministic, time invariant spatial function depending on the parameter vector θ (t is equivalent to the PCTF in the frequency domain). The two measured image intensities C are disturbed by a stochastic process $\underline{n}(x)$.

Unfortunately, practical measuring systems (photographic material or a videocamera) could introduce extra, more dominant, noise (DQE < 1). This noise is modelled as a zero mean, two-dimensional, discrete process which is purely random (the noise contribution to one image point is independent of the contribution to another image point), additive to the image and stationary. The image is considered to be one particular, fixed realization of a different stochastic process, independent of the noise.

Therefore, a measured image can be modelled as a two-dimensional discrete and deterministic image, disturbed by a stochastic process, see fig. 5. Consider two images, $\underline{C}_1$ and $\underline{C}_2$, formed with parameter vectors θ_1 and θ_2 respectively,

$$\underline{C}(x;\, \theta_1) = C_1(x;\, \theta_1) + \underline{n}_1(x), \tag{20}$$

$$\underline{C}_2(x;\, \theta_2) = C_2(x;\, \theta_2) + \underline{n}_2(x), \tag{21}$$

where $\underline{n}_1$ and $\underline{n}_2$ are noise terms (underlined quantities are stochastic processes) and θ_1 and θ_2 vectors of TEM parameters corresponding to image C_1 and C_2 respectively.

The phase spectrum $\underline{\Phi}_{uv}$ of images $\underline{C}_1$ and $\underline{C}_2$ can be written as

$$\underline{\Phi}_{uv} = P(k_{uv};\, \theta) + \underline{\epsilon}(k_{uv};\, \theta_1;\, \theta_2), \tag{22}$$

with

$$P(k_{uv};\, \theta) = \arg\left[\Gamma_1(k_{uv};\, \theta_1)\; \Gamma_2^*(k_{uv};\, \theta_2)\right], \tag{23}$$

where Γ denotes the PCTF (eq. (9)) at frequency k_{uv}, $\arg\{\cdots\}$ the argument of the bracketed complex quantity, * a complex conjugate, Φ_{uv} represents the phase at frequency k_{uv}, P models the phase spectrum and ϵ the phase disturbances due to the noise. Note that the expectation of the phase spectrum is independent of the object η, as defined in (1). Furthermore, the parameter vectors θ_1 and θ_2 influence the stochastic process ϵ (see appendix A).

The phase spectrum Φ_{uv} can be estimated from two images with [31]

$$\Phi_{uv} = \arg\left[\sum_{k=1}^{N}\sum_{l=1}^{N} X_{1kl}(u,\, v)\; X_{2kl}^*(u,\, v)\right], \tag{24}$$

where $X_{1kl}(u, v)$ and $X_{2kl}(u, v)$ denote the two-dimensional discrete Fourier transform (DFT) of the klth weighted segment of samples from the images $\underline{C}_1$ and $\underline{C}_2$, respectively. There are N^2 (possibly overlapping) square image segments. The two-dimensional DFT of an image segment, supposed to contain M^2 samples, is calculated with the fast Fourier transform (FFT) algorithm. Under asymptotic conditions the phase estimates have a Gaussian distribution with

$$E\{\underline{\Phi}_{uv}\} = P(k_{uv};\, \theta), \tag{25}$$

$$\mathrm{var}\{\underline{\Phi}_{uv}\} = \frac{1}{|W_{uv}|} - 1, \tag{26}$$

$$\mathrm{cov}\{\underline{\Phi}_{uv},\, \underline{\Phi}_{kl}\} = 0 \quad \text{for} \quad uv \neq kl, \tag{27}$$

where E denotes the expectation operator, $\mathrm{var}\{\cdots\}$ the variance and $\mathrm{cov}\{\cdots\}$ the covariance. W_{uv} represents the (if not known: the estimated) complex coherence spectrum [41,42] at frequency k_{uv}, given by:

$$W_{uv} = \frac{S_{12}(u,\, v)}{\left[S_{11}(u,\, v)\; S_{22}(u,\, v)\right]^{1/2}}, \tag{28}$$

where $S_{12}(u, v)$ is the complex cross-spectral density function of the images $\underline{C}_1$ and $\underline{C}_2$, respectively, at frequency k_{uv}. $S_{11}(u, v)$ and $S_{22}(u, v)$ are the power spectral density functions (PSDFs) of the images $\underline{C}_1$ and $\underline{C}_2$, respectively, at frequency k_{uv}. It can be shown that the asymptotic conditions are met, when images are analysed of 512^2

points using a segment size of 64 ($N = 8$ and $M = 64$).

Summarizing, the stochastic properties of the phase spectrum are modelled and expressed in terms of a signal $E\{\underline{\Phi}_{uv}\}$ and a noise term $\mathrm{var}\{\underline{\Phi}_{uv}\}$ (phase disturbances). Next, the estimator of defocus and astigmatism can be designed.

2.3. Estimation of the TEM parameters

First, the achievable precision with which defocus and astigmatism can be estimated will be derived. Secondly, the optimal estimator of defocus and astigmatism is designed, followed by the estimator of beam tilt misalignment. Finally, a practical performance criterion of the estimator of defocus and astigmatism is proposed.

2.3.1. Achievable precision of defocus and astigmatism estimates

The achievable tuning precision is given by the Cramer–Rao lower bound (CRLB) [33]. The CRLB is a lower bound on the variance of any unbiased estimator and can therefore be used to assess the relative performance of any estimator designed.

Let $\mathrm{cov}(\theta_i, \theta_j)$ be the ijth element of the $L \times L$ covariance matrix V of θ, where θ_i is an unbiased estimator of the ith parameter of the $L \times 1$ TEM parameter vector θ. Then, for all unbiased estimators θ_i, the diagonal elements of $\mathrm{cov}(\theta_i, \theta_j)$ (the variances) cannot be smaller than the corresponding diagonal elements of the CRLB, or

$$\mathrm{var}(\theta_i) \geq M_{ii}^{-1} \quad \text{for} \quad i = 1, \ldots, L,$$

with M_{ii}^{-1} the ith diagonal element of M^{-1}, which is the inverse of the $L \times L$ information matrix M, with the ijth element given by

$$M_{ij} = \sum_{B,\alpha}\sum \left(\sigma_{uv}^{-2} \frac{\partial P_\alpha(k_{uv};\, \theta_\alpha)}{\partial \theta_i} \frac{\partial P_\alpha(k_{uv};\, \theta_\alpha)}{\partial \theta_j} \right), \tag{29}$$

where σ_{uv}^2 is the variance of the phase disturbances $\mathrm{var}\{\underline{\Phi}_{uv}\}$, $\alpha = 1, 2$ accounts for the two phase spectra as defined in eq. (19), B is the frequency region used in the estimation, $\partial P_\alpha / \partial \theta_i$ denotes the first derivative of the model with respect to the parameter θ_i.

So, given the model P_α and the variance of the phase disturbances $\mathrm{var}\{\underline{\Phi}_{uv}\}$, the achievable precision can be computed with which defocus and astigmatism can be tuned using the two phase spectra. The maximum likelihood (ML) estimator achieves this precision asymptotically.

2.3.2. Estimator of defocus and astigmatism

Consider the phase model for the estimation of defocus and astigmatism (19) and (22), and fig. 5. Note that the model is linear in defocus D, but nonlinear in the astigmatism components A_x and A_y. Therefore, no closed form for the estimator of defocus and astigmatism exists, and we are forced to use an iterative method for numerical estimation. Fortunately, the phase disturbances have a Gaussian distribution and the equation errors are white (appendix A). Consequently, the ML estimator of the TEM parameter vector θ is equivalent with a weighted least squares (LS) estimator [33]. Furthermore, as the phase disturbances are mutually uncorrelated, the LS criterion for the LS estimator is

$$J_1(\theta;\, \Delta\theta) = \sum_{B,\alpha}\sum \left\{ \Omega_{uv} \left[\Phi_{uv} - P_\alpha(k_{uv};\, \theta_\alpha) \right]^2 \right\}, \tag{30}$$

where Ω_{uv} is the inverse of the variance of $\underline{\epsilon}$ given by (26) (the weighting function). The parameter vector θ is estimated by minimizing this criterion.

Unfortunately, the phase measurements Φ_{uv} give phases only in the range $[-\pi, \pi]$, and can therefore differ from the actual phase by an integral multiple of 2π. However, these problems caused by periodic phase estimates can be avoided with the criterion [43]

$$J_2(\theta;\, \Delta\theta) = \sum_{B,\alpha}\sum \left\{ \Omega_{uv} \cos\left[\Phi_{uv} - P_\alpha(k_{uv};\, \theta_\alpha) \right] \right\}. \tag{31}$$

The estimator using the cosine of the phase differences will be referred to as the COS estimator. The importance of the weighting function is illustrated in fig. 6; the phase estimates at frequencies where the modulus of the cross-spectrum is

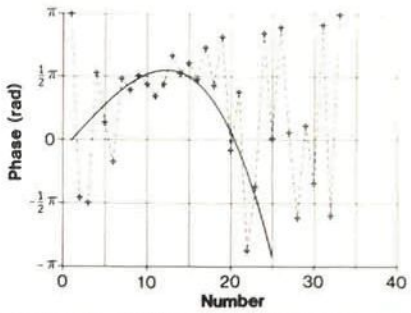

Fig. 6. A section of the simulated phase spectra, used to generate the results presented in table 3, as an illustration of the dependence of the variance of the phase on the modulus of the cross spectrum. The Fourier coefficients numbered 8–15 correspond to a strong transfer, the other coefficients correspond to a weak transfer, and consequently, the phase estimates have a relatively large variance.

strong have a smaller variance than the phase estimates where the modulus of the cross-spectrum is weak.

Having thus designed the optimal estimator of defocus and astigmatism, we next discuss the estimator of beam tilt misalignment.

2.3.3. Estimator of misalignment

Beam tilt misalignment is estimated from three images, one formed without beam tilt ($t_1 = 0$), and two with equal but opposite tilt angles ($t_2 = -t_3$). Consider the phase model for the estimator of misalignment (18). The difference between the phase spectrum of the pair of images formed with a tilt t_1 and t_2, and the phase spectrum of the pair of images formed with a tilt t_1 and t_3 defines the misalignment of the TEM.

Similar to the model of defocus and astigmatism (19), the phase model can be fitted to the measured phase spectrum with respect to the parameters describing misalignment. An optimal estimator of misalignment can be derived analogous to the estimator of defocus and astigmatism, but is not presented in this paper.

However, the model for the estimation of misalignment differs in some respects from the model for the estimation of defocus and astigmatism and one should be careful in designing the optimal estimator. First, the components of misalignment are linear in the model, and a closed-form estimator can be designed. Secondly, the equation errors are colored, see appendix A. Generally, this is highly undesirable in estimation problems since it leads to bias in the estimates. The remedy is here to set the defocus of the TEM such that the equation errors are whitened as well as possible.

2.3.4. Performance criterion for the estimation of defocus and astigmatism

Three parameters are required to model defocus and astigmatism of the TEM (D, A_1 and A_2). Each parameter is estimated with a certain precision. To evaluate the performance of the autotuning method a simple performance criterion is proposed which takes into account the precision of the corrections of defocus and astigmatism (result) and the required electron dose for tuning (costs).

The definition of precision of correction for defocus and astigmatism P_d is subjective. It depends on the specific experiment performed on the TEM. We define the precision P_d using the maximum of the effective directional defocus [36] for each azimuthal angle as

$$D_{\text{eff}} = |D| + \tfrac{1}{2}A. \tag{32}$$

The tuning precision of the correction of defocus and astigmatism will be defined as the standard deviation of D_{eff} after correction, which is a stochastic variable $\underline{D}_{\text{cor}}$ given by:

$$\underline{D}_{\text{cor}} = |\underline{D} - D| + \tfrac{1}{2}\left[(\underline{A}_1 - A_1)^2 + (\underline{A}_2 - A_2)^2\right]^{1/2}. \tag{33}$$

In the previous sections we showed that the estimators $\underline{D}$, $\underline{A}_1$ and $\underline{A}_2$ are unbiased, and have a jointly Gaussian distribution with a covariance matrix V. The derivation of the probability density function is cumbersome due to the severe correlation between $\underline{D}$, $\underline{A}_1$ and $\underline{A}_2$. Therefore, the precision of correction of defocus and astigmatism $P_d(V)$ is calculated numerically [44], as explained in appendix B.

In the next section two types of numerical experiments are described concerning the estima-

tion of defocus and astigmatism. First, the measuring strategy is designed for the optimum choice of variation of the TEM parameters, by calculating the achievable precision, independent of the specific estimator applied (CRLB). Secondly, a series of image simulations is carried out to compare the performance of our specific estimator design to this achievable performance (CRLB).

3. Practical design of the autotuning method

The autotuning method has to be optimally organized, or designed to minimize the tuning precision, given a certain electron dose incident on the specimen.

The precision of autotuning depends on several, so called "independent" variables (related to the electron dose, image recording system, spectral analysis, the PSDF of the specimen and TEM) which have to be chosen, if possible, to design the autotuning method. The range of values which these variables can assume during the measurements is called the "domain of action". Optimal experimental design [45] is now defined as choosing a combination of independent variable values in the domain of actions for the best tuning precision, with the lowest number of electrons.

Unfortunately, the tuning precision depends strongly on the "dependent" variables: the vector of unknown TEM parameters which has to be estimated. Moreover, the phase disturbances in the estimated phase spectra are also depending on the unknown TEM parameters. Conventional experimental design techniques are not applicable to this kind of problem, and therefore, in what follows, we will follow an intuitive approach.

A two-step tuning procedure is suggested, which can be described conveniently in mathematical terms. Let the status of the TEM, with respect to the unknown TEM parameters, be defined by a vector of TEM parameters in the multi-dimensional parameter space. The origin represents a perfectly tuned TEM (that is: the TEM parameters have the desired setting). Points within a subspace T around the origin represent a satisfactorily tuned TEM. A second subspace R can be defined, representing an area where tuning will be relatively precise (hereafter reference area). Suppose that from the current TEM status (starting point), the tuning will be relatively imprecise when the TEM is adjusted directly into T. The two-step tuning procedure will first adjust the TEM from the starting point into R and then into T. The two-step procedure will be much more precise than tuning in one single step, when using the same dose.

It is clear that the procedure to adjust the TEM from the starting point to the reference area is quite different from the procedure to adjust the TEM from the reference area to the tuning area. Before the first step, the status of the TEM is unknown. So, the lack of a priori knowledge hampers the tuning method described in the previous sections. First the weighting function has to be estimated from the images. Secondly, the frequency region used to determine the DSB region is not exactly known, and has to be estimated. After the first tuning step, we can use the knowledge on the weighting function and frequency region, and allow the autotuning method a precise second tuning step. Note that the second tuning step requires a starting point within the reference area. Therefore, it might be necessary to repeat the first tuning step using more electrons than in the first tuning attempt, to improve the precision of estimation to ensure a starting point within the reference area.

In the next sections, we discuss the second tuning step, for the estimation of defocus and astigmatism. First, the independent variables of the autotuning method are discussed.

3.1. Instrumental parameters determining the precision

Four types of independent variables can be distinguished. First, the variables related to the dose. Dose rate and measuring time can freely be chosen, provided that the total dose has a predefined value. Moreover, the dose distribution between the two tuning steps can freely be chosen. The best dose rate and measuring time depends on the characteristics of the image recording system. A high dose rate combined with a short measuring

time (flashed illumination) has the advantage that drift, vibration and stray field effects can be overcome. The feasibility of flashed illumination is discussed in a paper by Van der Mast and Koster [46].

Secondly, there are variables related to the image recording system: the sampling interval Δx and the number of samples, in both x- and y-direction respectively. Consider an ideal image recording system with a DQE = 1 (for the non-ideal case [14]), with square adjacent pixels and an equal number of pixels in x- and y-direction. The estimator will be less precise with increasing (reduced) sensor dimensions Δx^2. Therefore, Δx^2 should be chosen to be maximum, i.e., just no aliasing may occur. The ratio of the sensor size in reduced coordinates to the physical sensor size is inversely proportional to the magnification of the TEM. Therefore, the physical sensor size is not of importance, as the magnification can always be chosen so as to attain the required value for the reduced sensor size. Thus, only the number of sensors is left to optimize. The size of the image that can be recorded is limited. Consequently, to increase the number of sensors, the physical sensor size has to be decreased.

In the third place, variables related to the spectral analysis are present. These are: segment size M, segment overlap O, number of segments N and window type. These variables have to fulfill two requirements: (1) The phase disturbances must be sufficiently small to justify the autotuning method described in section 2. (2) The spectral estimate must attain an adequate resolution compared to the bandwidth of the theoretical real and imaginary part of the cross spectrum of the two images. This leads to the following requirements: (1) The ratio of the number of segments (N) to the segment size (M) should be large to reduce the variance of the phase estimates. (2) The Fourier transform of the weighted segment should have a main lobe that is narrower than the finest detail in the real or imaginary part of the cross spectra of the images. (3) The window shape must be chosen so as to reduce the sidelobes of the Fourier transform. (4) Segment overlapping must be used to increase both M and N with a given number of pixels. As the percentage of overlap increases, however, the computer requirements increase rapidly.

Finally, the variables related to the TEM are discussed. When estimating defocus and astigmatism, the beam tilt components T_x and T_y are independent variables. The choice for these independent TEM parameters is strongly related to the two-step tuning procedure, and implies therefore an analysis of the size and shape of the reference area R. The actual design of the two-step procedure is carried out in the next section.

3.2. Design strategy of the two-step autotuning procedure

An important aspect of the two-step autotuning method is the definition of the reference area R from which the TEM is adjusted very precisely into the tuning area T. The reference area is determined by the value of the independent variables. The CRLB, as defined in section 2.3.1, is a powerful tool to find this reference area. The CRLB can be used to calculate, a priori, the maximum achievable tuning precision as a function of the independent variables and assumed values of the unknown TEM parameters. In other words, the CRLB defines the "best" covariance matrix, and consequently, the "best" tuning precision.

The calculation of the CRLB is carried out using a negative exponential form for the PSDF of the specimen, modelling a thin carbon film [47]. The spectrum of the phase disturbances will be equal to N_0^2. N_0 will be referred to as noise level. Both PSDF of the specimen (S_s) and phase disturbances (S_n) will be normalized and are defined by

$$S_s(u, v) = e^{-|k_u| / k_0} \quad \text{where } k_0 = 1.8, \tag{34}$$

$$S_n(u, v) = N_0^2, \tag{35}$$

with

$$N_0^2 \sim (\bar{d} T M^2 \Delta x^2 \, \mathrm{DQE})^{-1} \tag{36}$$

where $\bar{d}$ is the dose rate and T the measuring time.

We assume an ideal image recording system with 512^2 square adjacent sensors. We choose a

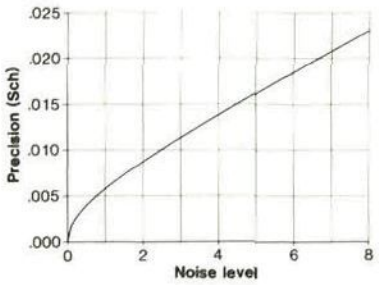

Fig. 7. The tuning precision P_d as a function of the noise level N_0 (calculation of the CRLB). Relevant TEM parameters are: defocus $D = 1$, no astigmatism and a beam tilt $\boldsymbol{t} = (0.2, 0)^T$.

segment size M equal to 64, a satisfactory compromise between variance and resolution with respect to the Fourier coefficients. The maximum frequency in the case of the DSB imaging is 2, which leads to optimal square sensor dimensions in reduced coordinates of 0.25 (just no aliasing). This can be accomplished by a suitable choice of magnification. The PCTF is taken as that of a 120 kV TEM with a constant of spherical aberration of 2 mm (so 1 Gl = 0.52 nm, and 1 Sch = 82 nm), a defocus spread of 0.2, and a beam divergence of 0.14. The noise level is equal to two. The relation between noise level and electron dose is complicated [29] and summarized in section 4.4. Under certain measuring conditions a noise level of two is equivalent to a dose of 26000 electrons per nm^2. The dose required for tuning D_{aut} is approximately related to the noise level N_0 by $D_{aut} \sim N_0^2$.

The influence of the noise level on the tuning precision is given in fig. 7. When the noise level is higher than 0.5, the relation between tuning precision and noise level is linear. The tuning precision values, which will be presented in the next section for specific noise levels, can therefore be easily rescaled to other noise levels.

The next section describes a number of numerical experiments, which give insight to the complex optimization problem under study. Some intuitive understanding of the results is possible considering the following. The value of the precision depends on the elements of the CRLB which can be separated into three factors (eq. (29)). The first factor is the variance of the phase estimates. These are small when transfer is strong. The second and third factors are equal to the derivative of the phase model with respect to a TEM parameter. Consider the diagonal elements of the product of the second and third factors: the squared derivatives of the phase model with respect to one parameter. These diagonal elements can be interpreted as "sensitivities" to changes in the phase model with respect to the parameter varied. Intuitively, it can be understood that strong transfer combined with high sensitivity will lead to precise estimates. Furthermore, the size of the frequency region (B) will be highly relevant with respect to the precision. In the numerical experiments, the DSB frequency region (defined by (15)) is approximated by that frequency region for which the ratio of $e(\boldsymbol{k}_0 - \boldsymbol{k})$ to $e(\boldsymbol{k}_0 + \boldsymbol{k})$ is between 0.8 and 1.25. The effects mentioned above are continually competing; high sensitivity often leads to weak transfer and a small frequency region of interest. Therefore, one may expect that there exists a setting optimally compromising both effects.

3.3. Reference area for the estimation of defocus and astigmatism

The tuning precision is first calculated as a function of the direction of astigmatism. Fig. 8 shows that the tuning precision is relatively insensitive to the direction of astigmatism. Although the square roots of the individual elements of the CRLB (the standard deviations of D, A_x and A_y) vary, their combined effects cancel out. Moreover, the roles of A_x and A_y are reversed when the angle of astigmatism exceeds $\pi/2$, because the two phase spectra are calculated from images with orthogonal tilt directions. It is concluded that the angle of astigmatism is of little influence for the tuning precision.

The tuning precision as a function of defocus has also been calculated and the influence of defocus appeared to be large. All elements of the CRLB behave similarly. For a noise level equal to two, a beam tilt of $(0.2; 0)^T$, and astigmatism of 0.2, the tuning precision is best for defocus values just above, and just under focus. Very near focus (0.2), the estimation will be imprecise. The depen-

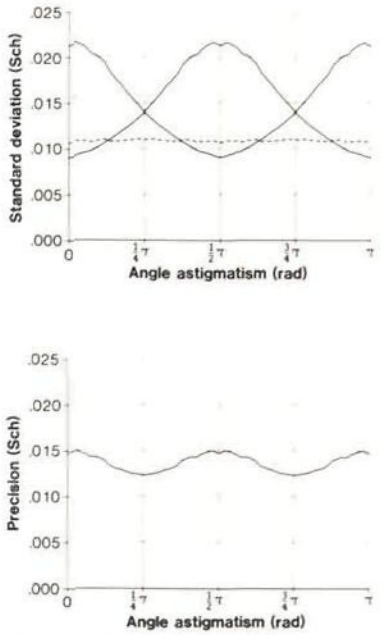

Fig. 8. The standard deviations of D, A_x and A_y and tuning precision P_0 as a function of azimuthal angle of astigmatism (calculation of the CRLB). Relevant TEM parameters are: defocus $D = 1$, beam tilt $t = (0.2, 0)^T$ and a noise level $N_0 = 2$.

dence on focus is understandable considering the strength of transfer, which is optimal for $D = 1$, and minimal for $D = 0.2$.

The reference area for the defocus and astigmatism values is given in fig. 9. Again the reference area is large: astigmatism variation from 0 to 3, combined with a defocus variation between 1 and 3, gives the best tuning precision. A smaller reference area exists for defocus values of 0 to -1 combined with an astigmatism of 0 to 1. The area to be avoided is for defocus values between 0 and 1 combined with an astigmatism between 0 to 0.5.

We conclude from figs. 8 and 9 that the tuning precision will be optimal for a defocus value of 1 combined with an amount of astigmatism of 1. These values of astigmatism and defocus will tune the TEM with a tuning precision of 0.02, given a noise level of two and a beam tilt of 0.2.

The reference area for defocus and beam tilt has also been calculated and appeared to be large: the tuning precision is best for beam tilt values 0.2 to 1.2, combined with a defocus value between 1 and 4.

In conclusion, it is recommended to induce a beam tilt of 0.2, and to set the defocus to 2 combined with an astigmatism value of 1. With this setting of defocus and astigmatism the best tuning precision can be expected for a large reference area.

4. Simulations of the estimation of defocus and astigmatism

Although the usefulness of the CRLB in optimal design is beyond doubt, it might be unreliable in predicting the achievable tuning precision. It is impossible to predict theoretically the consequences of non-asymptotic conditions, finite image size, and high noise levels in regions of weak image transfer which introduces folding of the distribution of phase disturbances, as described in section 2.3.2 and illustrated in fig. 6.

However, the statistical properties of the estimator can be determined by means of simulations. This is done by analysing the results of a series of parameter estimates from simulated noisy TEM images. In this section the estimation of defocus and astigmatism in the absence of beam tilt misalignment is studied.

The simulations are carried out to answer five basic questions: (1) Does a TEM setting within the reference area ensure the estimator to converge to a global minimum, and not to a local minimum? (2) Does an incorrect setting of the frequency region introduce substantial bias? (3) How important is the weighting function and the form of weighting with respect to the phase disturbance? (4) What is the practically achievable precision of the COS and LS estimators compared to the CRLB? (5) Does a high noise level introduce bias due to folding of the phase disturbances?

The simulations are carried out using an IBM-AT compatible personal computer using the scientific programming system ASYST [48].

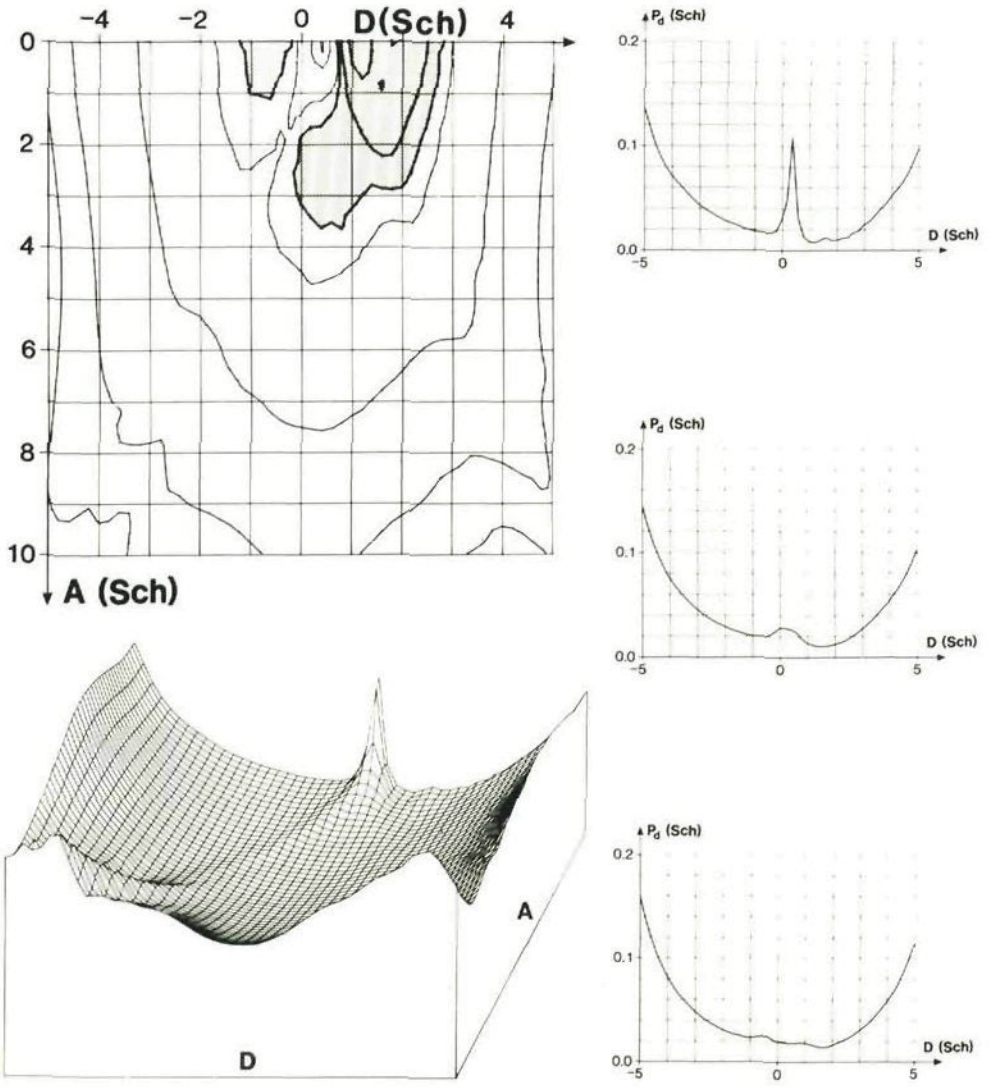

Fig. 9. The tuning precision P_d as a function of defocus D and astigmatism A (calculation of the CRLB). A contour plot (top left, dotted: $P_d < 0.02$), an axonometric plot (bottom left) and sections along the defocus axis for three astigmatism values: $A = 0$, $A = 1$ and $A = 2$ are shown (top right, middle and bottom graph). Relevant TEM parameters are: an azimuthal angle of astigmatism of $\frac{1}{4}\pi$ rad, beam tilt $t = (0.2, 0)^T$, and a noise level $N_0 = 2$.

4.1. Generation of noisy images

A noisy high resolution image of an amorphous carbon film is simulated [49] as the output of a linear filter S_η, with as input signal ν (white noise having a Gaussian distribution):

$$\tilde{\eta}(k_{uv}) = S_\eta(u, v)\, \tilde{\nu}(k_{uv}), \tag{37}$$

where $\tilde{\nu}$ denotes the Fourier transform of ν, S_η in the PSDF (power spectral density function) of the specimen and $\tilde{\eta}$ the Fourier transform of the electron wave emerging from the specimen (1), respectively. The image contrast is then given by

$$c(x_m; \theta) = F^{-1}\left[S_\eta(u, v)\, \tilde{\nu}(k_{uv})\, \Gamma(k_{uv}; \theta)\right]. \tag{38}$$

Noisy image contrast is obtained by adding white noise to the images, having a Gaussian distribution.

4.2. Numerical minimization

The parameters are estimated minimizing the COS and LS criteria (eqs. (30) and (31)). The plane model is linear in defocus D, but non-linear in the astigmatism components A_x and A_y (eq. (19)). Therefore a numerical minimization procedure has to be used. The procedure used is the Gauss–Newton method, especially developed for LS estimation problems [33].

It is known for non-linear minimization procedures that convergence problems may occur if the initial conditions are poor, and it is of importance to know whether the numerical minimization procedure requires a setting of the TEM parameters within the reference area to ensure the estimator to converge to a global minimum, and not to a local minimum. Therefore, calculation of the area where the DSB method converges with certainty to the global minimum are carried out (no noise added to the images). A two-dimensional section is calculated involving the influence of astigmatism and defocus. Fig. 10 shows the result. As can be seen, the first tuning step must adjust defocus and astigmatism with a precision of 2 to ensure iteration to the global minimum. Considering the reference area (section 3.3), we conclude that the second tuning step is not affected by the presence of local minima in the criterion.

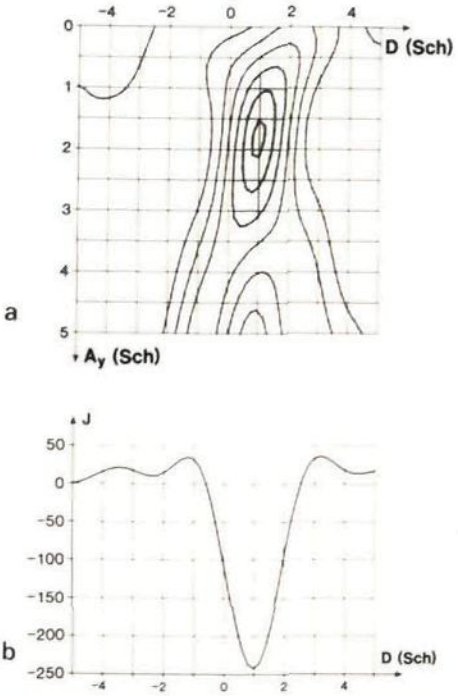

Fig. 10. Contour plot of the cosine criterion (a). The area where the DSB method converges with certainty to the global minimum is shaded. A cross-section of the criterion as a function of the defocus ($A = 1.7$) is shown (b).

4.3. Simulation results

To calculate sample variances, 100 runs of simulations are carried out. Each run consists of adding noise to the images, followed by the parameter estimation procedure (see fig. 11). In each run the same set of images are used, the setting of the TEM parameters is summarized in table 1.

If the image and the segment size are equal to 512 and 64 respectively, there are 64 segments to be processed. Therefore, the Fourier coefficients are calculated by averaging 64 coefficients availa-

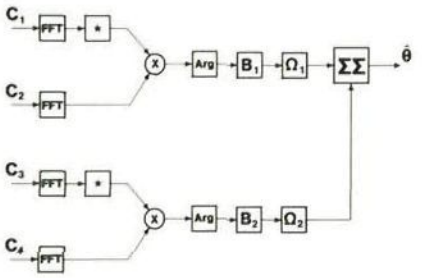

Fig. 11. Diagram of the parameter estimation procedure of the defocus and the astigmatism. All segments of the images C are Fourier transformed (FFT) and multiplied by the corresponding complex conjugate Fourier transformed image. The resulting phase spectra (Arg) are averaged and a numerical minimization procedure is used (within an appropriate frequency region (B) and with weighting function (Ω)) to estimate ($\Sigma\Sigma$) the TEM parameter vector (θ).

ble from the Fourier transform of each segment. In order to reduce the calculation time, the simulations are carried out using only one segment of 64^2 pixels. Considering the linearity of the Fourier transform, this can be done without loss of generality, only the power of the noise added to the segment must be reduced by a factor of 64. The Gauss–Newton procedure was found to iterate to the minimum in one or two steps using the LS criterion, and in less than eight using the COS criterion.

Next, the performance of the COS estimator is compared to the LS estimator, followed by a comparison of the optimal weighting function with an approximate weighting function. As approximate weighting function a frequency band is selected with uniform weighting (fig. 12), at frequencies between 0.4 and 1.2.

Table 1
The setting of the TEM parameters, as used for calculating the CRLB and for the simulations

TEM parameters	Setting
Induced beam tilt (t)	$(0.2, 0)^T$
Defocus (D)	1
Astigmatism (A)	2
Azimuthal angle astigmatism	$\frac{1}{4}\pi$ rad
Noise level (N_0)	2

First, the simulation procedure is carried out, without adding noise to determine the influence of an incorrectly selected frequency region (B). The results are given in table 2. Using optimal weighting, there is a slight bias, due to the fact that the DSB frequency region includes frequencies where no pure DSB imaging occurs. These systematical errors may be avoided by including only frequencies where only pure DSB imaging occurs (smaller frequency region). When the approximate weighting function is used, the estimates are more seriously biased. Again, this is due to the presence of frequencies lying outside the DSB frequency region.

Finally, the influence of the noise level in the images on the performance of the estimators is studied. The results are summarized in table 3. Apparently, non-systematical errors introduce no substantial bias. Furthermore, the form of the criterion is not highly important. The COS estimator performed slightly better than the LS estimator. It is expected that with increasing noise level, the performance of the COS estimator will improve, relative to the LS estimator due to folding of phase disturbances. This is confirmed in table 4 by the fact that the precision of the periodic LS estimator with $N_0 = 4$, is worse than that of the COS estimator, while with $N_0 = 0.4$, the estimators are equally precise. An estimate of the weighting function will not necessarily lead to substantial loss of precision; both estimators get near the achievable precision.

4.4. *Numerical example: electron dose required for tuning*

In this section a numerical example is given to compare the dose needed for tuning a TEM with that needed for detection of image detail.

Table 2
The bias of the estimator of defocus and astigmatism as a function of the frequency region, with the noise level $N_0 = 0$; for other relevant TEM parameters, see table 1

Estimation procedure	D	A_x	A_y
Optimal weighting	−0.0049	−0.0037	−0.0044
Uniform weighting	−0.0120	0.0086	0.0160

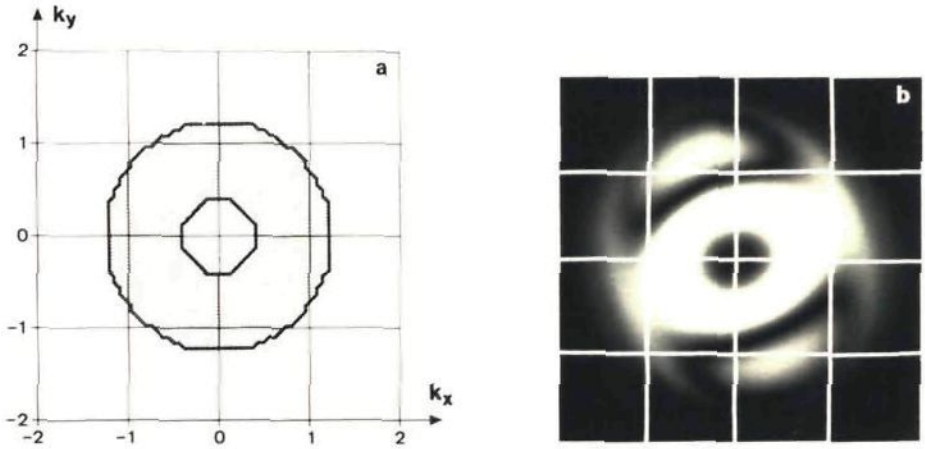

Fig. 12. Contour plot of the approximate weighting function (a) and the magnitude of the cross spectrum of two images formed with a defocus of 1, a beam tilt of +0.2 and −0.2, and without astigmatism (b).

Let the contrast of an image detail be defined as $C = \Delta N_b / N_b$, where N_b denotes the background dose (electrons per nm^2), and ΔN_b is an increment of the image intensity, referred to the object plane. In order to detect and image detail of a^2, the additional number of electrons $a^2 \Delta N_b$ accumulated in this detail has to overcome significantly the standard deviation of shot noise (or Poisson noise): $a_s \sqrt{N_b}$. Therefore, the dose N_b has to be chosen so as to meet the Rose equation: $a^2 \Delta N_b = 5 a_s \sqrt{N_b}$ [47]. It can be derived that a dose of

$$N_b = 25 (a^2 C^2 \, \mathrm{DQE})^{-1} \tag{39}$$

is needed to detect an image detail in the recorded image.

Table 3
The bias of the estimator of defocus and astigmatism (in Sch) as a function of the estimation procedure and criterion, with the noise level $N_0 = 4.0$; for other relevant TEM parameters, see table 1

Estimation procedure	D	A_1	A_2
COS criterion	−0.0034	−0.0057	−0.0014
LS criterion	0.0033	−0.0055	−0.0079
Uniform weighting	−0.0120	0.0210	0.0150

Let the image be recorded with a camera with a DQE = 1, and square adjacent sensors of 100 μm. Suppose a finest image detail of 0.5 nm is recorded with a magnification of 400,000. The scaled image sensor size is then 0.25 nm. A realistic value of image contrast is $C = 0.01$. Consequently, a dose of $N_b = 2500$ electrons per sensor is needed for detection of the image detail. Given the magnification of the sensor dimensions, the electron dose incident on the specimen is given by

$$D_{\mathrm{detection}} = 40{,}000 \text{ electrons per nm}^2.$$

The dose required to tune the TEM up to a predefined precision depends on the PSDF of the specimen (eq. (34)), noise level (eq. (35)) and on

Table 4
The tuning precision P_d (in Sch) of the estimator of defocus and astigmatism (in Sch) as a function of the estimation procedure for several noise levels. For relevant TEM parameters, see table 1

Estimation procedure	$N_0 = 0.4$	$N_0 = 4.0$
COS criterion	0.0090	0.047
LS criterion	0.0093	0.057
Uniform weighting	0.0138	0.043
Achievable precision	0.0066	0.033

the fractional intensity deviation (σ_i) of the image measured (e.g. the ratio of the standard deviation of the image to the mean of the image intensity) and on the DQE of the image pickup system [35]. The exact relation between noise level and dose is difficult to calculate [29], but can be approximated by

$$D_{\text{aut}} \sim \frac{N_0^2}{\sigma_i} \text{DQE}^{-1} \tag{40}$$

with $D_{\text{aut}} = 6500$ electrons per nm^2 for a σ_i of 0.05, DQE = 1, noise level $N_0 = 4$, an image of 512^2 pixels and a segment of 64^2 pixels.

In order to calculate the dose required to tune the TEM up to a predefined precision, this numerical exercise can be repeated with another noise level N_0. It can be derived that the dose needed for the first imprecise tuning step is negligible compared to the dose needed to tune TEM with the second, high precision tuning step.

5. Discussion and conclusions

A new method has been proposed to measure and correct defocus, astigmatism and beam tilt misalignment of a transmission electron microscope (TEM) automatically. The method is applicable to low dose, high resolution electron microscopy, if the specimen is described as a weak phase object. Defocus and astigmatism are estimated from two different pairs of images. These are obtained respectively by tilting the illumination in two perpendicular directions over two equal but opposite angles. Prior to the estimation of defocus and astigmatism, beam tilt misalignment is estimated from three images, one formed without beam tilt and two with equal but opposite tilt angles. The TEM is aligned to a coma-free axis. In all cases use is made of phase of the cross spectra of the images involved.

The optimal measuring strategy for the estimation of defocus and astigmatism has been designed. This design strategy was based on a measure of the achievable precision with which defocus and astigmatism can be estimated from the phase spectra. The best tuning strategy consists of two tuning steps. The first step is imprecise, and is used to adjust defocus and astigmatism to about 2 with a precision of 1, in order to create optimal tuning conditions for the second step. The total dose needed for tuning depends mainly on the precision required by the second tuning step. This second, high precision, tuning step has been tested with simulations, which show the relation between the tuning precision and the required dose. Defocus and astigmatism can be estimated with a precision of 0.02, using a dose of 6500 electrons per nm^2 with a camera having 512^2 pixels and 100% efficient in detection of the incident electrons.

An optimal estimator of defocus and astigmatism has been designed, and tested with simulations for several realistic measuring conditions. A numerical minimization procedure was used, and was tested with several criteria and weighting functions. The most practical criterion appears to be the sum of the cosine of the differences between the phase model and the phase estimates. The choice of the weighting function is not critical; uniform weighting over a band of frequencies is the most practical one considering computational load. The simulations are performed with a Gauss–Newton iteration scheme and were found to converge in one to eight iterations.

The method described in this paper is based on the estimation of parameters from the phase of cross-spectra and can be extended to estimate other lens aberrations with high precision. However, the method will only work if the model of the specimen is correct. An incorrect model will result in biased estimates of defocus and astigmatism. Therefore, attention must be paid to choose a suitable frequency region for which phase contrast theory is valid. The method has been tested with simulation of a thin carbon film, and probably modifications are necessary for thicker specimens.

The autotuning method aligns the TEM onto a coma-free axis. This axis will, in general, not be dispersion-free. However, the deflection coils underneath the objective lens can be used to shift the image such that this additional (dispersion-free) imaging condition is met.

The mathematical formulation of the autotuning method is such that it is easily extended to SSB imaging conditions. For the DSB imaging conditions, other mathematical formulations of the autotuning method are possible. As described in ref. [50], the effect of beam tilt is, in fact, a combination of a mere image displacement and image blurring due to the beam tilt. The image blurring can be removed by applying a special (digital) filter. After pre-filtering the images, the image displacements are measured using cross-covariance functions. Finally, the TEM parameters can be estimated from these measured image displacements.

Practical implementation of the method requires a video camera and computing power to handle the video images and to perform Fourier transforms within seconds. Furthermore, computer control of the objective lens for focus, deflection coils for beam tilt, and the stigmator coils for the correction of astigmatism is essential. The method proposed in this paper has been worked out for a final high precision tuning step. However, external control of other parameters, such as magnification, video image contrast, spot size and gun alignment are indispensable for a total autotunable TEM.

Practical limitations are set by the costs of the computing power, the noise introduced by the camera and the accuracy and speed to correct the currents of the objective lens, deflection coils and stigmator. Furthermore, the software needed for a reliable autotunable TEM will be complicated.

In Delft the implementation of the autotuning method is in progress. The experimental set-up consists of a Philips EM 420 TEM, a Gatan 622 video camera, a TEMDIPS computer system with special hardware for handling two-dimensional images and calculating Fourier transforms, and a DEC PDP 11/23 controlling the TEM under supervision of the TEMDIPS computer. The first, relatively imprecise, tuning step is made using the lower spatial frequencies (at lower magnifications) for dose efficiency. This tuning step is made by

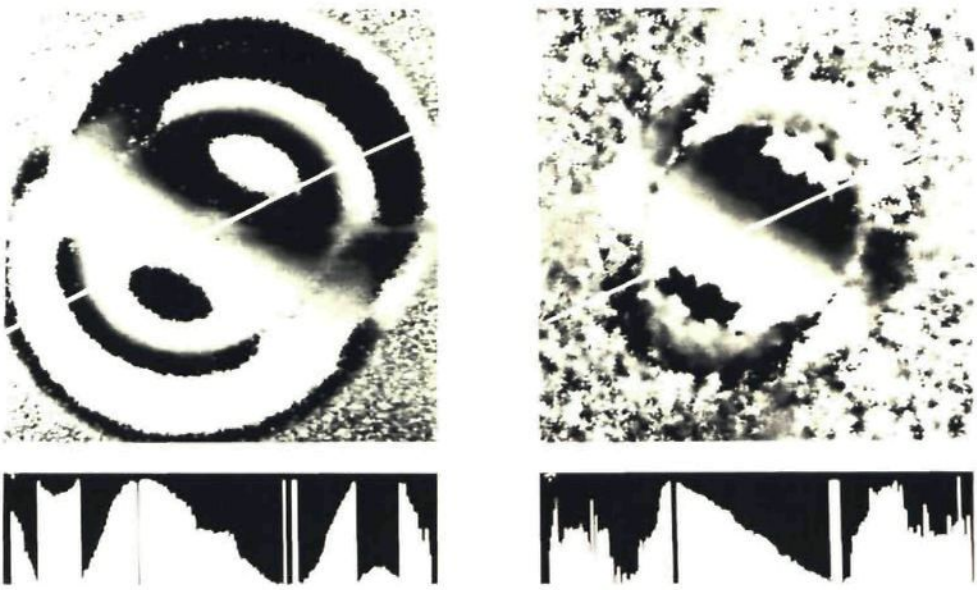

Fig. 13. A 256^2 pixel grey level images of a simulated and measured phase spectrum of two images of carbon film with a beam tilt of ± 0.3, a defocus of 1.5 and without astigmatism. The maximum frequency in the images is 2.5.

estimating image displacements, see refs. [27,50], and works well. The second tuning step, based on the estimation of parameters from cross-spectra as described in this paper, is currently tested in practice. The first preliminary measurements have been made (see fig. 13), and are promising. A paper on the practical implementation of the autotuning method for both the first and second tuning step will be published shortly.

Acknowledgements

Thanks are due to Dr. D. Typke for his valuable remarks and suggestions on the improvement of the autotuning method. These investigations were supported by the Netherlands Technology Foundation (STW) and by Philips Nederland B.V.

Appendix A. The influence of the TEM parameter vector on the equation errors

In this appendix a number of remarks are made with respect to the influence of the parameter vectors θ_1 and θ_2 on the stochastic process ϵ, as defined in eq. (22).

First, consider the input–output relation between the images used to estimate the phase spectrum, see eqs. (20) and (21), and fig. 5. The parameters are estimated from observations of both the input and the corresponding response of the linear model (t). Furthermore, the input $\underline{C}_1$ consists of the sum of a true image C_1 and a stochastic process $\underline{n}_1$. Similarly, the output $\underline{C}_2$ consists of the sum of C_2 and $\underline{n}_2$.

Next consider the equation errors, that is, the difference between the observations and the model describing those observations due to nonsystematical errors. Considering fig. 5, we can derive that the equation errors (here formulated in the frequency domain) are given by

$$\tilde{\underline{n}}_1\, \Gamma_2(\boldsymbol{k}, \Theta_2) - \tilde{\underline{n}}_2\, \Gamma_1(\boldsymbol{k}, \Theta_1),$$

where $\tilde{\underline{n}}$ is the Fourier transform of $\underline{n}$.

Consistency of any estimator is dependent on the properties of the equation errors. An estimator $\underline{t}_n$ is defined as consistent for θ if for any $\tau > 0$, $P(|\underline{t}_n - \theta| < \tau) = 1$ for $n \to \infty$, where n is the number of observations, and $P(\mathrm{A})$ denotes the probability of event A. If the equation errors are white, consistent estimation of the parameters is possible. If the equation errors are colored, estimators of θ are generally biased.

Consequently, for the estimation of defocus and astigmatism, the equation errors are white since the modulus of the PCTF is the equal for opposite beam tilt. When the beam tilt misalignment is estimated, the modulus of the PCTF is not equal for an opposite induced beam tilt. As result, the equation errors will be colored, and the estimator of θ is generally biased.

Appendix B. Numerical computation of the tuning precision

In this appendix the numerical computation of the tuning precision is discussed. The estimated parameters $\theta = (D, A_x, A_y)^{\mathrm{T}}$ have a jointly Gaussian distribution, hence their probability density function $f(\theta)$ is given by:

$$f(\theta) = (2\pi)^{-N/2} (\det V)^{-1/2} \mathrm{e}^{-\theta^{\mathrm{T}} V^{-1} \theta/2},$$

where N equals the number of parameters to be estimated (e.g. three for the estimation of defocus and astigmatism), V the covariance matrix of the parameter vector θ, and $\det V$ the determinant of V. The variance of a function $\rho(\theta)$ is given by:

$$\mathrm{var}\{\rho(\theta)\} = E\{\rho(\theta)\}^2 - E\{\rho(\theta)^2\},$$

where E denotes the expectation operator. The terms on the right-hand side can be written as:

$$E\{\rho(\theta)\} = \int_{-\infty}^{\infty} \rho(\theta)\, f(\theta)\, \mathrm{d}\theta,$$

$$E\{\rho(\theta)^2\} = \int_{-\infty}^{\infty} \rho(\theta)^2\, f(\theta)\, \mathrm{d}\theta.$$

So, calculating the precision P_{d} (as defined in eq. (33)) is equivalent to calculating these integrals numerically, where $\rho(\theta)$ denotes D_{cor}, given by eq. (33).

References

[1] J.M. Cowley, Ultramicroscopy 18 (1985) 463.
[2] W.O. Saxton, W.K. Jenkins, L.A. Freeman and D.J. Smith, Optik 49 (1987) 505.
[3] H. Lichte, Ultramicroscopy 20 (1986) 293.
[4] P. Bonhomme and A. Beorchia, Ultramicroscopy 17 (1985) 127.
[5] J.R. Fryer, Ultramicroscopy 23 (1987) 321.
[6] D. Lichtman, Ultramicroscopy 23 (1987) 291.
[7] D.T. Grubb, Ultramicroscopy 12 (1984) 279.
[8] R.F. Egerton, P.A. Crozier and P. Rice, Ultramicroscopy 23 (1987) 305.
[9] M. van Heel, Ultramicroscopy 8 (1981) 331.
[10] S.J. Erasmus and K.C.A. Smith, in: Electron Microscopy and Analysis 1981, Inst. Phys. Conf. Ser. 61, Ed. M.J. Goringe (Inst. Phys., London–Bristol, 1982) p. 115.
[11] W. Krakow, Ultramicroscopy 18 (1985) 197.
[12] R. Guckenberger, C. Kösslinger, R. Gatz, H. Breu, N. Levai and W. Baumeister, Ultramicroscopy 25 (1988) 111.
[13] W.O. Saxton, T.J. Pitt and M. Horner, Ultramicroscopy 4 (1979) 343.
[14] K.H. Herrmann and D. Krahl, J. Microscopy 127 (1982) 17.
[15] B. Kraus, O.L. Krivanek, N.T. Swann, C.C. Ahn and P.R. Swann, in: Proc. 11th Intern. Congr. on Electron Microscopy, Kyoto, 1986, Vol. 1, Eds. T. Imura, S. Maruse and T. Suzuki (Japan. Soc. of Electron Microscopy, Tokyo, 1986) p. 455.
[16] E.J. Kirkland and B.M. Siegel, Optik 53 (1979) 181.
[17] D.J. Smith, W.O. Saxton, M.A. O'Keefe, G.J. Wood and W.M. Stobbs, Ultramicroscopy 11 (1983) 263.
[18] E.J. Kirkland, Ultramicroscopy 15 (1984) 151 (Part I. Theory).
[19] E.J. Kirkland, Ultramicroscopy 17 (1985) 84 (Part II. Experiment).
[20] F. Zemlin, K. Weiss, P. Schiske, W. Kunath and K.H. Herrmann, Ultramicroscopy 3 (1978) 49.
[21] F. Zemlin, Ultramicroscopy 4 (1979) 241.
[22] R. Henderson, J.M. Baldwin, K.H. Downing, J. Lepault and F. Zemlin, Ultramicroscopy 8 (1986) 147.
[23] D. Typke and D. Köstler, Ultramicroscopy 2 (1977) 285.
[24] W. Kunath, F. Zemlin and K. Weiss, Optik 76 (1987) 122.
[25] W.O. Saxton, D.J. Smith and S.J. Erasmus, J. Microscopy 130 (1983) 187.
[26] D.J. Smith, A. Higgs and P. Perkes, in: Proc. 45th Annual EMSA Meeting, Baltimore, 1987, Ed. G.W. Bailey (San Francisco Press, San Francisco, 1987) p. 62.
[27] K.D. van der Mast, in: Proc. 8th European Congr. on Electron Microscopy, Budapest, 1984, Vol. 1, Eds. A. Csanády, P. Röhlich and D. Szábo (Hungarian group for Electron Microscopy, Budapest, 1984) p. 3.
[28] A.J. Koster, A. van den Bos, K.D. van der Mast and P. Kruit, in: Proc. 11th Intern. Congr. on Electron Microscopy, Kyoto, 1986, Vol. 1, Eds. T. Imura, S. Maruse and T. Suzuki (Japan. Soc. of Electron Microscopy, Tokyo, 1986) p. 501.
[29] A.J. Koster and A. van den Bos and K.D. van der Mast, Ultramicroscopy 21 (1987) 209.
[30] S. Nomura and S. Isakozawa, J. Electron Microsc. 36 (1987) 157.
[31] M.B. Priestly, Spectral Analysis and Time Series (Academic Press, New York, 1981).
[32] L. Reimer, Transmission Electron Microscopy, Springer Series in Optical Sciences, Vol. 36 (Springer, Berlin, 1984).
[33] A. van den Bos, Parameter estimation, in: Handbook of Measurement Science Fundamentals (Wiley, New York, 1982).
[34] P.W. Hawkes, Optik 55 (1980) 207.
[35] W.O. Saxton, Computer Techniques for Image Processing in Electron Microscopy (Academic Press, New York, 1978).
[36] S.C. McFarlane, J. Phys. C8 (1975) 2819.
[37] W. Hoppe, D. Köstler, D. Typke and N. Hunsmann, Optik 42 (1975) 43.
[38] K.H. Downing, Optik 43 (1975) 199.
[39] D. Typke and D. Köstler, Optik 45 (1976) 495.
[40] R.H. Wade and W.K. Jenkins, Optik 50 (1978) 1.
[41] E.J. Hannan and P.J. Thomson, IEEE Trans. Acoust., Speech, Signal Processing ASSP-29 (1981) 485.
[42] G.C. Carter, IEEE Trans. Acoust., Speech, Signal Processing ASSP-29 (1981) 463.
[43] B.V. Hamon and E.J. Hannan, Appl. Statist. 23 (1974) 134.
[44] A. Papoulis, Probability, Random Variables and Stochastic Processes (McGraw-Hill, New York, 1965).
[45] V.V. Fedorov, Theory of Optimal Experiments (Academic Press, New York, 1972).
[46] K.D. van der Mast and A.J. Koster, in: Proc. 46th Annual EMSA Meeting, Milwaukee, 1988, Ed. G.W. Bailey (San Francisco Press, San Francisco, 1988).
[47] J.C.H. Spence, Experimental High Resolution Microscopy (Oxford Univ. Press, London, 1981).
[48] ASYST, a scientific system (manual) (Adaptable Laboratory Software, Macmillan, New York, 1985).
[49] G.Y. Fan and J.M. Cowley, Ultramicroscopy 21 (1986) 125.
[50] A.J. Koster, A. van den Bos and K.D. van der Mast, in: Proc. 6th Pfefferkorn Conf. on Image and Signal processing, Niagara Falls, NY, 1987, Eds. P.W. Hawkes, F.P. Ottensmeyer, A. Rosenfeld and W.O. Saxton, Scanning Microscopy International, p. 83.

5 Practical Autotuning of a TEM

1	**Introduction**	**82**
2	**Theory of autotuning**	**86**
2.1	Effect of beam tilt : a mere image displacement	86
2.2	Measurement and correction of TEM parameters	89
2.3	Effect of beam tilt : image blurring	91
2.4	Expected accuracy and speed considering the noise	94
3	**Implementation of the autotuning method**	**96**
3.1	Requirements on the instrumentation	96
3.1.1	The Transmission Electron Microscope	96
3.1.2	The Camera	96
3.1.3	The computer - control of the TEM	98
3.1.4	The computer - image processing	98
3.1.5	The computer - the user interface	98
3.1.6	Some examples of measuring set-ups	99
3.2	The experimental set-up in Delft	99
3.2.1	The Philips EM420 TEM	99
3.2.2	The Gatan 622 camera	100
3.2.3	The DEC PDP 11/23	100
3.2.4	The TVDIPS image processing device	101
3.2.5	The IBM PC/AT	101
4	**Experimental results**	**101**
4.1	Calibration	101
4.2	Automatic rotation alignment	102
4.3	Automatic coma-free alignment	104
4.4	Automatic focusing and correction of astigmatism	104
4.5	Instrumental limitations for low SNR images	105
5	**Discussion and conclusions**	**107**
	References	**108**

PRACTICAL AUTOTUNING OF A TRANSMISSION ELECTRON MICROSCOPE

A.J. KOSTER, L.K. van VLIET, T.S. HOEKSTRA, M. HOEK, A. van den BOS and K.D. van der MAST

Research Group Particle Optics, Department of Applied Physics, Delft University of Technology, Lorentzweg 1, 2628 CJ Delft, The Netherlands

Summary

A method for the automatic correction of TEM misalignment, defocus and astigmatism, based on measuring image displacements when the illuminating beam is tilted, is proposed. Its performance has been tested on a Philips EM 420 TEM connected to a Gatan 622 video camera and a TVDIPS image processing system. The method works with weak phase objects and amplitude contrast specimens. The accuracy of the (coma-free) alignment procedure was measured to be 0.1 mrad and 5 nm for the correction of defocus and astigmatism. Properties and possible improvements of the measuring set-up are discussed. The automatic correction of the beam tilt misalignment, defocus and astigmatism of a transmission electron microscope (autotuning) is desirable for low dose and high resolution electron microscopy. Autotuning will enhance the number of meaningful micrographs when the signal-to-noise ratio of the image is too low and/or the desired accuracy in tuning the TEM too high for accurate manual control.

1 Introduction

The automatic correction and control of the defocus, astigmatism and beam tilt misalignment (autotuning) of a Transmission Electron Microscope (TEM) enables the user to record images of a specimen under well defined imaging conditions. Accurate and known setting of the defocus, astigmatism and beam tilt misalignment (TEM parameters) is required for reliable interpretation of images, especially when the signal-to-noise ratio (SNR) in the images is low [1], [2]. Unfortunately, when the signal-to-noise is low (for example due to low dose conditions) the TEM operator may have difficulties to tune the TEM with the required accuracy. An autotuning system is, therefore, desirable. It will increase the number of meaningful micrographs recorded, if it can tune the TEM with a pre-defined accuracy using a minimum electron dose for a broad range of specimens and imaging conditions.

Several papers on autotuning of a TEM were published. An overview can be found in Erasmus and Smith [3] and in Saxton and Chang [4]. Basically, three different types of methods have been

proposed, and we will describe them briefly.

The diffractogram can be used as (manual) tuning aid, because it gives an impression of the amount of defocus and astigmatism in the TEM. When no misalignment is present, the astigmatism can be corrected with the stigmator controls until the diffractogram becomes circular. Nowadays, the diffractogram of the image (modulus of the Fourier transform of the image) can be calculated and displayed within seconds, see Baba et al. [5] and Ogasawara et al. [6].

It is not often recognized that the TEM has to be aligned on a coma-free axis, before the correction of the astigmatism and defocus by observing the granularity or the diffractogram of the image. From one diffractogram it is not possible to derive the misalignment. If more than one diffractogram is used, under different imaging conditions, the misalignment can also be derived, see Typke and Kostler [7]. An elegant aid for aligning the TEM on a coma-free axis is by calculating a number of diffractograms as a function of the azimuthal angle of beam tilt. The diffractogram is the same for opposite beam tilt angles when the TEM is aligned on a coma-free axis. For some papers using the diffractograms of images to tune the TEM, see Zemlin [8], Henderson et al. [9] and Kunath et al.[10]

The diffractogram based methods are, in principle, not suitable for full automatic instrumental adjustment as the shape of the diffractograms is not specimen independent. The realization of an autotuning method which 'recognizes' the shape of the diffractogram (as used for the coma-free alignment procedure) will be difficult.

The second type of method is based on measuring the image contrast. An image in a TEM has minimum contrast when it aligned, focused and the astigmatism well corrected, see Saxton et al. [11]. The method iterates to an accurate setting of the TEM parameters using deliberate variation of defocus, astigmatism and alignment, but is dose inefficient (Koster et al. [12]) and works only when the TEM parameters are very near their correct setting. However, the method proved to work in practice (Smith et al.[13]), and is presently being improved (de Ruijter [14]).

The third type of method is based on measuring image displacements when the illuminating beam is tilted. In 1947 this method was introduced by LePoole for the manual correction of defocus (wobbler) [15], and was later extended to the correction of other aberrations (Koops [16]). In 1984 it was proposed by van der Mast to correct the defocus in one step using the linear relation between image displacement and defocus [17], and it was found that the method is inherently very precise and specimen independent (Koster et al. [18]). In 1987 a similar approach was used by Nomura and Isamozwa to correct the defocus by tilting the beam and, in addition, varying the defocus until the image coincides with the image if not beam tilt was induced [19]. The method proved to work at lower magnifications, but not to be dose efficient.

In this paper, this third type of method (based on measuring image displacements), is extended to the correction of astigmatism and beam tilt misalignment (section 2), and will be referred to as the autotuning method. The accuracy and speed of the method have been experimentally tested (sections 3 and 4). The present experimental set-up, the accuracy in aligning the TEM is 0.1 mrad, in focusing 5 nm and 10 nm for the correction of astigmatism, at an electron optical magnification of 96000. The time needed for the alignment is 7 s, for the correction of defocus and astigmatism 6.5 s.

Also described in this paper is a way to reduce the influence of image blurring when the beam is tilted over a large angle (section 2.3). This extension of the autotuning method was recently proposed and tested in simulations by Koster et al. [20].

The autotuning method is based on measuring the effect of beam tilt on an image in a TEM. The TEM parameters (beam tilt misalignment, defocus and astigmatism) are estimated from pairs of images formed with differently tilted beams, see fig. 1.

The beam tilt misalignment has to be estimated and corrected, prior to the correction of defocus and astigmatism. Due to mechanical limitations to the construction of a TEM, the condensor lenses, the objective lens and projector lens system are not perfectly aligned. Therefore, several types of beam tilt misalignment can be defined. We will briefly discuss three types of beam tilt alignment procedures using pairs of deflection coils in a TEM: the coma-free, dispersion-free and rotation alignment procedure.

Coma-free alignment is considered to be the most important. For a coma- free alignment the effect of spherical aberration of the objective lens is rotational symmetric around the primary beam

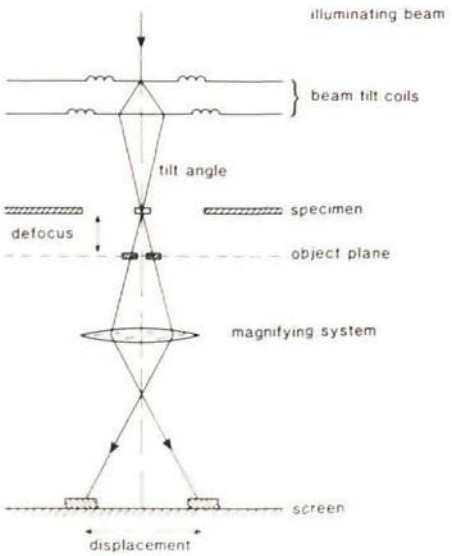

Fig.1: Effect of an induced beam tilt on the low spatial frequencies of the specimen. A beam tilt will result in an image displacement if the TEM is not focused, or the astigmatism not corrected. If astigmatism is present, the image displacement is not necessarily in the same direction as the induced beam tilt.

emerging from the specimen [8], [21]. The coma-free alignment procedure is formulated mathematically in section 2.1.

Next to the coma-free alignment, dispersion-free alignment is of importance. The energy spread of the electrons emerging from the specimen limits the

resolution of the image. In general, dispersion-free alignment can be obtained by varying the high tension. When the high tension is varied, two effects influence the image simultaneously: an image rotation with its centre defined by the interception of the objective lens axis with the (intermediate) image plane, and a (de)magnifying effect with its centre defined by the interception of the beam pointed at the centre of the objective lens and the (intermediate) image plane, see fig. 2. At only one point in the image plane both effects are eliminated (the stationary point) and no effect is visible. The position of this stationary point is determined by the beam tilt angle, as this angle determines the position of the centre of (de)magnification. So, dispersion-free alignment is obtained by tilting the beam in such a way that the stationary point is on the projector lens axis (and consequently at the centre of the fluorescent screen).

Simultaneous coma-free and dispersion-free alignment of the illuminating beam can be obtained when the deflection coils underneath the objective lens are used to shift the projector lens axis in order to position the stationary point at the centre of the fluorescent screen. So, first the TEM is coma-free aligned, then the high tension is varied and the projector lens system axis shifted to obtain dispersion-free alignment. In the experimental set-up in Delft, described in section 3, the high tension and the deflection coils underneath the objective lens cannot be controlled externally. Therefore, a dispersion-free alignment procedure was not implemented.

Rotation alignment is important when we consider the effect of focusing (changing the objective lens current). Variation of the objective lens current has features similar to the variation of the high tension, and the rotation alignment procedure is in most respects similar to the

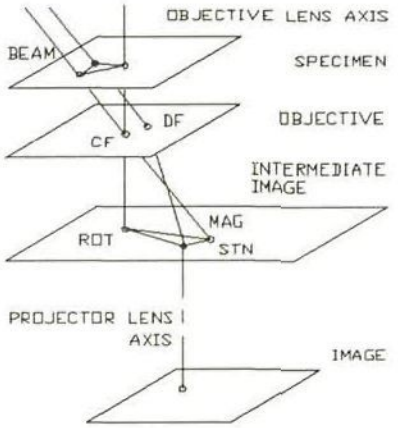

Fig.2: Dispersion-free (DF) alignment of the illuminating beam. When the high tension is varied, two effects influence the image: an image rotation around ROT and a (de)magnification. At one point in the image, both effects are eliminated (at the stationary point STN). The position of the stationary point is determined by the beam tilt angle. A simultaneously coma-free (CF) and dispersion-free alignment of the beam is possible by using the deflection coils underneath the objective lens to shift the projector lens axis towards the stationary point, instead of shifting the stationary point towards the projector lens axis by changing the tilt angle of the illuminating beam.

dispersion- free alignment. The image of a specimen structure on the fluorescent screen, will shift off from the screen when the stationary point is not positioned on

the projector lens axis, and a large focus change is induced (relative to the magnification of the TEM). So, the rotation alignment procedure induces a beam tilt in such a way that the stationary point is on the projector lens axis. The rotation alignment procedure is used for low and medium resolution work, as the coma-free and rotation alignment may differ a few mrad. The rotation alignment procedure is described mathematically in section 2.1. The implementation and test is discussed in sections 3 and 4.

The autotuning of the TEM is most efficiently done in two steps, because of two reasons.

Firstly, a two step procedure is more dose efficient than a single step procedure, which is an important requirement in many applications [22], [23]. The first step tunes the TEM parameters with a relatively low accuracy to a setting of the TEM which corresponds with a higher image contrast (for instance near Scherzer focus). The second step is done with a high accuracy (using the high contrast images), and can be used to focus the TEM to Gaussian focus, or to any other setting of the TEM.

Secondly, more than one procedure may be used to tune the TEM, each of the procedures having been designed to work optimally under different imaging conditions. An example of a first tuning step is the autotuning method described in this paper. The second tuning step may use higher spatial frequencies than the first step and consequently, be more accurate, slower and less robust than the first step (as it may incorporates the effect of image blurring in the procedure). An example of such a second tuning step is described in section 2.3.

Implementation of the autotuning method is described in section 3, followed by the experimental results in section 4.

2 Theory of autotuning

2.1 Effect of beam tilt : a mere image displacement

The autotuning method measures the effect of beam tilt on the image of the specimen. For the lower spatial frequencies of the specimen, this effect is a mere image displacement. The image displacement can be measured from the cross covariance function of the two images (section 2.2). The procedure used for the coma-free alignment requires five images; for the correction of defocus and astigmatism three images are required.

From linear image theory it can be derived [24] that the effect of beam tilt is a mere image displacement **d**, given by

$$\mathbf{d} = \{-|\mathbf{t}+\mathbf{m}|^2 + (\mathrm{D}\text{-}0.5\mathrm{A})\}(\mathbf{t}+\mathbf{m}) + \mathrm{A}((\mathbf{t}+\mathbf{m}).\mathbf{a})\mathbf{a}\} \qquad (1)$$

provided that the highest spatial frequency $|\mathbf{k}|$ in the image is lower than $\{-|\mathbf{t}+\mathbf{m}|^2 + (\mathrm{D}\text{-}0.5\mathrm{A})|\}^{0.5}$ to ensure that the effect of image blurring due to the spherical aberration of the objective lens is smaller than the image displacement due to defocus D, astigmatism A**a** and/or misalignment **m**, with the induced beam tilt represented by **t**. The TEM

parameters are given in the normalised units Sch and Gl, with 1 Sch = $(C_s\lambda)^{0.5}$, 1 Gl = $(C_s\lambda^3)^{0.25}$, C_s the constant of spherical aberration and λ the wavelength of the electrons.

plying a low pass (digital) filter to the images. A more dose efficient approach is to incorporate the effect of image blurring within the autotuning method, as is described in section 2.3.

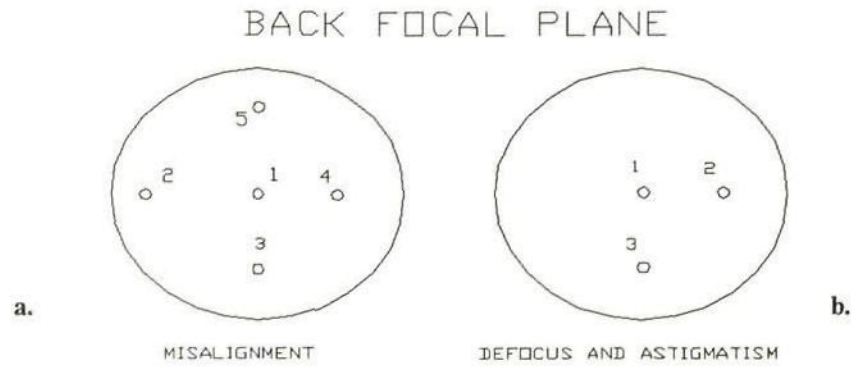

Fig.3: The induced beam tilt angles used for coma-free alignment of the illuminating beam and the correction of defocus and astigmatism, represented by a position in the back focal plane. Figure (a) corresponds with the coma-free alignment procedure. One image is formed without an induced beam tilt (1), and two pairs of images are formed with equal, but opposite and perpendicular angles (2,4 and 3,5). Figure (b) corresponds with the correction of defocus and astigmatism. Three images are required to estimate the defocus and astigmatism. One image is formed without an induced beam tilt (1), the other images are formed with beam tilt angles equal in magnitude but perpendicular (2,3).

Some remarks can be made on the relation between image displacement and beam tilt (1). Firstly, from fig.1 and (1) it is clear that the direction of the induced beam tilt (**t**) is, in general, not equal to the direction of image displacement (**d**). They are equal only if no astigmatism and misalignment is present (so there is only defocus). Therefore, the parameters **m**, D, A and **a** can only be estimated if more than one image displacement is measured. Secondly, to suppress the blurring effect due to the spherical aberration, the highest spatial frequency in the image must be lower than the limit mentioned. This can be effected by ap-

Prior to the correction of defocus and astigmatism, the TEM has to be aligned. If the TEM is not aligned on the coma-free axis, it is not possible to distinguish between the effect of misalignment and the effect of astigmatism in the image, by observing the texture of the image. Consequently, the compensation of misalignment may be mistaken for the correction of astigmatism. The beam tilt angle corresponding with a coma- free alignment, is estimated using five images. One image is formed without an induced beam tilt, one pair of images is formed with equal, but opposite tilt angles $\pm\mathbf{t}_1$,

beam tilt, one pair of images is formed with equal, but opposite tilt angles $\pm\mathbf{t}_1$, and the other pair of images is formed by tilting the beam perpendicularly over two equal, but opposite tilt angles $\pm\mathbf{t}_2$, see fig. 3. The difference in the image displacements relative to the image formed without an induced beam tilt, is the estimator for the misalignment. It is not difficult to derive from (1) that these differences between the displacements $\mathbf{d}_c$ are given by

$$\mathbf{d}_{ci} = -4(\mathbf{m}.\mathbf{t}_i)\mathbf{t}_i - 2t_i^2\mathbf{m}, \qquad (2)$$

with $\mathbf{t}_i$ induced and known for i = 1,2. Note that the estimation of misalignment is independent of the defocus or astigmatism. When this type of misalignment is corrected, the effect of spherical aberration is rotational symmetric around the primary beam and therefore aligned on a coma-free axis.

Another beam tilt alignment procedure is the rotation alignment. The rotation alignment is needed to minimize the movement of the image on screen when the defocus is changed. The procedure measures the image displacement $\mathbf{d}_r$ following a defocus change $(D_1\text{-}D_2)$, given by

$$\mathbf{d}_r = (D_1\text{-}D_2)\mathbf{m} \qquad (3)$$

with $D_1\text{-}D_2$ induced and known. From (3) it follows that the alignment is independent of the defocus and astigmatism. Note that not included in this model of image formation is the effect of image rotation and change in magnification, due to the change in objective lens current. Furthermore, the variation of defocus not only causes a displacement of the image, but may also result in contrast reversal if the defocus values are chosen on either side of Gaussian focus. This contrast reversal may result in an erroneous estimate of image displacement if no attention is paid to this effect, as is described in section 2.2.

Defocus and astigmatism are estimated after the coma-free alignment procedure. The relation between the image displacement $\mathbf{d}_f$ and the defocus and astigmatism for an induced beam tilt $\mathbf{t}$ follows from (1) and is given by

$$\mathbf{d}_f = \{-t^2 + (D\text{-}0.5A)\}\mathbf{t} + A(\mathbf{t}.\mathbf{a})\mathbf{a}\} \qquad (4)$$

where $\mathbf{t}$ is induced and known. Note that the relation between the image displacement and the defocus or astigmatism is linear for a beam tilt t smaller than $(D\text{-}0.5A)^{0.5}$. For larger beam tilts, the term t^2 has to be included within the correction algorithm. Furthermore, the direction of image displacements is important for the correction of defocus and astigmatism, as is obvious when astigmatism is considered as a direction dependent amount of defocus. Consequently, two-dimensional image displacement

measurements are necessary for the correction of the TEM parameters.

2.2 Measurement and correction of TEM parameters

Several methods are available to estimate an image displacement [25]. In this paper the image displacements are measured using cross covariance functions of pairs of images: the position of the maximum of the cross covariance function is an estimator for the image displacement. Another method is to minimize the sum of the (absolute) differences between the pixel values of two images [17].

The maximum cross covariance estimator is preferred for two reasons. Firstly, the stochastic properties of this method are well known [25], which is important when the signal-to-noise ratio in the images is low. Secondly, a cross covariance function can be calculated using Fourier transforms of images, which enables us to incorporate (digital) low/high pass filtering of the images within the estimation procedure of the TEM parameters. Moreover, the Fourier transform can also be used to calculate the diffractogram of an image, or the cross spectrum of two images as needed for the extended autotuning method (section 2.3). Note that the time needed to calculate the displacement is proportional to the time needed to calculate the Fourier transform of an image.

So, the displacement between two images ($I_1(\mathbf{x})$ and $I_2(\mathbf{x})$) is measured using the following algorithm

$$\mathbf{d} = \max_{\mathbf{x}} F^{-1}\left[F\{I_1(\mathbf{x})\}F^{*}\{I_2(\mathbf{x})\}\right] \qquad (5)$$

where F denotes the Fourier transform, F^{-1} the inverse Fourier transform, * the complex conjugate and $\mathbf{x}$ the (discrete) image coordinates in pixels. In principle, the position of the maximum is known within one pixel, and is thus related to the magnification of the specimen to the camera. The accuracy can be increased with interpolation techniques. For example, prior to the inverse Fourier transform in (5) the image size can be increased (within the computer memory) by adding pixel values with the average value of the image, following the Fourier transform of each image. In this way, loosely speaking, the displacement is estimated with a smaller pixel size. However, to apply this method in practice, the computational load might be too heavy to perform the estimation of displacement within reasonable time.

Another interpolation approach is to fit a function (for instance a polynomial) through the top of the cross covariance function, see fig. 9. The position of the maximum of this function has an accuracy better than one pixel. However, when the shape of the measured cross covariance function near the maximum does not correspond with the model, a biased estimate of the position of the maximum is obtained which limits the practical accuracy of the interpolation technique. In our measuring set-up we fit a second order polynomial through the maximum (using 9 pixels), and find that the effect of mismodelling (and instrumental limitations) results in a bias

less than 0.2 pixel for magnifications lower than 124,000.

The coma-free alignment procedure measures the differences between image displacements $\mathbf{d}_c$ using five images. During the procedure the displacements are scaled to specimen level, the magnification dependent image rotation is corrected for, the misalignment **m** is estimated and a correcting beam tilt opposite to **m** is induced. Rotation alignment is performed similarly, by measuring the displacement $\mathbf{d}_r$ using two images, estimating the misalignment **m** and inducing a correcting beam tilt opposite to the estimated misalignment. When the images are recorded on either side of focus the cross covariance may give an erroneous estimate of the displacement because of contrast reversal in the images, see fig. 4. The contrast reversal can be interpreted as an extra phase shift of π in the frequency domain, and can be corrected for prior to the inverse Fourier transform in (5), by multiplication of the sum of the phases of the complex Fourier transformed images by a factor of two. The estimate of displacement is then correct, provided that it is divided by two.

The estimator of defocus and astigmatism are derived form (4). The parameters describing the defocus and astigmatism are estimated by measuring several (N) displacements $\mathbf{d}_n$ (n = 0,..,N-1) between images formed with equal, but opposite beam tilts in different (N) directions (magnitude of tilt t, azimuthal angles $\tau_n = 2\pi n/N$ with n = 0,..,N-1 for N even and ≥ 4 (see fig.3). Each image displacement measurement is perturbed by noise due to the noisy images, or instability of the TEM parameters. Therefore, a least squares estimator is used to estimate the TEM parameters from

$$D = (2tN)^{-1} \sum_{n=0}^{N-1} [d_{nx}\cos(\tau_n) + d_{ny}\sin(\tau_n)] \quad (6)$$

$$A_a = (tN)^{-1} \sum_{n=0}^{N-1} [\delta_{nx}\cos(t_n + \gamma) - d_{ny}\sin(\tau_n + \gamma)] \quad (7)$$

$$A_b = (tN)^{-1} \sum_{n=0}^{N-1} [\delta_{nx}\sin(\tau_n + \gamma) + d_{ny}\cos(\tau_n + \gamma)] \quad (8)$$

where t is the magnitude of tilt, τ_n the azimuthal angle with $\tau_n = 2\pi n/N$, N the number of measured image displacements with d_{nx} and d_{ny} the components of the image displacement **d**, γ the angle between the stigmator and coordinate system relative to the deflection coils, and A_a, A_b the astigmatism modelled as $A_a = A\cos(2\alpha)$ and $A_b = A\sin(2\alpha)$, where A is the magnitude of the astigmatism and α the angle. When the number of measured image displacements N increases, the accuracy in estimating defocus and astigmatism will increase accordingly.

The minimum number of image measurements needed to estimate the TEM parameters with (6-8) is four (N = 4). However, because the TEM has been aligned on the coma-free axis, the effect of beam tilt is symmetric with

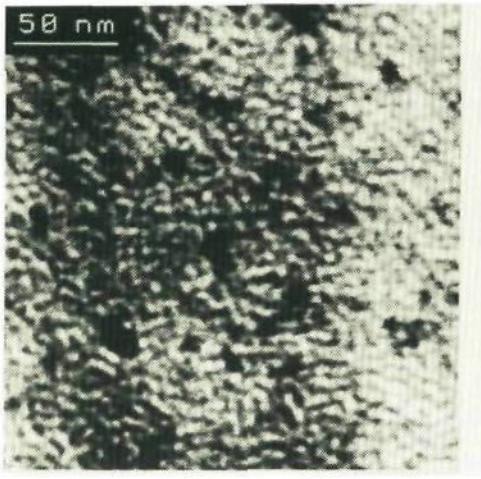

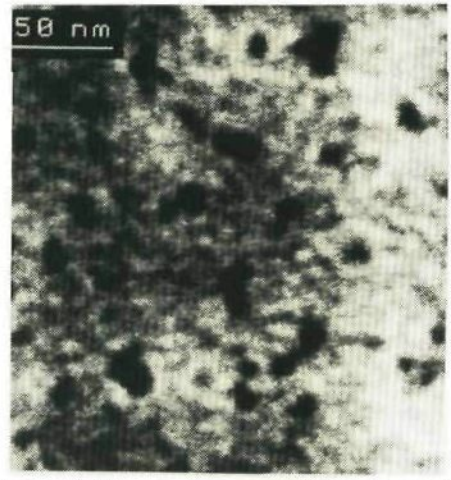

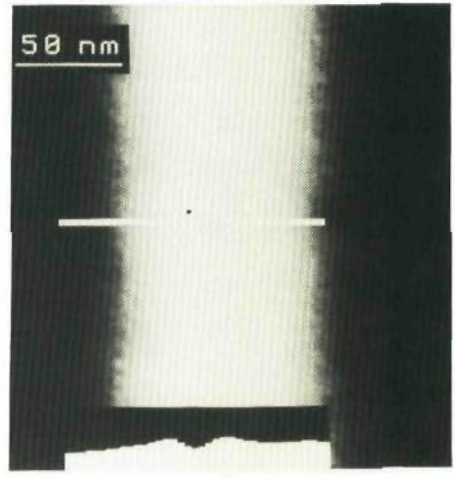

Fig.4: Contrast reversal due to change in defocus will give an erroneous estimate of image displacement. The images of a carbon foil evaporated with gold at a defocus of -/+ 2.5 μm are shown (above). Due to the contrast reversal, the position of the global maximum of the cross covariance function does not correspond with the image displacement (right): a local minimum of the cross covariance function is present at the position which corresponds with the image displacement. No correction was made for the shading pattern of the camera, which results in a cross covariance function having artifacts near zero image displacement (centre of (right)). When a correction is made for the shading pattern by dividing by a zero image, most of these artifacts disappear, as is illustrated by fig. 9.

respect to zero beam tilt. Because of this symmetry, it is sufficient to measure only three images: one image formed without an induced tilt, and the other two images formed with a beam tilt equal in magnitude but with $\pi/2$ rad difference in azimuthal angle, see fig.3.

2.3 Effect of beam tilt : image blurring

Due to the spherical aberration of the objective lens, the displacement of the specimen image is not equal for all spatial frequencies of the specimen; the high spatial frequencies are influenced more strongly by the objective lens than the low

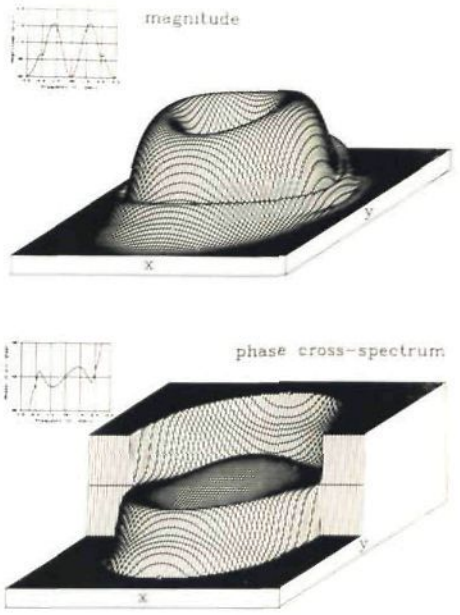

Fig.5: The magnitude and phase of the PCTF for a defocus of 1.5, no astigmatism and a beam tilt of 0.2.

spatial frequencies. This effect is visible as image blurring, and can be described as extra phase shifts due to the (complex) transfer function of the objective lens, see fig. 5. These phase shifts of the transfer function cannot be measured from one single image. However, if two images are recorded, the phase shifts can be measured and be used for autotuning. This method was recently proposed and tested in simulations [20].

For a weak phase object these phase shifts are described by linear image formation theory [24], are given by

$$P(\mathbf{k}) = \arg\{\Gamma_1(\mathbf{k})\Gamma_2(\mathbf{k})^*\} \qquad (9)$$

where Γ_1,Γ_2 are the phase contrast transfer functions corresponding with images $I_1(\mathbf{x})$ and $I_2(\mathbf{x})$, the * denotes the complex conjugate and $\mathbf{k}$ the spatial frequency scaled to specimen level and expressed in GI^{-1}. This model of phase shifts will be referred to as phase model.

Provided that double sideband imaging is a valid description of image formation, the phase model of a pair of images formed with two opposite beam tilts $\mathbf{t}$, is given by

$$P(\mathbf{k}) = 4\pi\{[k^2 + t^2\text{-}(D\text{-}0.5A)]\mathbf{k}.\mathbf{t} \\ -A(\mathbf{k}.\mathbf{a})(\mathbf{t}.\mathbf{a})\} \qquad (10)$$

Note that the blurring effect is due to the term k^2, which is neglected in (1). Furthermore, when we compare (1) with (10) the relation between a phase shift and an image displacement is clear: a linear phase shift is a mere image displacement [25]. The phase shifts are dependent on the TEM parameters and not on the (power spectrum of the) specimen.

To measure the phase shifts, the following estimators ($P'(\mathbf{k})$) of the phase angles of the cross spectrum are taken:

$$P'(\mathbf{k}) = \arg\{\sum_{i=1}^{4}\sum_{j=1}^{4} I_{1ij}(\mathbf{k})I_{2ij}(\mathbf{k})^*\} \qquad (11)$$

where $I_{1ij}(\mathbf{k})$, $I_{2ij}(\mathbf{k})\}$ denote the Fourier transformed ij^{th} image segment of the image $I_1(\mathbf{x})$ and $I_2(\mathbf{x})$, respectively. In our experiments, one image of 256^2 pixels consists of 4^2 image segments of 64^2 pixels, and each segment is weighted with

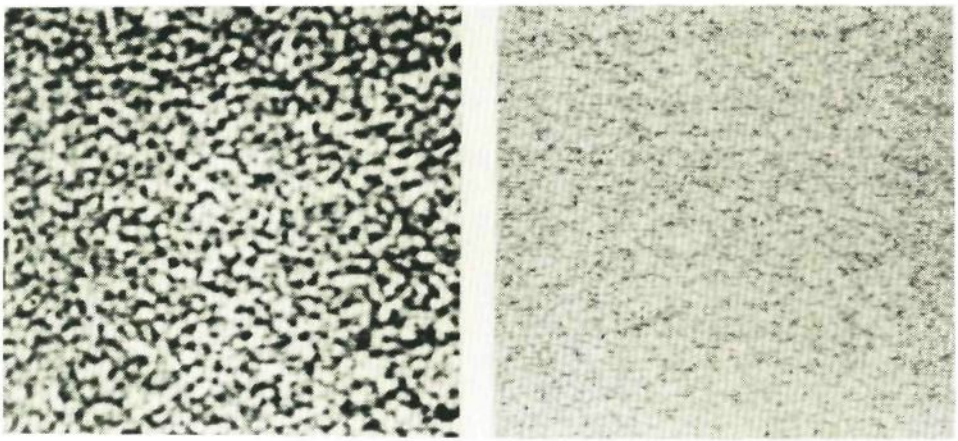

Fig.6: Illustration of the mathematical model of a measured image of a carbon foil. The image is assumed to be the sum of an image described by phase contrast image formation (such as a carbon foil filtered by the PCTF) (left), and the instrumentation noise or Poisson noise (right). The SNR is defined as the ratio of the image variance of (left) to the noise variance of (right).

a Hamming window as weighting function [25].

Coma-free alignment is obtained using three images, one formed without an induced tilt ($\mathbf{t}=\mathbf{0}$) and two formed with equal but opposite tilt angles $\pm\mathbf{t}$. The difference between two phase models $P_1(\mathbf{k})$ and $P_2(\mathbf{k})$, with $P_1(\mathbf{k})$ corresponding with beam tilts $\mathbf{0}$ and $+\mathbf{t}$ and $P_2(\mathbf{k})$ with beam tilts $\mathbf{0}$ and $-\mathbf{t}$, is given by

$$P(\mathbf{k}) = 4\pi\{t^2(\mathbf{k}.\mathbf{m}) + 2(\mathbf{m}.\mathbf{t})(\mathbf{k}.\mathbf{t})\}. \qquad (12)$$

As is clear from (12), the coma-free alignment can be obtained, independent of defocus and astigmatism. First, the three images (with the appropriate beam tilts) are recorded. Then the phase spectra are computed and, with (12), the misalignment m esitmated.

Defocus and astigmatism are estimated and corrected, subsequent to coma-free alignment. Two pairs of images are used for this. One pair is formed with tilted beams over two equal but opposite angles $\pm\mathbf{t}_1$, the other pair of images is formed by tilting the beam perpendicularly over two equal, but opposite directions $\pm\mathbf{t}_2$ ($\mathbf{t}_1.\mathbf{t}_2=0$ and $|\mathbf{t}_1| = |\mathbf{t}_2|$). Each phase model is described by (10). Using these four images two phase spectra are computed. From the two measured phase spectra and the phase model (10), the parameters describing defocus and astigmatism can be estimated.

The estimation of defocus and astigmatism from the measured phase spectra is carried out by minimizing the criterion [20]:

$$J = \sum_{i=1}^{2} \sum_{B} \{\cos[P_i'(\mathbf{k}) - P_i(\mathbf{k})] \qquad (13)$$

where B denotes the frequency region for which double sideband imaging theory is valid, and i the index use of the two phase spectra used for the estimation of the TEM parameters. Some remarks can be made with respect to (13). When the measured phase spectrum P'(**k**) is perturbed by noise, the phase will exhibit phase jumps of 2π (as the phase is defined between π and $-\pi$). If in (13) the sum of the squares of the differences had been used, these jumps would have increased the variance of the estimator. The cosine in (13), however, is not influenced by these phase jumps. Note that for small differences between the measured (P'(**k**)) and modelled phase spectrum (P(**k**)), the criterion is similar to a least squares criterion.

The frequency region B chosen for the experiments is a frequency band with $0.4 < k < 1.2$, as for this frequency band, the mathematical model of the cross spectrum (DSB model) is a valid description of image formation. For higher or lower spatial frequencies, the mismodelling will introduce extra bias in the estimates. A Levenberg-Marquardt algorithm is used [26] as numerical minimization procedure. From the simulations presented in [20], it has been concluded that iteration to the correct values of defocus and astigmatism (global minimum) is ensured, provided that a preceding tuning step has corrected misalignment with an accuracy of 3 mrad and the defocus and astigmatism with an accuracy of 150 nm.

In conclusion: four images, and the measurement of two phase spectra, are required to estimate the defocus and the astigmatism.

2.4 Expected accuracy and computation speed versus the noise properties

The performance of the method as a function of the noise in the images has been evaluated with a measure for the achievable accuracy in tuning the TEM using a beam tilt [20]. The achievable accuracy has been calculated using a mathematical model of the specimen, the TEM and the noise in the measured images. To measure the accuracy of the autotuning method as a function of the SNR of the images, that is: to measure the stochastic properties of the autotuning method, the tuning method has to be applied many times under the same measuring conditions. Unfortunately, due to specimen drift, radiation damage, focus drift and other instabilities this is difficult to do in practice.

To obtain information on the stochastic properties of the autotuning method simulations were done. Simulations are only useful when the mathematical model used for the experimental system is a valid approximation of reality. And even then, the conclusions drawn from the simulations must be interpreted with care.

In the simulations carried out [20], the power spectrum of a thin carbon foil was modelled with a negative exponential, the TEM was modelled with the phase contrast transfer function (PCTF), the image pickup device was modelled with a 512^2 pixel camera and the noise was considered to be white (all frequencies present and of equal intensity). In general, these assumptions hold in prac-

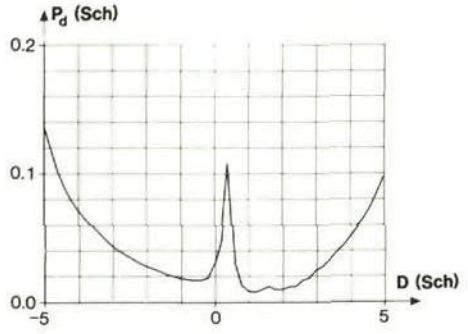

Fig.7: The achievable accuracy in tuning the TEM (P_d) as a function of the defocus, for a beam tilt of 0.2 and a SNR of 0.5. The achievable accuracy near focus is worse than the accuracy at Scherzer focus. Consequently, a more accurate estimate of defocus can be made if the TEM is tuned near Scherzer focus in a previous step.

tice, as is confirmed in other papers (for instance in [27]). The (signal) image of a carbon film can be described using the PCTF, the noise as a realisation of a (white) stochastic process having a Gaussian distribution. To illustrate this model of a recorded image, see fig. 6. Thus, for a Philips EM 420 TEM operated at 120 kV, a number of simulation experiments were carried out, believed to be sufficiently realistic.

In the simulations it was shown that the accuracy in tuning the TEM has a dependence on defocus as shown by fig. 7, provided that the SNR is about 1, the induced beam tilt equals 0.2, the defocus spread 0.2 and the beam divergence 0.14, respectively. As fig. 7 shows, for a TEM in Scherzer focus, the achievable accuracy in tuning a TEM (P_d) is better than for a TEM in Gaussian focus, as the image contrast is higher. Another conclusion drawn was that the tuning accuracy is proportional to the SNR in the images, provided that the SNR is larger than 0.5, as is shown in fig.2. By accumulating images, the accuracy in tuning the TEM will increase according to the simulations, up to some point where the instrumentation limits the accuracy in controlling the TEM parameters. When the dose is decreased, the accuracy in tuning the TEM will gradually worsen, until the effects introduced by the camera system limit the performance of the autotuning method.

3 Implementation of the autotuning method

The autotuning system of a TEM is, in general, a feedback system consisting of three parts: a TEM, a camera as image pick-up system, and a computer for the computations and control. Essential is that the TEM can be controlled externally; defocus, stigmator and deflection coils in particular. For practical autotuning it is crucial that the computation of image displacement and the application of digital low/high pass filters, is done with high speed (within seconds). Therefore, a fast Fourier transform facility must be available to calculate the image cross covariance functions and cross spectra. Numerous papers on the computer control of electron microscopes have been published [28], [29], [30] and [31]. Next, the required specifications for autotuning of each part of the feedback system are discussed.

3.1 Instrumentation requirements

3.1.1 The Transmission Electron Microscope

For our purposes, the TEM must have facilities for external control of the beam tilt, objective lens stigmator and focus. External control of the condensor lens system (electron intensity on the camera, beam divergence), position of pivot points and the magnification of the TEM, is convenient for the calibration of the computer control, but is not essential for the autotuning procedures. In addition, it is convenient when the communication between TEM and computer is two-way; that the TEM is able to give specific information on its status when the external computer prompts for it.

3.1.2 The camera

In this paper the camera is loosely defined as that part of the feedback system which transforms the electron intensity distribution in the TEM present at the image plane, to a grey level distribution in the framestore of a digital computer. This transform consists of many steps. A recent overview of existing systems is given in [4]. Several methods are available to record an image.

A method to record the image by using only one detector element (such as a transmission detector), scanning the electron intensity distribution over the detector, and measuring at time intervals the electron current. The advantage of this approach is that the electron intensity distribution is recorded with exactly the same detector: no shading pattern is visible in the recorded image due to variation in the sensitivity of the image recording elements. A disadvantage is that the method is not dose efficient, as only one detector is used for the (serial) intake of the image. So, for practical systems a single-detector recording system is not sufficient.

Another way to record the image is to use a one-dimensional CCD array instead of a single detector. The advantage compared to the single detector is a higher dose efficiency. The disadvantages are the inhomogeneous sensitivity of the detector elements (shading

pattern) and the necessity to protect the CCD chip against the high energy electrons (hundreds of keV). A fluorescent or YAG screen is often used to transform the electron intensity distribution to a light intensity distribution which is recorded with the CCD chip. This transformation contributes to the shading pattern of the camera.

A more dose efficient approach is to use a two-dimensional CCD array or a vidicon type of camera. In the remaining part of the paper, it is assumed that this type of image pickup device is used.

The camera influences the performance of an autotuning method considerably, because it has a finite pixel resolution and sensitivity. The resolution limits the choice of electron optical magnification as the camera is only capable to detect images up to some spatial frequency. Presently, images of about 256^2 pixels of a specimen recorded with a camera are normally used for processing, but cameras with 1024^2 pixels are commercially available. The pixel size of a vidicon type of camera is adjustable, and in practical situations adjusted to the resolution of the fluorescent (or YAG) screen (in practice 25 to 50 μm). A CCD camera has a fixed pixel size of about 5 to 25 μm, smaller than the resolution of the fluorescent or YAG screen. Therefore, demagnification of the image on the screen to a smaller image on the CCD camera is needed to use the resolution of the CCD camera effectively. This demagnification is done either by means of fibre coupling or optically, and may introduce extra image distortions.

The sensitivity of the camera determines the applicability of the autotuning method for low dose work. When an image intensifier is connected to the camera, a sensitivity of 5.10^5 electrons per cm^2 per second (specifications of a Gatan 622) can be obtained, without an intensifier 5.10^3. To suppress noise in the recorded images, accumulation of a number of images, possibly using special hardware, is essential. The sensitivity of the camera is not the same for all pixels (shading pattern). The shading pattern will not shift when the illuminating beam is tilted and has to be corrected for. A correction method is to devide and image with an image recorded without a specimen (so called zero image). This correction method has been found to be sufficient.

A digital high pass frequency filter has been found to be helpful to remove the low frequencies of the shading pattern (a smooth change in sensitivity of the pixel elements across the camera, or a smooth change in the illumination intensity across the camera). If the image has hexagonal structures in its shading pattern due to the coupling of optical fibres, the effect of this pattern can also be eliminated using a digital filter. Note, that this filtering is needed only for tuning, and may not be needed for the interpretation, or display, of the actual images. For the application of digital filters within electron microscopy see [32].

The afterglow of an image on the camera determines a minimum time span between the input of each new image (due to the fluorescent or YAG

screen on camera) and, therefore, is a limiting factor to the speed of the autotuning procedure. In practice, a time span of a second between the intake of each image (for instance, after inducing a beam tilt) is needed.

3.1.3 The computer - control of the TEM

A digital, or serial interface to control of beam tilt, stigmator and defocus is preferable to analogue control as it is less sensitive to electronic noise. Furthermore, the interface must be fast and flexible to perform complex control procedures with success. For instance, for the coma- free and dispersion free alignment procedures an external control of the beam tilt, the defocus, the magnification and the condensor lens system is indispensable. Commercially, available TEMs are mostly equipped with a serial communication port, but are presently rather slow in handling the instructions given (in the order of seconds).

3.1.4 The computer - image processing

In general, the speed of an autotuning method is determined by the computational power of the image processing system. The autotuning method described in this paper requires the calculation of cross *covariance functions and cross spectra of* pairs of images. Therefore, the specifications of the image processing computer with respect to speed and accuracy of Fast Fourier Transform (FFT) of images are of importance.

An image is such a vast amount of data that micro- and mini-computers have difficulties processing it within minutes. An image of 512^2 pixels of 16 bits deep requires 0.5 Mbyte of RAM to store it. An IBM PC, with DOS as operating system, is not able to multiply images without using the (time- consuming) hard disc, and will take minutes in doing so. In addition, the Fourier transform of an image is such a computational load that it will take minutes on a PC.

Consequently, the processor, bus, memory and operating system must be suitable to process Mbytes of data and to perform FFTs of images within fractions of a second. Therefore, special hardware for an FFT of an image (array processor or FFT processor) must be available. Furthermore, the images have to be transferred between RAM and the special hardware units within fractions of a second, which requires a high speed picture transfer bus. Finally, special hardware to accumulate (at video-rate) images to suppress noise, and to subtract, add, multiply and divide images is virtually inevitable for implementation of a practical autotuning system.

3.1.5 The computer - the user interface

The operator of the TEM is interested in solving the problems concerning the specimen under study, and not in the computers connected to the TEM. Yet, in practice, the interface between computer and TEM operator is often poorly designed: the output is a nice color picture, but the input is only a keyboard (with, again, another monitor) near the TEM. The user interface should be designed in such a way that the operator is able to influence continuously the status of TEM and image processor. For

this reason is the accessibility and user-friendliness of the highest software level available of importance, as at this level the TEM and computer are used during experiments. It is not possible to define a 'best' user interface, as it is application and problem dependent. Perhaps the most friendly way to control the computer is using a few commands, invoked with a mouse. For example, a command to accumulate images, calculate a diffractogram, or to correct the defocus and the astigmatism.

Application programming must be feasible to develop more specific commands. Normally, this lower level programming is done in Pascal, Fortran, C or assembler.

3.1.6 Some examples of measuring set-ups

The least expensive set-up consists of a PC configured as user interface, image processing device and TEM interface simultaneously. A video image is stored, and a Motorola 68020 (Macintosh, Atari) or Intel 8086 (IBM PC) processor is used for image processing. It is doubtful whether this set-up is suitable for practical applications, as it will take minutes to process the images. Nevertheless, when special extension boards are added to this system (Fourier board, video-rate image integration board, array processor board, transputer boards), it will enhance the performance considerably.

Presently, a limitation of PC-based systems is that the commercially available image processing software is not designed to the hardware extensions specific for autotuning. However, impressive PC-based image processing systems are becoming available (SEMPER [33] and EMS [34]). Another point to consider is how suitable the system is for future demands on, for instance, image simulation (SHRLI [35]) or reconstruction techniques (IMAGINE [36]).

A flexible set-up consists of an image processing system for which a variety of extension boards and compatible software packages are available (VMEbus, Multibus, DEC Q-bus, operating systems VMS, UNIX, OS-9). A few examples of this type of set-up are the IMAGINE machine, a MicroVAX with SEMPER [33], or the system described in the next section (TVDIPS). For user convenience this system may be controlled by a separate (small) computer, dedicated to the specific application.

3.2 The experimental set-up in Delft

The experimental set-up in Delft consists of a Philips EM 420 TEM, a Gatan 622 camera without image intensifier, a DEC PDP 11/23 computer used as TEM interface, a TVDIPS image processing device with special hardware and an IBM PC/AT as user interface, see fig. 8. Each of these parts is discussed separately.

3.2.1 The Philips EM 420 TEM

The Philips EM 420 is a 120 kV TEM equipped with a tungsten filament and has a point resolution of 0.34 nm. The TEM is, in its standard configuration not equipped with external control of beam tilt, focus and objective lens stigmator. Therefore, modifications in the electronics were necessary to control

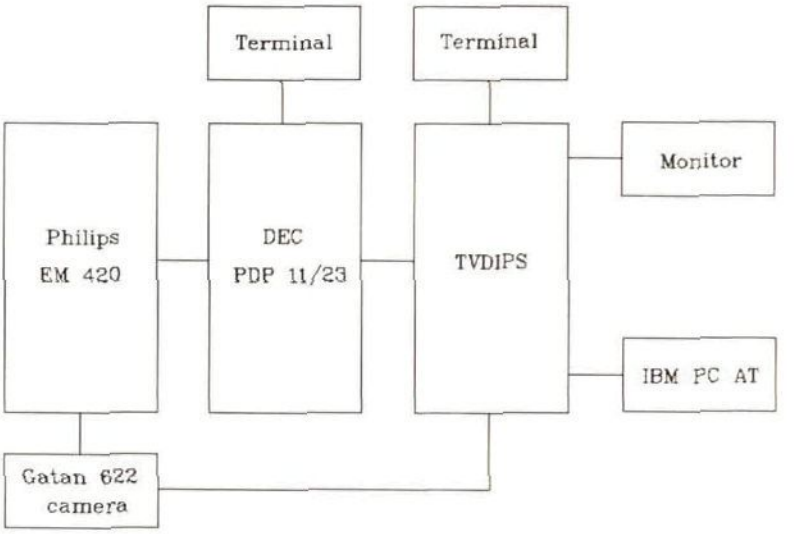

Fig.8: The experimental measuring set-up in Delft. A Philips EM 420 images a specimen on a Gatan 622 camera, which is connected to a Tietz Video Digital Image Processing System (TVDIPS). This system controls the TEM interface (DEC PDP 11/23) and uses an IBM PC/AT as intelligent terminal.

these parameters externally. Other parameters, like the magnification and the beam divergence, are controlled manually.

3.2.2 The Gatan 622 camera

Connected to the TEM is a Gatan 622 video camera with a YAG crystal to convert the electron intensity distribution to a light distribution. For the computations an image size of 256^2 pixels appeared to be sufficient. At a magnification of 12,400 the pixel size corresponds with 0.346 $\pm$ 0.010 nm. An image is clearly visible at a vidio monitor when the average intensity of the image corresponds with an exposure time of 50 s at an emulsion setting of 1. The minimum time span before storing a new image (after, for example, a beam tilt), is due to the afterglow in practical situations about 0.5 s.

3.2.3 The DEC PDP 11/23

The TEM interface consists of a DEC PDP 11/23 computer, to control the beam tilt, focus and objective lens stigmator. The DEC is controlled by the image processing computer through a serial port. If an instruction cannot be carried out (for example, because the range of the DAC is not sufficient for some specific task), the image processing computer is informed.

The DEC is fitted with 256 kByte of RAM, an 8 bit digital I/O boards of which 3 bits are used to control the focus of the TEM, eight 12 bit DACs (-5 to + 5 V) of which two are used to control the objective lens stigmator and two for the beam tilt. Focus is controlled in steps of 6.47 $\pm$ 0.09 nm and 1000 steps/s. The DACs con-

nected to the x-coil and y-coil tilt the beam with 8.56 ± 0.03 mrad/volt and 10.06 ± 0.04 mrad/volt, respectively (depends on the position of the pivot point) and with 40 mrad/s. The DACs connected to the stigmator introduce astigmatism with 3.90 ± 0.06 μm/volt for both stigmator coils with 20 μm/s. For development purposes, the TEM interface can be also be controlled with a separate terminal.

3.2.4 The TVDIPS image processing device

As image processing device TVDIPS, a commercially available system [37], is used. The system is equipped with a special software shell to perform a number of basic operations on images, without the need of programming. For example, the averaging of images for noise suppression, calculation of diffractograms, or automatic image contrast enhancement is done without any programming. More application dependent tasks, like the computation of cross spectra or Fourier filtering, require programming in Pascal, C or assembler.

The system is built around the VME bus, the Motorola 68020 processor and the multi-user multi-tasking operating system OS/9. The system is equipped with 5 Mbyte of RAM, 80 Mbyte of hard disk and two floppy disk drives. Furthermore, the system consists of a high speed picture bus, an image Arithmetic Logical Unit (ALU) for the accumulation of images at video-rate, and a 16 bits integer FFT processor. Fourier operations are done at high speed: a diffractogram of 256^2 pixel image in 0.8 s and a cross covariance function in 2.5 s. Division of images is done with the Motorola 68020 processor and will take about 2 s. For images with a high signal-to-noise ratio it was found to be sufficient to subtract the shading pattern, which takes about 0.2 s.

The image processing system is controlled using one of the two serial ports of an IBM PC/AT configured as terminal. The second serial port is used to control the TEM interface (DEC computer).

3.2.5 The IBM PC/AT

An IBM PC/AT is configured as the user interface and is connected to the image processing system. For any PC a vast amount of graphical software is available to help the operator to control the TEM and image processing system conveniently. As high level language the scientific language ASYST is used. Application dependent programs are developed in this language. If needed, lower level application programming of the image processing system can be done in Pascal or assembler.

4 Experimental results

The performance of the autotuning method is tested on a Philips EM 420 TEM, operated at 120 kV. Experimental results will be presented obtained with the autotuning method for magnifications between 12,400 and 124,000.

4.1 Calibration

The relation between the TEM parameters, and the currents through lenses and coils in the TEM is measured. This calibration of control has to be repeated when the pivot point of the

beam tilt, the centering of the stigmator, or the video amplifier setting is changed.

The magnification from specimen level (nm) to camera level (pixel) is calibrated at a magnification of 12,400. This is an important calibration, as the calibration of all the other magnification settings are related to this one. A crystalline specimen (catalase, with two orthogonal frequencies of 8.75 and 6.85 nm) is imaged and its diffractogram is calculated. From the distances between the diffraction spots (the spatial frequencies) the corresponding scaling factor (0.346 $\pm$ 0.010 pixel/nm) is computed.

Next, the relation between the beam tilt (mrad) and the voltages applied to the deflection coils is calibrated. The diffraction pattern of an amorphous gold film is imaged. Using Bragg's law, the beam tilt is related to the distance between the diffraction rings visible on the screen. The proportionality constants between the voltages applied to the deflection coils were found to be 8.56 $\pm$ 0.03 mrad/V (x-coil) and 10.06 $\pm$ 0.04 mrad/V (y-coil).

The focus step size (nm) is calibrated using the previously calibrated beam tilt angle and magnification. First, the beam is tilted, and the image is recorded. Next, a number of focus steps are induced and a second image is recorded. Then the displacement between the two images is measured using the cross covariance function (pixels). Finally, the defocus difference is calculated and the focus step is known (6.47 $\pm$ 0.09 nm at 120 kV.

The other magnification settings are calibrated using the same amount of defocus and beam tilts. From the measured displacements, and the calibration of magnification 12,400, all the other magnification settings are calibrated (27,500: 0.720 $\pm$0.02 pixel/nm, 75,000: 1.890 $\pm$ 0.079 pixel/nm, 160,000: 4.268 $\pm$ 0.723 pixel/nm.

Finally, the stigmator coils a and b are calibrated by inducing a change in the voltages applied, and measuring the amount of astigmatism introduced. The sensitivity of stigmator coil a, and of b, was found to be 3.90 $\pm$ 0.06 μm/V.

Another approach is to calibrate the TEM during autotuning. During each attempt, the ration between the induced change in the TEM parameter and the corresponding displacement can be measured. The advantage of this approach is that it results in a very robust autotuning procedure. A drawback is that extra images are required and thus a larger dose. For this reason, we chose to separate the calibration and autotuning procedures.

4.2 Automatic rotation alignment

The rotation alignment procedure corrects the beam tilt misalignment in such a way that the image does not shift when the defocus of the TEM is changed (section 2.1). Prior to the alignment, the TEM is automatically set in underfocus to avoid contrast reversal when the defocus change is induced (section 2.2).

The implemented algorithm requires as input the magnification. From the magnification the change in defocus, suitable for alignment at that specific magnification, is derived (see Table 1). The algorithm calculates the misalignment from two images formed at two

Table 1: The induced amount of defocus as used by the rotation alignment procedure as a function of the magnification. The accuracy in estimating the misalignment was better than 0.1 mrad.

Magnification	1st image	2nd
	μm	μm
12,4000	-30	-10
12,500	-15	-5
75,000	-8	-3
96,000	-4	-2

Fig.9: Illustration of the rotation alignment procedure. The images correspond with an underfocus of -9.1 μm (upper left) and -5.4 μm (upper right) at a magnification of 45,000. The maximum of the cross covariance function of the two images (lower left) indicates an image displacement as result of a beam tilt of 4.3 mrad. The image displacement is estimated with an accuracy better than 0.2 pixel, by fitting a quadratic polynomial through the top of the cross covariance function (lower right). The images are corrected for the shading pattern produced by the camera system by dividing by the zero image. If no correction is made for the shading pattern, artifacts will be present in the cross covariance function as is shown by fig. 4.

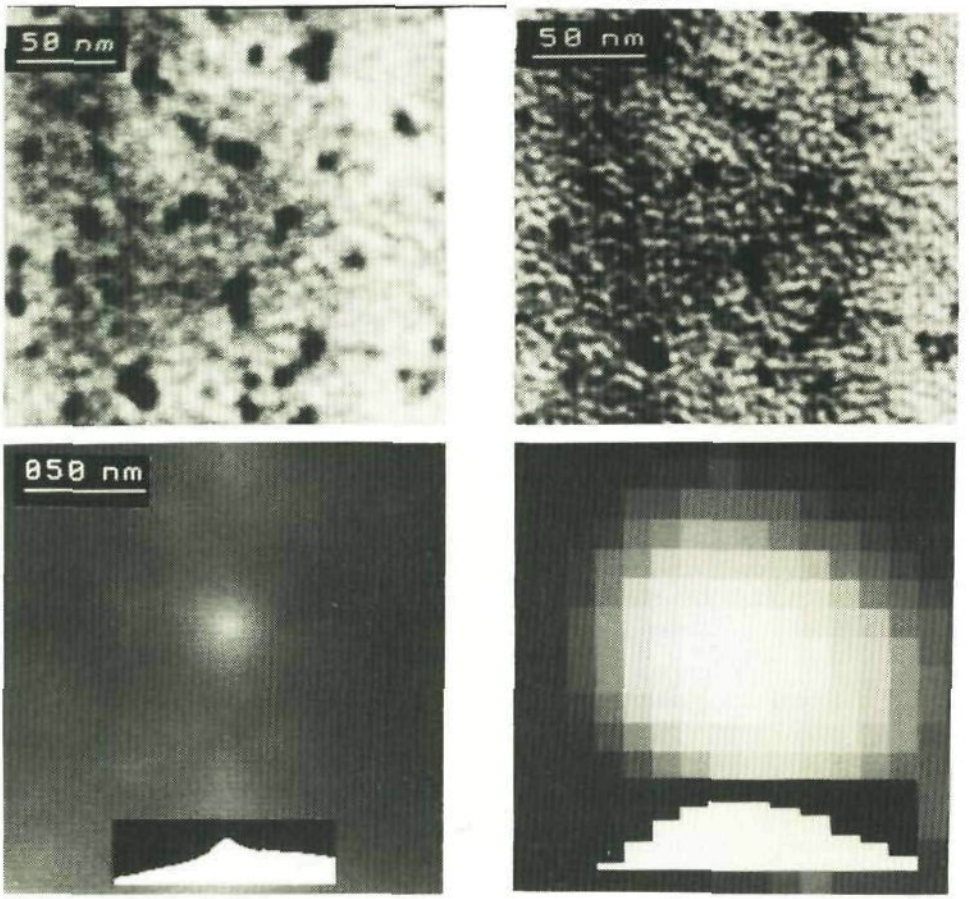

Table 2: The measured accuracy in estimating the defocus and astigmatism as a function of the magnification. The induced beam tilt angle is 8 mrad.

Magnificaton	defocus nm	astigmatism nm
12,400	36	72
27,500	18	36
75,000	8	16
96,000	5	10

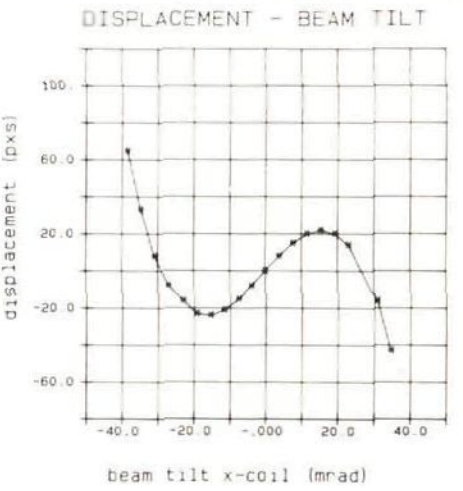

Fig.10: The image displacements as a function of the induced beam tilt at a magnification of 27,500 and a defocus of 2.5 μm. The effect of spherical aberration is clearly visible for tilt angles larger than 10 mrad. From these measurements the constant of spherical aberration was estimated to be 2.30 ± 0.03 μm.

accuracy of the algorithm depends on the accuracy of the image displacement measurement, which is, apart from the effects due to noise in the images, 0.2 pixel for magnifications up to 124,000. The accuracy in aligning the TEM is 0.1 mrad. The alignment procedure takes 7 s, of which 4 s are used for the computations.

The procedure is shown by fig. 9. At a magnification of 45,000 two images are recorded at -9.1 and -5.4 μm underfocus. The initial misalignment was 4.3 mrad, as indicated by the position of the global maximum of the cross covariance function.

4.3 Automatic coma-free alignment

The coma-free alignment procedures estimates the misalignment from the differences in image displacement for opposite beam tilts. It is described in section 2.1. Five images are recorded: one without a beam tilt, and four with equal, but oppositly tilted beams. Prior to alignment, the TEM is set automatically in underfocus, in order to have optimal image contrast. The optimal beam tilt and defocus is magnification dependent.

The implemented algorithm requires as input the magnification, induces the beam tilts and estimates the misalignment from the image displacements. The measured accuracy is better than 0.1 mrad, with induced beam tilts of 8 mrad. The procedure takes about 15 s to align the TEM, of which 10 s are used to calculate the four cross covariance functions.

When the TEM is not aligned coma-free, the image displacements corresponding with opposite beam tilt, differ in magnitude. When the image displacement is measured as a function of the beam tilt angle, the constant of spherical aberration can be estimated (4). For the experiment shown in fig.10, the misalignment was 0.7 mrad, and the constant of spherical aberration 2.30 ± 0.03 mm.

4.4 Automatic focusing and correction of astigmatism

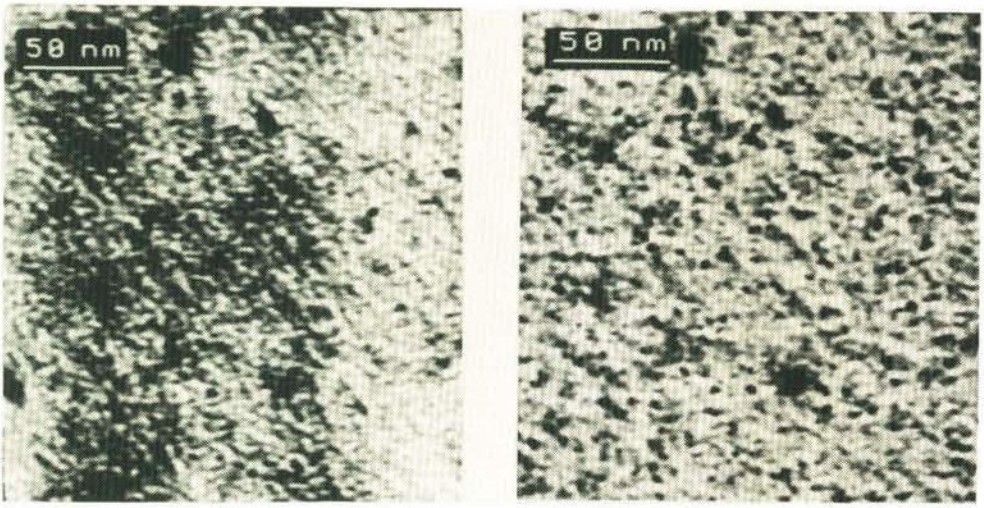

Fig.11: Illustration of the correction of defocus and astigmatism. One image corresponds with a defocus of -2.5 μm and an astigmatism of 3.9 μm (left) at a magnification of 45000 with a beam tilt of 8 mrad. The other image is the result after the correction of defocus and astigmatism (right).

The correction of defocus and astigmatism requires the recording of three images: one formed without an induced beam tilt, and two of the images with equal beam tilts in perpendicular directions (section 2.1). Prior to the recording of the images, the TEM is aligned coma-free. As in the previous sections, the accuracy of correction depends on the accuracy of the displacement estimates, which is illustrated by Table 2. The procedure takes 6.5 s, of which 5 s are used for the computations.

An illustration of the correction procedure is given in fig.11, at a magnification of 45,000, a defocus and astigmatism of 2.5 μm, respectively, 12.0 μm, using a beam tilt angle of 8 mrad.

A more accurate estimate of the defocus and astigmatism is made when the image displacement is measured as a function of more than two azimuthal angles. Fig.12 shows the measured image displacements corresponding with 8 beam tilts ($\pi/8$ rad between each tilt), at a magnification of 75000. The values of defocus and astigmatism were -1.95 and 0.02 μm, respectively.

4.5 Instrumental limitations for low SNR images

In a previous paper [20], the achievable precision in tuning a TEM using the beam tilt method was calculated. These calculations gave a relation between the signal-to-noise ratio (SNR) in the images (related to the dose used for recording the images) and the achievable precision in estimating the TEM parameters from these images. This achievable precision can be used as to evaluate the perfor-

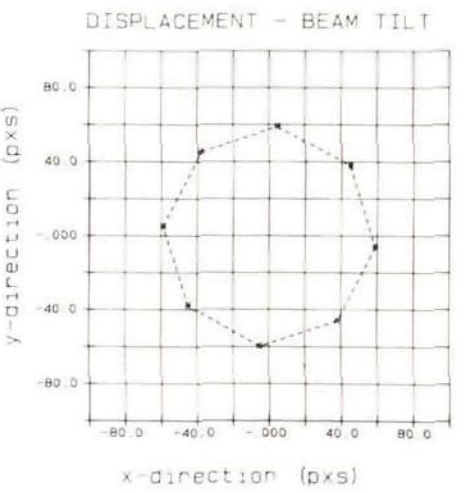

Fig.12: The image displacement as a function of the azimuthal angle of the induced beam tilt at a magnification of 75,000. From this figure the defocus and astigmatism were estimated to be -1.95 μm and 0.02 μm, respectively.

mance of the measuring set-up with respect to the of noise in the images (see section 2.4).

In this paper, the SNR of an image is defined as the ratio of the variance of the specimen image (signal) and noise. The signal variance is calculated from the accumulation of a large number of images. The noise variance is calculated from the difference between the accumulated image and a single image. Several methods to measure and suppress the noise in a recorded video image were proposed [38], [39] and [40]. This definition of SNR is chosen as a simple measure for the ratio of the power in the noise and the power in the image. For other purposes it may be more convenient to define a SNR per spatial frequency of the recorded image.

In the set-up in Delft, the Gatan camera, without image intensifier, is not limited by shot noise (with a Poisson distribution) but by instrumentation noise, for a dose between 5 and 50 electrons per pixel (fig.13); the SNR is proportional to the square of the dose and not proportional to the dose. Furthermore, the SNR of an image of a thin carbon film is, under these circumstances, less than 2. It is evident that for low dose experiments, an image intensifier is necessary. The SNR depends also on the defocus of the TEM, and varies by a factor of three in practical situations.

The practical limitation in measuring an image displacement appeared to be 0.2 pixel for a magnification lower than 124,000 (reproducibility of 0.2 pixel); an increase of the SNR did not result in a

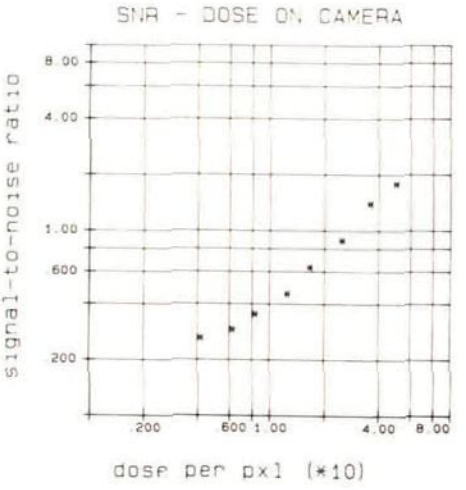

Fig.13: The SNR as a function of the electron dose per pixel. The SNR is proportional to the square of the electron dose, which indicates that the instrumentation noise of the camera is stronger than the shot noise (Poisson distribution)

better accuracy. Furthermore, the shading pattern of the camera system (section 3), frustrates the estimation of image displacement of low contrast images (roughly lower than 0.5) and makes pre-processing of the images necessary. To illustrate the influence of the shading pattern see fig. 4 and 9.The cross covariance function is distorted in the sense that it has high values near the position corresponding with no image displacement (the shading pattern stays positioned, independent of the beam tilt). These values may exceed the value of the peak corresponding with the image displacement. Fig. 9 shows a cross covariance function when a correction is made for the shading pattern. The peak corresponding with the image displacement is clearly visible, and shows the image displacement.

Finally, as the Fourier transform is calculated with a 16 bit integer accuracy and the cross covariance following the Fourier transform is available with 8 bits precision, the calculation of the cross covariance function is less accurate than that in the simulations.

In the next section the theoretical and practical autotuning results are summarized, and present developments are discussed.

5 Discussion and conclusions

Experimental results concerning automatic control of the misalignment, defocus and astigmatism of a TEM have been presented. The method used is designed for both amplitude and weak phase objects, and needs further extension to be applicable to cristalline or periodic material (strong phase objects). The autotuning method has been tested on a Philips EM 420 TEM equipped with a Gatan 622 video camera, connected to a TVDIPS image processing system with special fast computer-hardware, and controlled by a small DEC 11/23 computer.

The procedure uses only the lower ($< 0.4\ \mathrm{GI}^{-1}$) spatial frequencies in the images and measures image displacements when the beam is tilted. From these image displacements the TEM parameters are estimated and adjusted. The accuracy is magnification and noise dependent. At a magnification of 12,400 the defocus can be estimated with 36 nm accuracy, the astigmatism with 72 nm and the alignment with 0.1 mrad, respectively. At a magnification of 96,000 these values are 5 nm, 10 nm and 0.1 mrad respectively. The total time needed for alignment is 7 s, and for the correction of defocus and astigmatism 6.5 s.

The practical limitations were due to a finite reproducibility in controlling the beam tilt, defocus, stigmator, a finite accuracy in calculating Fourier transforms and the shading pattern of the camera.

To improve the performance of the autotuning system, it is necessary to use a computer controllable TEM (such as the Philips CM or the Jeol 4000 series) as basic instrument. The digital control of the deflection coils, objective lens and stigmator will may be more reproducable than the anologue control as used in the experiments described in this paper. Furthermore, when other parameters (other than defocus, astigmatism and beam tilt) are accessible and controllable, more

complex and robust autotuning procedures can be realised. For instance, the control of the magnification, combined with the control of the condensor lens system, in order to obtain the same spot size or the same intensity on the screen, makes autotuning at other magnifications than the one used for making the micrographs possible. Moreover, a simultaneous coma-free and dispersion free alignment is feasible (see Introduction), when the variation of the high tension is combined with the control of the deflection coils beneath the objective lens system.

The demands on the computer connected to the microscope are high. Essential is that image displacements can be measured by calculating the cross covariance function within a few seconds. The calculation of the cross covariance function should be done using Fourier transform with floating point arithmetic. Furthermore, to overcome the limitations due to the shading pattern of the camera, division of a recorded image by a so called zero image, is essential. Low- and/or high pass filtering of the recorded images before the estimation of image displacement may be needed at low dose work, or at high magnifications.

The application of automatic control of a TEM will lead to new methods of research and image recording in low and medium resolution electron microscopy. For instance, the method may be helpful for object reconstruction purposes. Furthermore, special techniques for low dose work, and the recording of small areas of tilted specimens at a correct defocus are presently developed [41] and [42].

The developments in automatic control of electron microscopes combined with the developments in image simulation software [35], image recording devices [43], image processing [44] and high resolution holography [45] will have a strong impact on high resolution electron microscopy [46] and [47]. New reconstruction techniques combined with an accurate setting of the beam tilt and defocus, may make on-line specimen structure reconstruction possible, with a resolution determined by the fundamental limits of the specimen, and not by those of the the microscope [48]. It is evident that image processing combined with accurate control of the TEM is essential for the further development of high resolution electron microscopy techniques.

Presently, the method described in this paper is implemented on several types of the Philips CM series of TEMs combined with the TVDIPS image processing system, to test the performance and flexibility for low dose electron microscopy at medium resolutions. Methods for automatic control of a TEM suitable for high resolution electron microscopy imaging conditions, combined with the integration of image simulation procedures on fast computer systems are under development.

Acknowledgments

These investigations were supported by the Netherlands Technology Foundation (STW) and by Philips Nederland B.V. Thanks are due to Dr.ir. P. Kruit for his support in improving the practical applicability of the autotuning method.

References

[1] E.J. Kirkland, Part I. Theory, Ultramicroscopy 15(1984)151.

[2] E.J. Kirkland, B.M. Siegel, N. Uyeda and Y. Fujiyoshi, Part II. Experiment, Ultramicroscopy 17(1985)84.

[3] S.J. Erasmus and K.C.A. Smith, J. Microsc. 127(1982)185.

[4] W.O. Saxton and M. Chang, Proc. 9th Eur. Cong. EM (York, UK) 1(1988)59.

[5] D. Typke and D. Kostler, Ultramicroscopy 2(1977)285.

[6] N. Baba, E. Oho and K. Kanaya, Scanning Microscopy, Vol.1, 4(1987)1507.

[7] M. Ogasawara, N. Baba, E. Oho and K. Kanaya, Proc. 9th Eur. Cong. EM (York, UK) 1(1988)199.

[8] F. Zemlin, Ultramicroscopy 4(1979)241.

[9] R. Henderson, J.M. Baldwin, K.H. Downing, J. Lepault and F. Zemlin, Ultramicroscopy 8(1986)147.

[10] W. Kunath, F. Zemlin and K. Weiss, Optik 76(1987)122.

[11] W.O. Saxton, D.J. Smith and S.J. Erasmus, J. Microsc. 130(1983)187.

[12] A.J. Koster, A. van den Bos and K.D. van der Mast, Proc. 6th Pfefferkorn conf. (Niagara Falls, Canada), Scanning Microscopy Suppl. 2(1988)83.

[13] D.J. Smith, A. Higgs and P. Perkes, Proc. 45th Annual Meeting EMSA (San Francisco, USA) (1988)62.

[14] W.J. de Ruijter, Arizona State University, Tempe, Arizona, USA, personal communication.

[15] J. Le Poole, Philips Tech. Rev. 2(1947)33.

[16] H. Koops, Proc. 6th Eur. Cong. EM (Jerusalem, Israel) 1(1976)334.

[17] K.D. van der Mast, Proc. 8th Eur. Cong. EM (Budapest, Hungary) 1(1984)3.

[18] A.J. Koster, A. van den Bos and K.D. van der Mast, Ultramicroscopy 21(1987)209.

[19] S. Nomura and S. Isamozwa, J. Electron Microsc. Vol. 36(1987)157

[20] A.J. Koster, W.J. de Ruijter, A. van den Bos and K.D. van der Mast, Ultramicroscopy 27(1989)251.

[21] D.J. Smith, W.O. Saxton, M.A. O'Keefe, G.J. Wood and W.M. Stobbs, Ultramicroscopy 11(1983)263.

[22] D.T. Grubb, Ultramicroscopy 12(1984)279.

[23] J.R. Fryer, Ultramicroscopy 23(1987)321.

[24] D.L. Misell, Image Analysis, Enhancement and Interpretation (North- Holland, 1978).

[25] M.B. Priestley, Spectral Analysis and Time Series (Academic Press, 1981).

[26] W.H. Press, B.P. Flannery, S.A. Teukolsky, W.T. Vetterling, Numerical Recipes (Cambridge University Press, 1986).

[27] G.Y. Fan and J.M. Cowley, Ultramicroscopy 21(1986)21.

[28] W. Krakow, Ultramicroscopy 18(1985)197.

[29] H.P. Rust and D. Krahl, Ultramicroscopy 8(1982)287.

[30] P. Rez and D.W. Williams, Ultramicroscopy 8(1982)247.

[31] H.Fujioka, K, Nakamae, K. Ura, S. Takashima, K. Harusawa, J.Electron Microsc., Vol. 35(1986)215.

[32] A.F. de Jong, W. Coene and D. van Dyck, Ultramicroscopy 27(1989)53.

[33] Synoptics Ltd, 15, The Innovation Centre, Cambridge Science Park, Milton Road, Cambridge, CB4 4BH, (0223)-322267.

[34] P.A. Stadelman, Ultramicroscopy 21(1987)21.

[35] M.A. O'Keefe, R. Kilaas, Proc. 6th Pfefferkorn conf. (Niagara Falls, Canada), Scanning Microscopy suppl. 2(1988)225.

[36] M. van Heel, Fritz Haber Institut of the Max Planck Society, Berlin, Federal Republic of germany.

[37] Hans Richard Tietz, Video and Image Processing Systems, Herbststrasse 7, D-8035 Gauting, Federal Republic of Germany, (089)8506567.

[38] S.J. Erasmus, J. of Microsc. 127(1982)29.

[39] A. Ishikawa, K. Fukushima and A. Fukami, Proc. 9th Eur. Cong. EM (York, UK) 1(1988)205.

[40] N. Baba, E.Oho, M. Mukai and K. Kanaya, J.Electron Microsc. Tech. 2(1985) 54.

[41] F. Zemlin, Proc. 9th Eur. Cong. EM (York, UK) 1(1988)139.

[42] P. Bullough and R. Henderson, Ultramicroscopy 21(1987)223.

[43] N. Mori, T. Oikawa, T. Katoh, J. Miyahara, Y. Harada, Ultramicroscopy 25(1988)195.

[44] K. Kanaya, J. Electron Microsc. Tech. 10(1988)319.

[45] H. Lichte, Ultramicroscopy 20(1986)293).

[46] J.A. Eades, Ultramicroscopy 24(1988)1.

[47] A. Bourret, Proc. 9th Eur. Cong. EM (York, UK) 1(1988)165.

[48] D. van Dyck and W. Coene, Optik 77(1987)125.

6 Conclusions and Discussion

In this report the theoretical and experimental possibilities and limitations of an automatic method to correct the defocus, astigmatism and beam tilt misalignment of a transmission electron microscope (TEM) were discussed. The method is based on measuring the effect of a beam tilt on a specimen image in a TEM. This autotuning method was implemented designed and tested, and was found to be successful for low-dose electron microscopy, and for high resolution electron microscopy, if the specimen is a weak phase object.

The effect of a beam tilt on the specimen image is a mere image displacement for the low spatial frequencies of the specimen (low magnification). For higher magnifications not only a displacement is visible, but also image blurring. The image blurring is due to the spherical aberration of the objective lens, which influences the diffracted electron beams corresponding with the higher spatial frequencies of the specimen differently from those corresponding with the lower spatial frequencies. This image blurring frustrates autotuning based on estimating mere image displacements. Four methods to autotune the TEM, in spite of this blurring effect, were described.

The first approach is to tune the TEM at a lower electron optical magnification than the magnification used for recording the micrographs (chapter 2). At lower magnification ($<20{,}000$) the effect of the spherical aberration on the estimation of image displacements is nigligible. This approach is sufficient when the structures on the specimen do not contain high resolution information (<20 nm), and when the specimen is not highly radiation sensitive.

The second approach is to remove the blurring effect due to those higher spatial frequencies, by applying a low-pass digital filter to the images, prior to the estimation of image displacement. If this low-pass filtering is applied to the images, autotuning of a TEM based on measuring image displacements, will work at both low and high electron optical magnifications. Consequently, autotuning is then possible at the same magnification as used for recording the images on micrographs. A drawback of this approach is the dose inefficiency. Firstly, high spatial frequencies of the specimen image are important to the tuning precision. Secondly, the electrons contributing to the high resolution information are not taken into account for autotuning, and only used to damage the specimen.

The third approach is to correct for the blurring effect due to the spherical aberration, prior to the estimation of image displacement (chapter 3). The non-linear effect due to the spherical aberration on the phase of the cross spectrum of a pair of images formed at oppositely tilted illumination, can be corrected using a digital phase correcting filter. This phase correcting filter is only dependent on the induced beam tilt

angle. Thus, as the induced beam tilt angle is known, the blurring effect can be corrected for. Note that with this method the beam tilt misalignment and the astigmatism are assumed to be corrected previously.

The fourth approach is in most cases the most suitable: instead of removing, or correcting, the non-linear effect due to the spherical aberration is incorporated in the autotuning method (chapter 4). The phase angles of the cross spectra of pairs of images formed with oppositely tilted illumination are used to estimate the TEM parameters. This approach makes use of the highest frequencies in the images, and is, therefore, suitable for high resolution, and low-dose electron microscopy.

Simulations of a TEM and measuring set-up showed that the minimum dose needed to tune the defocus with 2 nm precision is about 6500 electrons per nm^2, for a TEM operated at 120 kV at an electron-optical magnification of 400,000, at Scherzer defocus, with a thin amorphous film as specimen, and an (digital) image size of 512^2 pixels (Chapter 2 and 4). The precision depends strongly on the setting of the TEM and type of specimen. For example, the precision in tuning the defocus is 2 nm if the TEM has been set previously in Scherzer defocus and 10 nm for a TEM in focus.

In addition, in the simulations it became evident that a two step autotuning procedure should be used for tuning. The first step adjusts the TEM with low precision to some setting from where the second tuning step can be done with high precision. This two step procedure is dose efficient, and each step may consist of different tuning procedures. For example, the first tuning step may be done at low magnification (for low-dose considerations) by measuring mere image displacements using the cross covariance function of pairs of images (chapter 5, section 2.1). The second tuning step may be done at a higher electron-optical magnification, and incorporates the non-linear effect due to the spherical aberration of the objective lens (chapter 5, section 2.3).

For a full implementation of this autotuning approach, the instrumental requirements are high. Firstly, most of the electron optical elements in a TEM must be computer controllable (the magnification, condensor lens system, objective lens, the deflection coils above and underneath the objective lens, a beam shutter). Secondly, the image processing device must be able to calculate Fourier transforms of (512^2 pixels) images within a fraction of a second. The latest types of TEMs and image processing systems meet these requirements.

The performance of the autotuning method was tested in Delft on a conventional Philips EM 420 TEM, a Gatan 622 video camera, a fast image processing system (TVDIPS), and a small DEC PDP 11/23 computer used for the external control of the TEM. The experimental set-up does not meet all the instrumental requirements as mentioned above, but was found to be sufficient to test the basic principles of the autotuning method. A Philips EM 420 TEM is not computer controllable, and was therefore modified for the external control of the defocus, the stigmator and the deflection coils

above the objective lens. The method was found to work fast and reliable. At a magnification of 12,400 the defocus was estimated with an accuracy of 36 nm and the astigmatism with 72 nm. At a magnification of 96,000 the defocus was estimated with 5 nm accuracy, the astigmatism with 10 nm and the misalignment with 0.1 mrad, respectively. The induced beam tilt angle for these experiments was 8 mrad. The total time needed for alignment was 7s, and for the correction of defocus and astigmatism 6.5 s.

The availability of a facility in the image processing system for Fourier transform of images is essential for practical autotuning of a TEM. The commercially available system connected to the TEM was able to calculate a cross covariance function within 0.8 s, with 16 bits integer arithmetic. The reproducibility in controlling the TEM parameters was found to limit the accuracy in estimating an image displacement to about 0.2 pixel. The shading pattern of the camera limited the estimation of image displacements for images with a very low signal-to-noise ratio. A correction for this shading pattern by dividing by a (so called) zero image was found to be sufficient.

For the next generation of the experimental autotuning system in Delft, it is essential to enhance parts of the experimental set-up to be able to continue the further development of the autotuning method. First of all the TEM should be modified extensively, or replaced by the latest Philips CM series of TEM, to realize the complex tuning procedures as are needed in practice (change in magnification during tuning, simultaneous rotation and coma-free alignment, low dose work). A computer controllable TEM makes the design and implementation of complex autotuning and imaging strategies feasible. Secondly, for low-dose electron microscopy, the camera system should be equipped with an image intensifier. Furthermore, the image processing system should be equipped with a floating point array processor to calculate Fourier transform of images, and have facilities for the external control of the TEM.

Presently, some of these enhancements are effectuated. The autotuning method described in this report is implemented on several TEMs of the Philips CM series of microscopes (computer controllable), to evaluate its performance in practical situations. The image processing system used (TVDIPS), has facilities for the external control of the CM type of microscope and a 80 Mflop array processor for a fast (200 ms) floating point calculation of Fourier transforms of 512^2 pixel images.

Existing low dose techniques may have considerably benefit from an autotuning facility. For instance, a well known method is to tune the TEM at a different area of the specimen than the area of interest. This method may be improved to cope with non-flat surfaces, or even specimen tilts [1-2]. A more accurate estimate of the defocus at the area of interest is possible if the defocus at areas surrounding the area of interest is measured. When the values of the TEM parameters are measured for the areas surrounding the area of interest, an in-

dication of the defocus at the area of interest can be derived by means of interpolation. This procedure to estimate the TEM parameters on areas surrounding the area of interest is rather complex to implement. The use of the deflection coils above and underneath the objective lens, the use of the condensor lens system combined with the electron optical magnification to illuminate a specific area on the specimen, and the use of a beam blanker within the TEM is necessary. Furthermore, estimating the defocus in several areas of a tilted specimen is of interest for the reconstruction of specimen structures from a specimen tilt series; the defocus can be corrected dynamically during the recording of micrographs of several areas on the specimen.

Another technique to obtain information on radiation sensitive structures which may benefit of autotuning, is the periodic averaging technique [3]. A large number of identical structures (the so called unit cells), hardly visible due to the (shot) noise in the images, are averaged (in place, not in time) to increase the signal-to-noise ratio of a unit cell. Limitations of these kind of methods are due to the projection of three-dimensional structures to two-dimensional structures and to the random orientation of all those structures.

A limitation to this technique is that the specimen area is too large to be recorded on one micrograph. If the large area is not flat, then the defocus of the specimen images recorded will differ. Therefore, a reproducable estimate of the defocus is useful to minimize the difficulties related to the reconstruction of the unit cell. The reconstruction requires the processing of thousands of video images and is not yet feasible on- line. However, with the developments in high resolution camera systems (2048^2 pixels), and the increase in computational power, the display of the on-line reconstructed structure might be feasible within the coming decade.

Another exciting possibility with an autotuning facility on a TEM is the on-line reconstruction of the specimen structure from a through focus series of specimen images [4-5]. For weak phase objects the phase contrast transfer function of the TEM determines which frequency region of the specimen image is directly interpretable. At a certain defocus, an image is not directly interpretable due to contrast reversal and amplitude filtering of the specimen image. Therefore, if at each defocus value for which an image is recorded, the TEM parameters are measured, a directly interpretable image can be displayed on a monitor, after composition of a number of specimen images formed at different focus. For this application, an accurate setting of the defocus and beam tilts, and a fast Fourier transform facility on the image processing system is necessary.

Other developments from which the research on radiation sensitive material, and high resolution microscopy may have benefit are related to the gun and the use of the deflection coils underneath the objective lens [6]. If, the so called, flashed illumination is possible (electron illumination of the specimen for only a few

msec), an autotuning system can be used to process the noisy images (only a few electrons contribute to the image formation) until the computer system has obtained enough information on the setting of the TEM to estimate the TEM parameters up to some desired accuracy [7]. Furthermore, when the specimen is moving, the computer system can align the video images obtained within the computer, or adjust the setting of the deflection coils underneath the objective lens as a dynamic shift to nullify the movement of the specimen. This technique requires prediction of the position of the specimen at a certain moment and is therefore not possible if the specimen movement is random. When the movement of the specimen image is due to instrumental instability, the movement should be eliminated by technical improvements and not with a computer system correcting for the movement.

For high resolution electron microscopy the autotuning method was tested in simulations. For the experimental testing of the method a high resolution TEM combined with image simulation software must become available For high resolution electron microscopy it is inevitable to compare the measured specimen images with simulated images. The specimen thickness, structure, orientation and TEM setting, influence the image severely [8]. The method described in this work is suitable for a weak phase object, but not for thick crystalline material. The development of an autotuning method applicable to thick cristalline material is highly desirable. Still, in many practical situations, the structures of interest are positioned on a thin amorphous film (weak phase object), which can be used for autotuning of the TEM.

Autotuning for high resolution electron microscopy is highly desirable as the comparison between measured and simulated high resolution images is less ambiguous when the setting of the TEM is known accuractely. Furthermore, the resolution of the images can be increased when a beam tilt is induced, combined with an appropriate amount of defocus [9]. From a series of images formed with different beam tilts and defocus values, a directly interpretable image of the specimen structure may be be reconstructed.

An interesting development in the interpretation of high resolution electron microscopic images, is the proposal of a new restoration procedure of the wave function emerging from the specimen [10]. The procedure proposed can be used for direct, unambiguous structure retrieval from a number of images. The instrumental requirements for the application of this proposed method are extremely high, but might be met with the latest generation of TEMs, computer systems and automatic control facilities. The autotuning method should be able to estimate and control the defocus of the TEM with an accuracy of at least 2 nm, but is never realized in an experimental set-up.

The developments in TEM and image processing show that within five or ten years, autotuning will be a facility on any new TEM. A camera, a framestore and image processing facilities will be integrated in the TEM. This is to be ex-

pected because the ratio of the computational power of computers to the costs increases. In addition, the importance of (on-line) image processing within electron microscopy increases, especially for the low dose and high resolution work.

Consequently, the quality and reliability of the TEM as an analytical tool will depend, more and more, on the design and implementation of automatic control facilities. Three levels of automatation are to be expected. The lowest level will be disigned for a full human control. For instance, the manual control of the defocus will be highly reproducable and fully calibrated. The next level of automatation will make specific tasks related to, for instance, low dose work (tuning the TEM at another area in the specimen than the area used for recording), less complicated and more reproducable. The highest level of automatation will be related to the facilities to design and incorporate, new, control procedures.

For successful development of procedures towards the requirements of the microscopist, with their various applications, a standardization of the instrumentation and software is essential. Unfortunately, only time will show what hardware and software will become a standard in the coming years. Nevertheless, it was one of the goals of this work to present a possible standard way of tuning the TEM parameters automatically. The method described is applicable for most commercially available TEMs, and useful for a variety of research done with a transmission electron microscope.

References

[1] Bullough P. and Henderson R. (1987). Use of spot-scan procedure for recording low-dose micrographs of beam-sensitive specimens. Ultramicroscopy 21, p.223.

[2] Zemlin F. (1988). A novel procedure for recording tilted samples in small-spot scanning with simultaneous compensation. Inst. Phys. Conf. Ser. No. 93, Vol. 1, p.139.

[3] Heel, M. van (1982). Detection of objects in quantum-noise-limited images. Ultramicroscopy 8, p.331.

[4] Bonhomme P. and Beorchia A. (1985). Image synthesis in the electron microscope. Ultramicroscopy 17, p.127.

[5] Vogel, R.H. and Provencher S.W. (1988). Three-dimensional reconstruction from electron micrographs of disordered specimens. Ultramicroscopy 25, p.223.

[6] Mast, K.D. van der and Koster A.J. (1988). Are major instrumental developments in TEM still to be expected? Proc. 46th Annual EMSA Meeting, Milwaukee.

[7] Bostanjoglo O., Tornow R.P. and Tornow W. (1987). Nanosecond-exposure electron microscopy of laser-induced phase transformations. Ultramicroscopy 21, p.367.

[8] O'Keefe M.A. and Kilaas R. (1988). Advances in high-resolution image simulation. Scanning Microscopy Supplement 2, p.225.

[9] Saxton W.O. (1988). Accurate atom positions from focal and tilted beam series of high resolution electron micrographs. Scanning Microscopy Supplement 2, p.213.

[10] Dyck D. van and Coene W. (1987). A new procedure for wave function restoration in high resolution electron microscopy. Optik 77, No. 3, p.125.

Samenvatting

Een transmissie electronenmicroscoop (TEM) is een belangrijk instrument voor het onderzoek van biologische en anorganische structuren. De toepasssing van een TEM wordt onder meer beperkt door het oplossend vermogen van het instrument, de gevoeligheid van het preparaat voor de bestraling met electronen, en door de kunde van de microscopist om het microscoop in te stellen. Met het instellen van het miscroscoop wordt in dit rapport bedoeld het corrigeren van het defocus en het astigmatisme, en het uitlijnen van de belichtingsbundel ten opzichte van de objectieflens.

Het doel van het onderzoek is om een methode te ontwerpen, te implementeren en te testen, die automatisch de TEM instelt. Het automatisch instellen van de TEM duiden we verder aan met autotuning of met zelf-instelling.

Een tweetal belangrijke eisen stellen wij aan de autotuning methode. Ten eerste behoort de methode geschikt te zijn voor zowel het werk met zeer stralingsgevoelige preparaten (low-dose) als hoog oplossend vermogen electronenmicroscopie. Bij low-dose electronenmicroscopie speelt vooral de gevoeligheid van het preparaat voor de electronenstraling een belangrijke rol, en bevatten de beelden veel ruis. Voor hoog oplossend vermogen electronenmicroscopie is niet zozeer de stralingsschade aan het preparaat een probleem als wel de zeer hoge nauwkeurigheid waarmee de TEM ingesteld dient te worden voor een eenduidige interpretatie van de preparaatafbeeldingen. De tweede eis die aan de methode gesteld wordt is dat hij het microscoop zo nauwkeurig mogelijk instelt met het gebruik van een minimaal aantal electronen.

De dissertatie is bedoeld voor degene die zich bezig houdt met de ontwikkeling van nieuwe technieken en methoden met betrekking tot de toepassing van transmissie-electronenmicroscopie.

De autotuning methode is ontwikkeld om de microscopist te helpen het microscoop zo nauwkeurig mogelijk in te stellen als het preparaat zeer gevoelig is voor de electronenstraling. De mogelijkheden en beperkingen van autotuning in de praktijk wordt uitvoerig beschreven.

De beschrijving van de autotuning methode, alsmede de eisen die gesteld worden aan de instrumentatie komen aan de orde. Er wordt een aantal suggesties gedaan hoe de autotuning methode van nut kan zijn voor low-dose electronenmicroscopie en voor reconstructie van drie-dimensionale structuren uit een reeks beelden opgenomen met verschillend defocus en/of bundelkanteling.

Het ontwerp en de uiteindelijke test van de autotuning methode wordt in een zestal hoofdstukken beschreven.

In hoofdstuk 1 wordt ingegaan op electronenmicroscopie en een aantal toepassingen. Er wordt benadrukt dat het van belang is de TEM nauwkeurig in te stellen, zonder dat het preparaat onnodig door electronen bestraald wordt.

Vervolgens wordt een overzicht gegeven van een aantal methoden die beschikbaar zijn om het defocus, astigmatism en de misalignering te corrigeren (handmatig en semi-automatisch). De conclusie van het hoofdstuk is dat de methode voor het instellen van de TEM, gebaseerd op het meten van een beeldverschuiving als gevolg van het kantelen van de belichtingsbundel, zeer geschikt is als autotuning methode.

Zoals gezegd is het van belang de TEM in te stellen met gebruik van een minimale aantal electronen. Dit heeft tot gevolg dat de beelden waarmee de instelling van de TEM afgeleid, en zonodig gecorrigeerd moet worden, veel ruis zullen bevatten. Daarom is een statistische, en niet deterministische, parameterschattingstheorie gebruikt om een schatter te ontwerpen die de TEM parameters (het defocus, het astigmatisme en de uitlijning) zo precies mogelijk schat (minimale variantie van de schatter). Bij de statistische schattingstheorie is de ruis in het model van de waarnemingen opgenomen. Juist in beelden van een transmissie electronenmicroscoop is de voorkennis omtrent de statistiek van de ruis groot aangezien ze voor een belangrijke mate door Poisson statistiek beschreven wordt (tel ruis).

In hoofdstuk 2 wordt vervolgens het preparaat, de TEM en het beeldopnamesysteem gemodelleerd. Met behulp van dat mathematisch model wordt bepaald wat de precisie (variantie van de schatter) zal zijn waarmee de TEM parameters onder realistische meetomstandigheden geschat kunnen worden. Als maat voor de haalbare precisie wordt de ondergrens van Cramer en Rao bepaald. De ondergrens van Cramer en Rao is afhankelijk van het preparaat, de TEM en het beeldopnamesysteem, maar niet afhankelijk van de uiteindelijk geimplementeerde schatter. De ondergrens van Cramer en Rao is dan ook een geschikt hulpmiddel voor het optimaliseren van de meetopstelling en de meetstrategie. De conclusie van het hoofdstuk is dat de haalbare precisie in het schatten van het defocus uit beeldverschuivingen ongeveer 5 nm zal zijn, met gebruik van 6500 electronen per nm^2, een vergroting van 400,000, een beeldopnamesysteem dat 512^2 beeldelementen bevat, en als het preparaat een dun amorf vlies is (koolvlies).

De autotuning methode bepaalt de instelling van de TEM uit het meten van beeldverschuivingen wanneer de belichtingsbundel gekanteld wordt. Bij lage vergrotingen, en dus voor de lage spatiele frequenties in het preparaat, is het effect van bundelkanteling een zuivere beeldverplaatsing wanneer de TEM niet gefocuseerd is. Echter bij hoge vergrotingen, is er naast beeldverplaatsing ook beeldvervaging waar te nemen. Als gevolg van de sferische aberratie van de objectieflens, is de beeldverplaatsing afhankelijk van de spatiele frequentie: hogere spatiele frequenties verplaatsen zich over een andere afstand dan de lagere spatiele frequenties. Het directe gevolg hiervan is dat de autotuning methode, gebaseerd op het meten van zuiver beeldverplaatsingen, niet goed zal werken bij hogere vergrotingen. Er zijn echter een aantal manieren om de invloed van de sferische aberratie op het

schatten van de TEM parameters te verminderen.

Hoofdstuk 3 beschrijft een methode om te invloed van sferische aberratie op het meten van een beeldverschuiving te corrigeren. Het blijkt mogelijk te zijn om het defocus te schatten met behulp van verschuivingsmetingen wanneer beide beelden (digitaal) gefilterd worden voordat een beeldverschuiving gemeten wordt. Het benodigde filter is slechts afhankelijk van de bundelkanteling, welke opgelegd wordt en dus bekend is (mits de TEM is uitgelijnd en het astigmatism vooraf gecorrigeerd is). Naast de beschrijving van deze filtering wordt de autotuning methode, gebaseerd op verschuivingsmetingen, vergeleken met een andere, in de literatuur voorgestelde, autotuning methode (variantie methode). De haalbare precisie van beide methodes wordt onder realistische omstandigheden berekend en vergeleken. De uitkomst van deze vergelijking is dat de verschuivingsmeting ongeveer 30 maal minder electronen gebruikt, en dus meer geschikt is voor low-dose electronenmicroscopie dan de variantie methode.

In hoofdstuk 4 wordt de voorgaande theorie, met betrekking tot het schatten van de parameters uit een aantal beelden opgenomen met gekantelde bundels, verder uitgediept. Zoals gezegd, is het mogelijk de TEM parameters te schatten uit beeldverschuivingen met behulp van kruiscovariantie functies, mits het effect van sferische aberratie verwaarloosbaar klein is, door de beelden op te nemen bij lage vergrotingen. Een andere mogelijkheid is de beelden vooraf te filteren met het (hierboven beschreven) correctie filter. Het is echter ook mogelijk de TEM parameters te schatten uit het fase gedeelte van kruisspectra van beelden opgenomen met gekantelde belichtingsbundels. Deze aanpak modelleert de sferische aberratie als een extra parameter, en heeft de voorkeur boven de verschuivingsschatting wanneer het preparaat zeer gevoelig is voor de electronenstraling. Aangezien de hoge spatiele frequenties in het preparaat gebruikt worden voor het automatische instellen van de TEM, is de methode geschikt voor hoog oplossend vermogen electronenmicroscopie. Deze methode is algemeen toepasbaar mits het preparaat beschreven kan worden als een zwak fase object. Voor dikke kristallijne preparaten zal de methode niet goed werken.

In hoofdstuk 5 wordt de voorgaande theorie samengevat, de experimentele opstelling en een aantal experimenten beschreven. De meetopstelling bestaat uit een Philips EM 420 TEM, een Gatan 622 camerasysteem, een DEC PDP 11/23 computer en een beeldverwerkend systeem (TVDIPS). De Philips EM 420 TEM is in haar standaarduitvoering niet geschikt voor computerbesturing. Een aantal (electronische) modificaties waren dan ook noodzakelijk om het focus, de stigmator van de objectieflens en de deflectiespoelen boven de objectieflens te kunnen besturen. De DEC PDP 11/23 computer is hiertoe voorzien van extra hardware en software. De Gatan camera is verbonden met de TEM, en met het beeldverwerkend systeem TVDIPS. De TVDIPS computer

bevat hardware om zeer snel verschuivingen en kruisspectra te berekenen. De snelheid is van belang voor de autotuning methode, aangezien de instelling van de TEM bepaald wordt uit beeldverplaatsingen die op hun beurt weer berekend worden met kruiscovariantiefuncties. Een kruiscovariantie functie van twee beelden (256^2 beeldelementen) wordt in 0.8 s berekend. De TVDIPS computer is verbonden met de DEC computer die op zijn beurt weer verbonden is met de TEM. De autotuning methode is geimplementeerd en blijkt betrouwbaar en nauwkeurig te werken. Bij een vergroting van 96000 is de reproduceerbaarheid in het schatten van de uitlijning 0.1 mrad, 5 nm van het focus en 10 nm van het astigmatisme te zijn. Dit is voldoende nauwkeurig voor toepassingen in de praktijk. De tijd die nodig is om het focus en het astigmatisme te bepalen en te corrigeren is 6.5 s. De uitlijning van de belichtingsbundel neemt 7 s in beslag.

Hoofdstuk 6 geeft een overzicht van de eerste vijf hoofdstukken en richt zich op de naaste toekomst met betrekking tot autotuning. Er wordt benadrukt dat de autotuning methode geimplementeerd is op een aantal systemen buiten Delft, om haar toepasbaarheid in praktische situaties te testen. In samenwerking met Philips (producent van electronenmicroscopen) en met de firma Tietz Image Processing Systems (producent van computer systemen geschikt om de Philips CM serie electronenmicroscopen te besturen) is de methode geimplementeerd op het meest recente type computerbestuurbare electronenmicroscoop.

Momenteel worden de industrieel/commerciele aspecten van de autotuning methode voor low-dose electronenmicroscopie geevalueerd, en vindt er een verdere ontwikkeling van de methode plaats om een bruikbaar hulpmiddel te zijn voor gebruikers van de nieuwste generatie computerbestuurbare electronenmicroscopen.

Korte levensbeschrijving

21 dec 1960	De schrijver van dit proefschrift wordt te Velsen geboren en krijgt de naam Abraham Johannes Koster.
september 1973	Hij besluit toe te treden tot de 'Mr. S. Vissering Scholengemeenschap', eveneens in Velsen.
mei 1979	Bram ontvangt het diploma voor het met succes doorlopen van het Voorbereidend Wetenschappelijk Onderwijs.
nazomer 1979	Enthousiast begint hij als student bij de afdeling der Technische Natuurkunde aan de Technische Hogeschool in Delft.
november 1982	Na het behalen van zijn Kandidaats diploma in 1982, schrijft hij zich in bij de Kamer van Koophandel als (mede-)oprichter van het automatiserings adviesbureau 'Microcontrol'.
voorjaar 1984	Hij mindert zijn adviserende activiteiten en richt zich meer op de studie waar hij al enige tijd bezig is met zijn vierdejaarswerk, onder begeleiding van Dr.ir. A. van den Bos, binnen de vakgroep Signaal/Systeem techniek, sectie Parameterschatten. De titel van zijn verslag luidt: 'Ontwerp van een gebruikersvriendelijke spectraal analysator op parametrische grondslag'.
zomer 1984	*Meerdere maanden verblijft hij in Canada, waarin hij* gedurende twee maanden onderzoek verricht bij de groep Micro-Structural Sciences van het National Research Council (NRC) in Ottawa, met betrekking tot 'Quadrupole Mass Spectrometry'.
nazomer 1984	Hij beseft dat parameterschatten van belang is voor de automatische besturing van transmissie electronenmicroscopen, en start een succesvol samenwerkingsprojekt tussen de sectie Parameterschatten en de vakgroep Deeltjes Optica.

februari 1985 — Het samenwerkingsprojekt mondt uit in zijn afstudeerverslag met de titel 'Achievable precision in autotuning of a transmission electron microscope' onder begeleiding van Prof.dr.ir. B.P. Veltman en Dr.ir. A. van den Bos.

april 1985 — Hij zet het samenwerkingsproject binnen de vakgroep Electronen Optiek voort, onder begeleiding van Prof.dr.ir. K.D. van der Mast en Dr.ir. A.van den Bos, maar nu als promovendus

april 1989 — Hij heeft zich vier jaar bezig gehouden met het ontwerpen, implementeren en testen van diverse manieren om een transmissie electronenmicroscoop automatisch in te stellen, in dienst van het de Stichting Fundamenteel Onderzoek der Materie (FOM). Hij weet dat de electronen microscopisten de autotuning methode goed kunnen gebruiken om onderzoek te doen aan zeer stralingsgevoelige, preparaten, en hoopt dat ze dat ook zullen doen.

Nawoord

Graag wil ik een ieder bedanken die heeft bijgedragen aan de totstandkoming van dit proefschrift. Mijn dank gaat in de eerste plaats uit naar mijn beide promotoren, Karel van der Mast en Aad van den Bos, die aan mijn zijde stonden in tijden van voor- en tegenspoed. Eveneens gaat mijn dank uit naar Pieter Kruit voor zijn kritische en aanmoedigende opmerkingen betreffende het autotuning project. Natuurlijk ben ik *iedereen binnen de vakgroep Deeltjes Optica dankbaar voor zowel de wetenschap-*pelijke bijdragen als voor de genoten gezelligheid.

Het was voor mij zeer leerzaam en plezierig om gedurende de afgelopen vier jaar samen met een aantal studenten te werken aan het zogenaamde 'Autotuning Project'. Ik ben dan ook Rolf, Folbert, Bert, Hans, Taco, Mario en Leo dankbaar voor hun *wetenschappelijke bijdragen en enthousiasme.*

Bijzonder dankbaar ben ik Petra en mijn ouders, voor de broodnodige steun buiten het universitaire wereldje.

Dit onderzoek is verricht met steun van Philips Electron Optics en van de Stichting Technische Wetenschappen (STW).

Bram Koster

12. If communication is defined as 'one or more persons making, having or continuing contact with one or more other persons by means of carrying out, or having carried out an observable activity - or activities - with the purpose to realize one or more goals,' and communication-failure as 'not being able to exchange information as a result of an insufficient capability to speak, listen, write and read,' then the medium television is not an aid for communication, but a cause for communcation-failure, because this medium encourages people to look at a screen without any other observable meaningful activity.

Neil Postman (1986). Amusing ourselves to death: public discourse in the age of show-business. New York, Viking.

C.J.J. Korswagen (1982). Mondelinge communicatie in theorie en praktijk. Groningen, Wolters-Noordhof.

13. In 1987 the average Dutchman used a motorcar more than a bicycle in comparison to 1980, if the increase in usage is measured as the ratio of the average distance driven and the average distance biked per day. This is an indication that the consideration of the average Dutchman given to environmental problems decreased in that period.

Centraal bureau voor de statistiek (1988). Statistisch Zakboek 1988. 's-Gravenhage, Staatsuitgeverij, 239.

Theses

connected to the dissertation

Autotuning of a Transmission Electron Microscope

A.J. Koster, Delft, June 6, 1989.

1. For the autotuning of a TEM, the electron dose required for a two-step method (consisting of a rough and a fine-tuning step, respectively) is, in general, smaller than that required for a one-step method.

2. The possibility to estimate parameters of structures in the specimen directly from electron microscopical images recorded with a videocamera will decrease the necessity to store the images on photographic material for off-line processing.

W.O. Saxton (1988). Accurate atom-positions from focal and tilted series of high resolution electron micrographs. in: Image and Signal Processing in Electron Microscopy, eds. P.W. Hawkes, W.O. Saxton, F.P. Ottensmeyer, A. Rosenfeld (Scanning Microscopy International, Chicago), 213.

3. It is preferable to combine autotuning of a TEM and the calibration of the TEM-control in one single procedure, as the reliability of autotuning will increase drastically while the required electron dose will be only a factor of two higher than without simultaneous calibration.

4. The acceptance of holography within electron microscopy as a method to study specimen structures is hindered by the fact that a human being is able to observe only the intensity of images and not complex images consisting of phase and magnitude. Therefore, the application of holography will increase as soon as a videocamera and an image processing system are part of a TEM and capable of transfering and displaying the complex holographic images as an intensity distribution on a monitor.

Lichte (1986). Electron holography approaching atomic resolution. Ultramicroscopy 20, 293.

5. In a discussion of the phase contrast transfer function in the weak phase approximation for tilted illumination, the frequency region should be mentioned for which the double side band imaging is a valid description of image formation, because this region is highly dependent on the setting of the TEM.

W. Hoppe, D. Kostler, D. Typke and N. Hunsmann (1975). Kontrastuebertragung fuer die Hellfeld-Bildrekonstruktion mit gekippter Beleuchtung in der Elektronenmikroskopie. Optik 42, No. 1, 43.

6. A method recently proposed to estimate the electron wave function emerging from a specimen using a series of images formed at different values of defocus, should be formulated statistically and not deterministically in order to get insight in the practical limitations of this method due to the noise in the images and inaccuries in the control of defocus.

D. van Dyck and W. Coene (1987). A new procedure for wave function restoration in high resolution electron microscopy. Optik 77, no.3, 125.

7. The reliability and applicability of an autotuning method based on measuring the variation in image contrast when the setting of the TEM is changed will increase when this method is combined with an autotuning method based on measuring the effect of beam tilt on the image.

W.O. Saxton, D.J. Smith, M.A. O'Keefe, G. Wood and W.M. Stobbs (1983). Procedures for focusing, stigmating and alignment in high resolution electron microscopy. Journal of Microscopy 130, Part 2, 187.

8. The evolution of the TEM during the past 10 years can be characterized by the integration of computers to control currents through coils and not by the improvement of electron optical components. It is to be expected that in the coming 10 years computers will play an even larger role with respect to the interpretation of images for high resolution electron microscopy and the imaging of radiation sensitive specimens for high resolution low dose electron microscopy.

9. Automatic control of a TEM will not increase the production (in terms of obtaining data of structures in specimens per time unit) when the knowledge and expertise of the user is inversely proportional to the level of automation.

10. In the Netherlands, the educational program at university level has changed in the past 20 years in such a way that the saying 'studying at a university' should be, in general, replaced by 'taking a course at a university'.

Koninklijk Instituut voor Ingenieurs (1989). Compact academisch pakket perst irstudie in 3 jaar. Ingenieurskrant, 20 april, 52.

11. For scientific research the price of material or instrumentation is not a valid criterion to justify a method or idea, since prices are time dependent.

11. In wetenschappelijk onderzoek is de kostprijs van benodigde materiaal of middelen geen juist kriterium om een methode of idee mee te rechtvaardigen, aangezien de kostprijs in de tijd zal fluctueren.

12. Als men communicatie definieert als: 'het in gemeenschap treden, zijn of blijven van een of meer personen met een of meer andere personen door het verrichten - of verricht hebben - van een waarneembare activiteit - of van waarneembare activiteiten -, teneinde een of meer doelstellingen te verwezenlijken,' en communicatie-stoornis als: 'een belemmering in informatie-uitwisseling tengevolge van het onvoldoende beheersen van elementaire vaardigheden zoals spreken, luisteren, schrijven en lezen,' dan is het medium televisie niet zozeer een hulpmiddel tot communicatie, maar eerder een oorzaak van communicatie-stoornissen, aangezien dit medium aanzet tot kijken naar een beeldscherm zonder dat dit kijken resulteert in een andere waarneembare betekenisvolle activiteit.

Neil Postman (1986). Amusing ourselves to death: public discourse in the age of show-business. New York, Viking.

C.J.J. Korswagen (1982). Mondelinge communicatie in theorie en praktijk. Groningen, Wolters-Noordhof.

13. Vergeleken met 1980 gebruikte de gemiddelde Nederlander in 1987 een automobiel meer dan een fiets, als de toename in het gebruik gemeten wordt als de verhouding tussen de afstand gemiddeld afgelegd per auto en die per fiets per dag. Dit geeft aan dat het besef van de gemiddelde Nederlander van de milieuproblematiek in deze periode is verminderd.

Centraal bureau voor de statistiek (1988). Statistisch Zakboek 1988. 's-Gravenhage, Staatsuitgeverij, 239.

Stellingen

behorende bij het proefschrift

Autotuning of a Transmission Electron Microscope

A.J. Koster, Delft, 6 juni 1989.

1. Voor het automatisch instellen van een TEM, is het benodigde aantal electronen bij een twee-staps methode (bestaande uit een grof en fijn- instelling) in het algemeen kleiner dan bij een één-staps methode.

2. De mogelijkheid om parameters van structuren in een preparaat direct (on-line) te schatten uit electronenmicroscopische beelden opgenomen met een videocamera onder bekende beeldvormingscondities zal de noodzaak om beelden op fotografisch materiaal op te slaan voor latere (off-line) verwerking verminderen.

W.O. Saxton (1988). Accurate atom-positions from focal and tilted series of high resolution electron micrographs. in: Image and Signal Processing in Electron Microscopy, eds. P.W. Hawkes, W.O. Saxton, F.P. Ottensmeyer, A. Rosenfeld (Scanning Microscopy International, Chicago), 213.

3. Het is beter om het automatisch instellen van een TEM en de calibratie van de TEM-besturing te combineren in één enkele procedure, aangezien dan de betrouwbaarheid van het automatisch instellen sterk zal toenemen en het benodigd aantal electronen slechts een factor twee groter zal zijn dan zonder deze gelijktijdige calibratie.

4. Het aanvaarden van holografie binnen de electronenmicroscopie als een techniek om structuren in preparaten te bestuderen wordt belemmerd door het feit dat een mens slechts intensiteitsverdelingen waarneemt en geen complexe beelden bestaande uit fase en magnitude. Het gebruik van holografie zal daarom pas sterk toenemen zodra een videocamera met bijbehorend beeldverwerkingssysteem een integraal onderdeel is van het electronenmicroscoop en de complexe holografische beelden direct (on-line) omgezet kunnen worden naar een preparaatafbeelding in de vorm van een intensiteitsverdeling op een beeldscherm.

H. Lichte (1986). Electron holography approaching atomic resolution. Ultramicroscopy 20, 293.

5. Ten onrechte wordt bij het presenteren van de contrast transfer functie in de zwakke fase benadering met gekantelde belichtingsbundel vaak het frequentiegebied waarvoor 'double sideband imaging' de beeldvorming in het microscoop beschrijft niet vermeld, hoewel dit frequentiegebied sterk bepaald wordt door de instelling van de TEM.

W. Hoppe, D. Kostler, D. Typke and N. Hunsmann (1975). Kontrastuebertragung fuer die Hellfeld-Bildrekonstruktion mit gekippter Beleuchtung in der Elektronenmikroskopie. Optik 42, No. 1, 43.

6. Een methode recentelijk voorgesteld om de golffunctie tredend uit het preparaat te bepalen uit een aantal beelden opgenomen met verschillend defocus zou niet op een deterministische, maar op stochastische wijze geformuleerd dienen te worden om de praktische beperkingen van deze methode als gevolg van ruis in de beelden en onnauwkeurigheden in het besturen van het defocus af te schatten.

D. van Dyck and W. Coene (1987). A new procedure for wave function restoration in high resolution electron microscopy. Optik 77, no.3, 125.

7. De betrouwbaarheid en toepasbaarheid van een automatische methode om de TEM in te stellen gebaseerd op het bepalen van minimum contrast in het beeld zal groter zijn als deze methode gebruikt wordt in combinatie met een automatische methode gebaseerd op het meten van het effect van bundelkanteling in het beeld.

W.O. Saxton, D.J. Smith, M.A. O'Keefe, G. Wood and W.M. Stobbs (1983). Procedures for focusing, stigmating and alignment in high resolution electron microscopy. Journal of Microscopy 130, Part 2, 187.

8. De ontwikkeling van TEM is de afgelopen 10 jaar in hoge mate bepaald door de integratie van computers met betrekking tot regelen van stromen door spoelen en niet door verbeteringen aan de diverse electronen optische onderdelen. Het is te verwachten dat in de komende 10 jaar computers een nog grotere rol gaan spelen, maar dan met betrekking tot beeldinterpretatie bij hoog oplossend vermogen electronenmicroscopie en bij het afbeelden van zeer stralingsgevoelige preparaten.

9. Automatisering van een TEM zal de productie (het verkrijgen van gegevens over structuren in het preparaat per tijdseenheid) niet doen toenemen wanneer de kennis en vaardigheid van de gebruiker omgekeerd evenredig is met de mate van automatisering.

10. Het universitair onderwijsprogramma is in de afgelopen 20 jaar in Nederland zodanig veranderd dat de zinsnede 'studeren aan een universiteit' in het algemeen beter vervangen kan worden door 'het volgen van een cursus aan een universiteit.'

Koninklijk Instituut voor Ingenieurs (1989). Compact academisch pakket perst irstudie in 3 jaar. Ingenieurskrant, 20 april, 52.